Chem Soc Rev

REVIEW ARTICLE

View Article Online
View Journal | View Issue

Cite this: *Chem. Soc. Rev.*, 2023, **52**, 5135

Electrochemical transformations catalyzed by cytochrome P450s and peroxidases

Neeraj Kumar, [a] Jie He *[ab] and James F. Rusling *[abcd]

Cytochrome P450s (Cyt P450s) and peroxidases are enzymes featuring iron heme cofactors that have wide applicability as biocatalysts in chemical syntheses. Cyt P450s are a family of monooxygenases that oxidize fatty acids, steroids, and xenobiotics, synthesize hormones, and convert drugs and other chemicals to metabolites. Peroxidases are involved in breaking down hydrogen peroxide and can oxidize organic compounds during this process. Both heme-containing enzymes utilize active Fe^{IV}=O intermediates to oxidize reactants. By incorporating these enzymes in stable thin films on electrodes, Cyt P450s and peroxidases can accept electrons from an electrode, albeit by different mechanisms, and catalyze organic transformations in a feasible and cost-effective way. This is an advantageous approach, often called bioelectrocatalysis, compared to their biological pathways in solution that require expensive biochemical reductants such as NADPH or additional enzymes to recycle NADPH for Cyt P450s. Bioelectrocatalysis also serves as an *ex situ* platform to investigate metabolism of drugs and bio-relevant chemicals. In this paper we review biocatalytic electrochemical reactions using Cyt P450s including C–H activation, S-oxidation, epoxidation, N-hydroxylation, and oxidative *N*-, and *O*-dealkylation; as well as reactions catalyzed by peroxidases including synthetically important oxidations of organic compounds. Design aspects of these bioelectrocatalytic reactions are presented and discussed, including enzyme film formation on electrodes, temperature, pH, solvents, and activation of the enzymes. Finally, we discuss challenges and future perspective of these two important bioelectrocatalytic systems.

Received 12th June 2023

DOI: 10.1039/d3cs00461a

rsc.li/chem-soc-rev

[a] *Department of Chemistry, University of Connecticut, Storrs, CT 06269-3136, USA. E-mail: jie.he@uconn.edu, james.rusling@uconn.edu*
[b] *Institute of Materials Science, University of Connecticut, Storrs, CT 06269-3136, USA*
[c] *Department of Surgery and Neag Cancer Center, Uconn Health, Farmington, CT 06030, USA*
[d] *School of Chemistry, National University of Ireland at Galway, Galway, Ireland*

Neeraj Kumar

Neeraj Kumar received his PhD in Chemistry from Indian Institute of Technology Roorkee, India (2019). Then he worked as Research Associate at the CSIR-Central Building Research Institute Roorkee and National Postdoctoral Fellow at the Department of Inorganic and Physical Chemistry, at the Indian Institute of Science (IISc) Bangalore. Currently, he works as a Postdoctoral Research Associate at the Department of Chemistry, University of Connecticut, Storrs, USA. His research interests include electrochemistry, electrochemical sensors/biosensor, photo-catalysis, and electro-/bio-catalysis.

Jie He

Jie He received his BS and MS degrees in Polymer Materials Science and Engineering from Sichuan University and his PhD in Chemistry from Université de Sherbrooke in 2010. He joined the faculty of the University of Connecticut after working as a postdoctoral fellow at the University of Maryland in 2011–2013. He is currently an Associate Professor of Chemistry and Polymer Program at the Institute of Materials Science, University of Connecticut. His research group focuses on design and synthesis of hybrid materials of polymers and metals that are capable activating small molecules as inspired by metalloenzymes.

1. Introduction

Chemical transformations of organic compounds are fundamentally and practically important for synthesizing essential chemical products like new and safe drugs, clean industrial chemicals, environmentally safe materials, and beyond.[1] A key to making these transformations practical is high yield at low cost. In comparison to traditional chemical syntheses, biological syntheses are most often catalyzed by enzymes and very often outperform chemical catalysis in terms of substrate specificity and product regio- and stereo-selectivity. Thus, the utilization of biological catalysts in chemical transformations can provide cost-effective, selective, rapid syntheses, often without separation of by-products or intermediates.[2,3]

Novel synthetic methods are needed to make strictly chiral pharmaceutical products. For example, often only one chiral form of a drug has the desired activity, while the other chiral form may have undesirable or even toxic activity. Biocatalysts offer alternative routes to chemical syntheses under mild conditions, low environmental toxicity, and excellent chiral selectivity, and can avoid toxic solvents and redox agents. Enzymes lead to high regio- and stereoselectivity in the reaction products.[1,3–5] The study of drug metabolites also plays a key role in uncovering therapeutic and toxicity effects.[6,7] Heme-containing enzymes especially Cytochrome P450 (Cyt P450s, Scheme 1), are involved in up to 75% of metabolic reactions of existing drugs and also covert toxic compounds like pollutant to less or more toxic products. Enzymes can also be efficient in the remediation of pollutants.[8–11] Thus, biocatalytic transformations have garnered lots of attention in organic and pharmaceutical syntheses, pollutant remediation, and metabolism studies.

In this review, we summarize recent advances of bioelectrocatalytic transformations of organic compounds using Cyt P450s and peroxidases. Cyt P450s are an extensive family of enzymes in mammals, bacteria and plants.[12,13] They have an iron heme cofactor (Scheme 1) imbedded within their polypeptide structures as the mediation center of all their catalyzed oxidation reactions (see Scheme 2). As mentioned, Cyt P450s metabolize drugs and other chemicals in humans, but in some cases produce toxic products.[7,14–19] Cyt P450s are biocatalysts for C–H hydroxylation, N- and S-oxidation, O-, N- and S-dealkylation, C–C bond cleavage, C=C double bond epoxidation, aromatic coupling, as well as more unusual reactions.[20,21] They are effective for synthesis of drugs, drug metabolites,[22–27] bioremediation,[28–30] and development of biosensors.[31–33]

Cyt P450s as monooxygenases incorporate one oxygen atom site-selectively into a reactive substrate.[23,34] In humans Cyt P450 reductases (CPRs) accept electrons from nicotinamide adenine dinucleotide (NADH) or nicotinamide adenine dinucleotide phosphate (NADPH).[35] In nature, CPR transfers two electrons from NADPH to Cyt P450s (Scheme 2). Other redox partners also exist for Cyt P450s,[23,36] *e.g.*, bacterial and mitochondrial systems with NADPH-ferredoxin reductase and ferredoxin partners. Cyt P450s also have alternative activation pathways utilizing hydrogen peroxide (called the H_2O_2 shunt) to facilitate oxidative reactions.[37,38] All these enzymatic reactions feature reduction of Fe(III) to Fe(II) that reacts with oxygen or H_2O_2 to yield reactive Fe(IV)=O species to oxidize substrates.[39] Cyt P450 oxidations have also been discussed in terms of heme iron–oxygen enzyme forms called compound I ($P^{\bullet+}Fe(IV)=O$), using terminology from peroxidases.[40]

Peroxidases use hydrogen peroxide (H_2O_2) as the oxygen source. The iron heme prosthetic group typically binds with a histidine residue that acts a proximal ligand. The catalytic cycle of all peroxidases is shown below and is similar to the H_2O_2 shunt process of Cyt P450s (eqn (1)–(3)). Peroxidases get activated by two-electron reduction of H_2O_2 to yield high valent Fe(IV)=O species.

$$PFe(III) + H_2O_2 \rightarrow PFe(III)\text{–}O\text{–}O\text{–}H \rightarrow P^{\bullet+}Fe(IV)=O \text{ (Compound } \mathbf{I}) + H_2O \quad (1)$$

$$P^{\bullet+}Fe(IV)=O + RH \rightarrow Fe(IV)=O \text{ (Compound } \mathbf{II}) + R^{\bullet} + H^{+} \quad (2)$$

$$PFe(IV)=O + RH + H^{+} \rightarrow PFe(III) + H_2O + R^{\bullet} \quad (3)$$

Initially, peroxidase PFe(III) is oxidized by H_2O_2 to produce the two-electron oxidized intermediate (compound **I**, eqn (1)) compound **I** ($P^{\bullet+}Fe(IV)=O$).[43–48] Compound I oxidizes a substrate to yield ferryl-oxy intermediate compound **II** (Fe(IV)=O, eqn (2)), which is reduced back to the Fe(III) by oxidizing another substrate molecule (eqn (3)).[44,49,50] In organisms, peroxidases destroy excess H_2O_2 and reactive oxygen species (ROS) as well as oxidize numerous compounds. Several types of peroxidases, *e.g.* lignin peroxidase,[47,48,51–56] horseradish peroxidase (HRP),[46,57–60] chloroperoxidase (CPO),[61–64] manganese peroxidase,[65,66] and haloperoxidases.[67–69] have been used extensively in biocatalytic oxidations (*e.g.*, the oxidation of alkanes to alcohols) or chromogenic reactions in chemiluminescence.[70] While oxidation of these enzymes by H_2O_2 is required, their inactivation by H_2O_2 may limit their use in industry.[71–73] Thus, recent studies have focused on *in situ* production of H_2O_2 that potentially overcomes the over-oxidation issue.[74]

James F. Rusling

James F. Rusling earned a BSc from Drexel University (1969), and PhD in Chemistry from Clarkson University (1979). He is Paul Krenicki Professor of Chemistry at University of Connecticut, Professor of Surgery and Neag Cancer Center member at UConn Health, and adjunct Professor of Chemistry at National Univ. of Ireland, Galway. Current research includes biocatalysis, electrochemical biocatalysis, microfluidic devices for point-of-care disease diagnostics, nano-energy for implantable medical devices, and mass spectrometry methods for peptide biomarkers, He has authored over 450 research papers and several books, and is a musician interested in Irish and American folk styles.

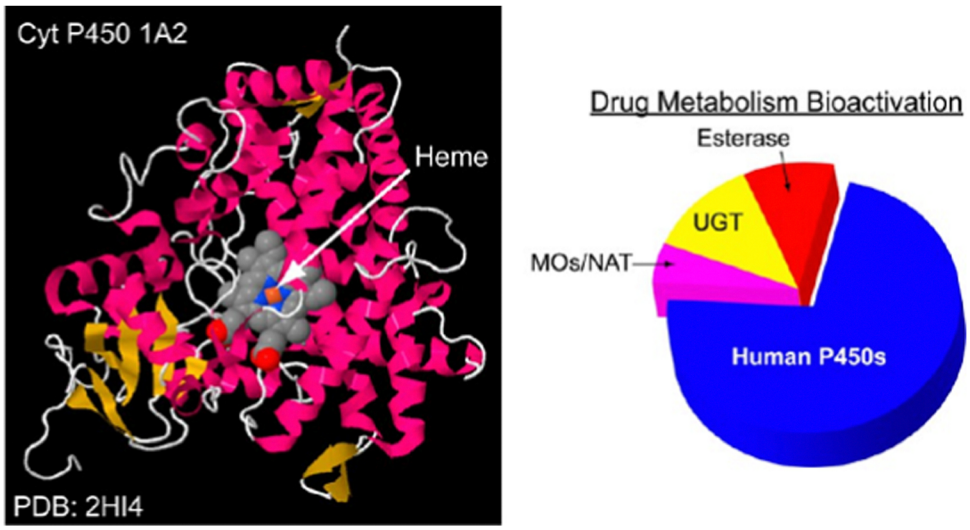

Scheme 1 Ribbon structure of human cytochrome P450 (CYPE14), identifying the iron heme cofactor that is central for all its biosynthetic reactions, and chart showing the relative importance of various liver enzymes in metabolizing known drugs. Reproduced from *Anal. Chem.*, 2016, **88**, 4584–4599 with permission.[26] Copyright, 2016, ACS publication.

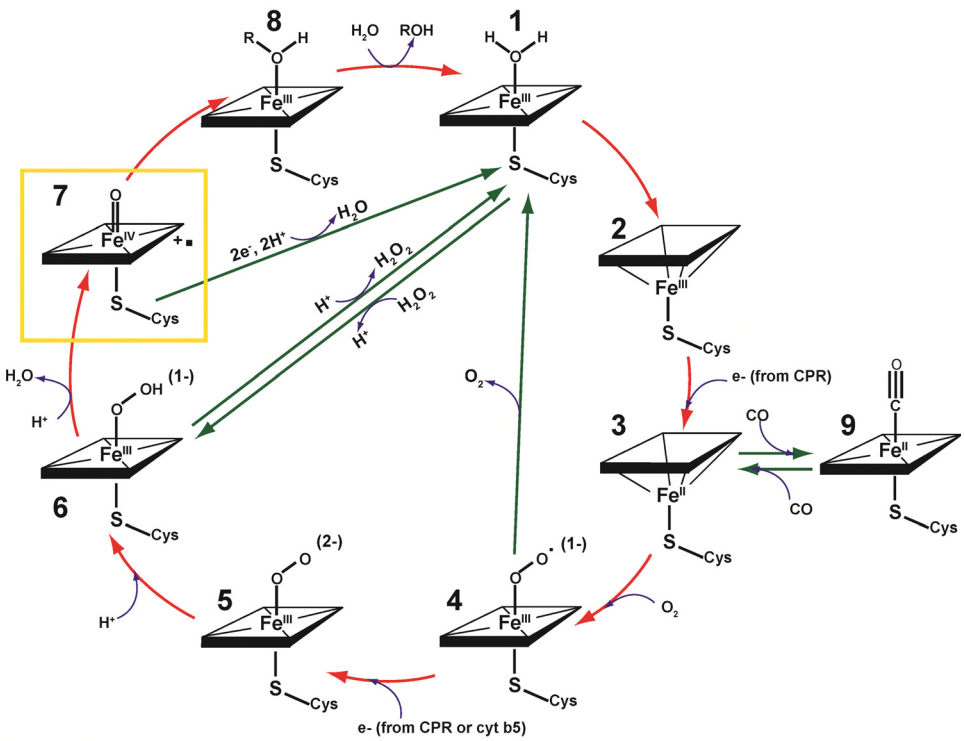

Scheme 2 Pathway for mammalian Cyt P450-catalyzed reactions.[8,13,35,41,42] The ferric iron-heme (P-Fe) Cyt P450 (1) first binds substrate RH to eliminate water (2). Next, 2 is reduced to 3 by NADPH-dependent reductase CPR to yield ferrous heme Cyt P450 3, which then binds dioxygen to form ferryl superoxy complex 4. This complex is reduced by NADPH reductase CPR to yield 5, which is then protonated to 6, which may also be generated by peroxide *via* the reversible peroxide shunt. Protonation of 6 and dioxygen cleavage lead to active heme-iron(IV)-oxo radical cation (7), considered the key reactive intermediate that transfers oxygen to the bound substrate to yield the product ROH. Exposure of ferrous form 3 to carbon monoxide (CO) yields P-Fe(II)-CO complex 9, which absorbs 450 nm light, which gave these enzymes the name Cyt P450s. Abbreviation: CPR, cytochrome 450 reductase.

1.1 Classification of Cyt P450s and peroxidases

Cyt P450s are commonly divided into two classes. Bacterial and mitochondrial P450s are in Class I, and use a two-component electron transfer system containing a ferredoxin reductase and iron–sulfur protein (ferredoxin). Ferredoxins are acidic, low molecular weight, soluble proteins including iron-sulfur

clusters, *e.g.* [2Fe-2S], [3Fe-4S] and [4Fe-4S], and a 7 Fe ferredoxin with both a [3Fe-4S] and a [4Fe-4S] cluster. The electron transfer pathway involves NAD(P)H donating an electron to ferredoxin reductase, which subsequently transfers to ferredoxin, and then to the Cyt P450.[75–81] Mammalian microsomal Cyt P450s are called Class II enzymes and the electron source is NADPH Cyt P450 reductase.[77–79] The generally accepted electron transfer and reductant oxidation pathway is presented in Scheme 2.[77,82,83]

While the short notation for these enzymes is Cyt P450s, specific enzyme notations are used for individual Cyt P450s, *e.g.*, CYP3A4, CYP1A2, CYP2E9, CYP2B6, CYP2E1, CYP2C8, CYP2C19 and CYP2D6, *etc.*[84] In those notations, CYP represents the superfamily followed by a number indicating the gene family, the capital letter after the first number represents the subfamily, and the last number denotes the individual gene.[85] The use of italics in the name usually denotes a gene, *e.g.*, *CYP2E1* gene (*i.e.*, the gene encoding the enzyme CYP2E1).[86] Cyt P450s can be found in every class of organism. In humans, there are 18 families of mammalian Cyt P450s. Many of these enzymes are associated with specific drug metabolism and xenobiotic reactions to oxidize drugs/toxins.[87,88] For example, CYP2E1 metabolizes paracetamol (acetaminophen) into *N*-acetyl-*p*-benzoquinoneimine.[89] CYP2B6 metabolizes cyclophosphamide into 4-hydroxy cyclophosphamide.[90] CYP2A6, CYP2B6, CYP3A4, CYP3A5, CYP2C9, CYP2C18, CYP2C19, show oxazaphosphorine 4-hydroxylation activity. High activity for 4-hydroxylation of cyclophosphamide is demonstrated by CYP2B6, and for 4-hydroxylation of ifosfamide by CYP3A4.[91] The numerous androgen-metabolizing Cyt P450s (CYP3A4, CYP3A5, CYP3A43 and CYP2B6) and CYP enzymes (CYP27B1, CYP27A1, CYP24A1, CYP3A4, CYP2J2, CYP2R1) are necessary for vitamin D metabolism.[85,92–94] Human CYP2B6, CYP2C19, CYP2D6, CYP2C9 and CYP3A4 metabolize 75–90% of existing phase I drugs. Among these, CYP3A4 is responsible for biotransformation of a very large number (close to 50%) of drugs.[84,95,96]

Peroxidase enzymes are found in plants, animal, and microorganism tissues. They are classified into three classes based on source.[97–100] Class I-intracellular prokaryotic peroxidases include catalase, ascorbate peroxidase and cytochrome *c* peroxidase. Class II-extracellular fungal peroxidases contain manganese peroxidase, lignin peroxidase and versatile peroxidase, and class III-secretory plant peroxidases comprise horseradish root peroxidase (HRP), wheat peroxidase (WP), lignin-forming tobacco peroxidase (TOPA), tomato peroxidase (TMP) and barley peroxidase (BP).[98,101] Peroxidases can use many types of peroxides as electron acceptors to catalyze oxidative reactions.

1.2 Synthetic scope of this review

Diverse applications of Cyt P450s and peroxidases, including biosensors, drug metabolism, synthesis reactions, catalysis, drug interactions and conversion have been reviewed by a number of research groups.[7,31,32,102–108] We address below the use of Cyt P450s and peroxidases for electroorganic synthesis where no additional electron donors are required (see below). We organize the reactions in the text below from a synthetic viewpoint, based on the types of chemistry, *e.g.*, C–H activation, S-oxidation, epoxidation, N-hydroxylation, oxidation of alcohols and oxidative *N*-, and *O*-dealkylation. There are four major goals of this review article,

(1) To provide a comprehensive overview of the status of Cyt P450s and peroxidases in bioelectrocatalysis, including suitability of electrode materials and immobilization methods.

(2) To identify reaction conditions required for high catalytic activity of these enzymes on electrode surfaces.

(3) To review recent bioelectrocatalytic applications of Cyt P450s and peroxidases for oxidative chemistry.

(4) To describe novel approaches used in bioelectrocatalysis with these enzymes.

2. Combining electrochemistry with biocatalysis

2.1 Rationales for electrochemical activation of heme enzymes

As shown in Scheme 2, two electrons are delivered sequentially to the iron heme in the complex Cyt P450 catalytic cycle. The first one reduces Fe(III) to Fe(II) in the heme group, and Fe(II) then reacts and binds with oxygen to yield Fe(III)–O–O$^{\bullet}$. The second electron reduces this species to Fe(III)–O_2, which eventually leads to the Fe(IV)=O species that oxidize the reactant RH (Scheme 2).[109] Cyt P450s are capable of oxidation or hydroxylation of non-activated carbon atoms, *i.e.*, oxidation of C–H bonds. The use of NADPH as an electron source and cytochrome P450 reductases (CRP) as in the natural catalytic cycle (Scheme 2) can serve as an multifaceted biocatalytic system with significant industrial potential, but also carries practical issues that need to be solved.[102,110–112] On one hand, the complex electron transfer mechanism of Cyt P450s in solution requires the use of expensive reductants such as NADH or NADPH. The monotonic eukaryotic Cyt P450 reductases, and bacterial redox partner system are more distinct but a bit complicated to apply to solution-based syntheses.[20,113,114] On the other hand, although being difficult to handle, CRP that is necessary to the direct electron transfer with Cyt P450s presents in commercially available Cyt P450 preparations known as microsomes (or baculosomes) and supersomes. The latter constructs feature specific single Cyt P450's (*e.g.*, CYP3A4) and include CRP in a predominantly lipid matrix. Microsomes are derived from specific organs and contain a collection of Cyt P450s, CPR, and other proteins in a lipid matrix. Cyt P450s catalyze regio- and stereo-selective activation of C–H bonds in organic reactants under optimal conditions.[78,115] This makes them suitable as biocatalysts for the synthesis of pharmaceuticals and other fine chemicals where control of stereochemistry is absolutely important and necessary.

There have been extensive efforts to overcome the limitations of Cyt P450s in the past.[116,117] Among those, electrochemical activation can improve performance of Cyt P450s without the use of additional chemicals. Replacement of biological electron transfers by electrochemical processes where electrons are

transferred directly between electrodes and enzymes, or enzymatic systems offers a promising approach to more feasible, cost-effective, and simplified pathways. The driving force for enzyme-based reactions can be regulated by the potential applied on the working electrode in the electrochemical cell under control of the user.[118] Immobilization of enzymes on working electrodes is an important tool to produce or generate the drug metabolites and other products with high yield and high selectivity for a fast toxicity screening.[116,119–127] Electrochemical techniques can also scale up the generation of metabolites in sufficient amounts for investigation of metabolite or structural characterization. However, activation has often been driven by the H_2O_2 shunt, and not by the accepted biological pathway in Scheme 2.[116] Nonetheless, electrochemical methods have many advantages for production of drug metabolites and other products, including: (i) simple approach; (ii) mild conditions in buffer solutions; (iii) avoid need for NADPH or NADH; and (iv) immobilization of enzymes on electrodes that greatly improves stability, and minimizes the amount of enzyme required.[94,128,129]

Cyclic voltammetry (CV) can be used to examine fundamental features of electrochemical transformations of enzymes. For example the standard heterogeneous electron transfer rate constant k_s for Cyt P450 reductions in thin layer-by-layer (LbL) polyion films (see Scheme 4 and associated discussion) on pyrolytic graphite (PG) electrodes was shown to depend on the heme iron spin state.[130] CVs of bacterial Cyt P450cam and human Cyt P450 2E1 in LbL film at pH 7.0 are shown in Fig. 1. These are background subtracted CVs of poly(ethyleneimine) (PEI)/(poly(sodium 4-styrene sulfonate) (PSS)/P450 2E1)$_4$ and PSS(/PEI/P450cam)$_4$ films on PG electrodes. The peak current was proportional to scan rate as predicted for surface bound species. In anaerobic buffers at pH ~7, human Cyt P450cam with low spin iron gave a 40-fold higher electron transfer rate constant (k_s, 95 s^{-1}) for reduction than the high spin human Cyt P450 1A2 (2.3 s^{-1}).[130] The mixed spin CYP2E1 has an intermediate value of k_s for reduction. In addition, comparison of experimental CVs with digital simulations was consistent with faster oxidation rates of the Fe(II) forms than reduction rates of Fe(III) forms. This suggested that Cyt P450s retain their enzymatic activity on the electrode where an underlying chemical conversion scheme involving oxidized and reduced forms of Cyt P450s underwent rapid conformational equilibria coupled with their electron transfer processes.[130] The rate constant for chemical oxidation of Fe(III)-Cyt P450s in these films by *t*-BuOOH to active Fe(IV)=O Cyt P450s obtained by rotating disk voltammetry (RDV) also showed dependence on spin state. Therefore, those enzymes can maintain native structures and enzyme activities in the LbL films, that is fundamentally important for electrochemical activation of heme enzymes.

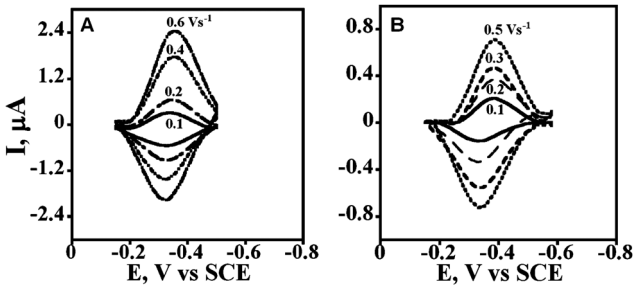

Fig. 1 Background subtracted LbL films of enzymes with polyions on a PG electrode in anaerobic 50 mM phosphate buffer with 0.1 M sodium chloride, pH 7: (A) Cyt P450 2E1/polyion, and (B) Cyt P450cam/polyion. Reproduced from *J. Am. Chem. Soc.*, 2009, **131**, 16215–16224 with permission.[130] Copyright, 2009, ACS Publications.

2.2 Activation of enzymes in electrochemistry

As suggested above, immobilization of Cyt P450s or peroxidases on an electrode surface does not stop their binding of substrates and their further catalysis. Immobilization on electrodes can also stabilize enzymes, minimize the amount of enzymes (*e.g.*, down to nM) needed, and eliminate the use of electron donors. The enzyme co-factors or initial acceptors like CPR can accept electrons directly from the electrode that can act as an electron source for P450s.[28–31] In bioelectrocatalysis, enzymes can mimic their natural pathway for Cyt P450-catalyzed oxidations on electrodes as demonstrated in the thin LbL films made from polyions, and Cyt P450 CPR microsomes containing pure Cyt P450.[131] These stable films consisted of thin layers of the polyions poly(diallyldimethylammonium chloride) (PDDA) and PSS as six alternating layers with CYP2A1 microsomes (containing CPR), denoted as PDDA/PSS(/CYP1A2/CPR)$_6$ films on PG electrodes. Comparing voltammetry with CYP1A2 and CPR films alone showed that electron flow proceeded from the electrode to CPR and then to CYP2A1 in the CYP1A2/CPR films, very similar to the biological pathway in Scheme 2. The background subtracted CVs of the CPR/CYP2A1 films are characteristic of the electrochemical reduction-oxidation reactions (Fig. 2A). The films of CPR/CYP2A1 showed a peak at −230 mV *vs.* normal hydrogen electrode (NHE) and there was no peak potential shift when carbon monoxide was added. The electron transfer rate constant (k_s) was ~40 s^{-1}, similar to films with only CPR or CPR/cytochrome b5 present. Fig. 2B shows that CYP1A2 alone has a peak potential −90 mV *vs.* NHE. There was a ~35 mV shift with addition of CO characteristic for Cyt P450s, and 20-fold smaller k_s values than films with CRP and CYP2A1. Similar results were observed when CYP2E1 was used in the same experiments. Those results support the sequential transfer of electrons from electrode to CPR to Cyt P450s when both are present in the film. Electrons are not directly transferred to Cyt P450, when CPR and Cyt P450s are both present.

Fig. 2C shows CV digital simulations of the model featuring electron transfer first to CPR then to Cyt P450 when both are present in the film. Simulations showed good agreement with experimental CV peak potentials and shapes. The simulation model features electron transfer from CPR to Cyt P450 and electrochemical–chemical–electrochemical (E_rCE_o) pathway (eqn (4)–(6)), where E_o is electrochemical oxidation and E_r is reduction of CPR. Initially, CPR accepts an electron characterized by electrochemical rate constant $k_{s,red}$ (eqn (4)). Eqn (5) represents redox equilibrium between the CPR_{red} and Cyt P450-

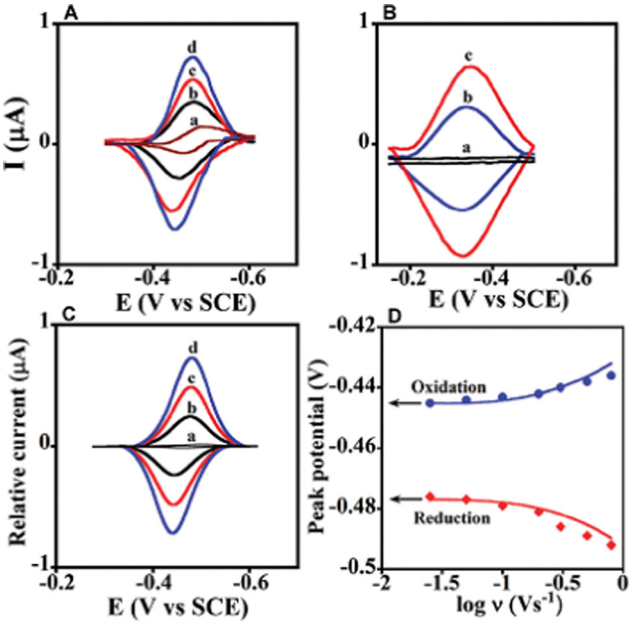

Fig. 2 Experimental and simulated voltammetry of CYP1A2 + CPR microsome films on pyrolytic graphite electrodes. (A) Background subtracted voltammograms of (a) CPR films at 0.3 V s^{-1} without CYP and (b)–(d) with CYP1A2 film with CPR films at (b) 0.1, (c) 0.2, and (d) 0.3 V s^{-1} scan rate. (B) Background-subtracted voltammograms of (a) polyion film and (b) and (c) CYP1A2 film without CPR at (b) 0.1 and (c) 0.2 V s^{-1} scan rate. (C) Digitally simulated theoretical voltammograms related to (a) reversible electron transfer at CPR film at 0.3 V s^{-1} scan rate and (b)–(d) E_rCE_o-model and parameters in Scheme 1 for CYP1A2 and CPR films at (b) 0.1, (c) 0.2, (c) 0.3 V s^{-1} scan rate, demonstrating the excellent agreement with experimental voltammograms in (A). (D) Effect of scan rate on reduction (red diamonds) and oxidation (blue circles) peak potential for CYP1A2/CPR films plotted with theoretical peak potentials (lines) simulated by using the E_rCE_o model. Reproduced from *J. Am. Chem. Soc.*, 2011, **133**, 1459–1465 with permission.[131] Copyright, 2011, American Chemical Society.

Fe^{III} to produce CPR_{ox} and Cyt P450-Fe^{II}, followed by oxidation of CPR_{red} (eqn (6)).

$$CPR_{ox} + e \rightarrow CPR_{red}\ E^\circ = -230\ \text{mV}\ vs.\ \text{NHE};\ k_{s,red} = 0.4\ s^{-1} \quad (4)$$

$$CPR_{red} + \text{P450-Fe}^{III} \rightleftharpoons CPR_{ox} + \text{P450-Fe}^{II}\ k_b \geq 5k_f\ s^{-1} \quad (5)$$

$$CPR_{red} \rightarrow CPR_{ox} + e\ E^\circ = -230\ \text{mV}\ vs.\ \text{NHE};\ k_{s,ox} = 40\ s^{-1} \quad (6)$$

Electrons flowing from electrode to CPR to Cyt P450 was confirmed by observing the catalytic limiting current from RDV for oxidation of 4-(methylnitrosamino)-1-(3-pyridyl)-1-butanone (NNK) to 4-hydroxy-1-(3-pyridyl)-1-butanone (Fig. 3) and by confirming the product formed in this reaction.[131] The Cyt P450 on the electrode surface increased the plateau current with increasing the concentration of NNK (Fig. 3). The increment in the current demonstrated that the oxidation of NNK was catalyzed by Cyt P450/CPR film.

In a related work, the Cyt P450 3A4 supersomes with CPR were immobilized on colloidal Au coated graphene electrode through electrostatic interactions. Electron transfer from electrode

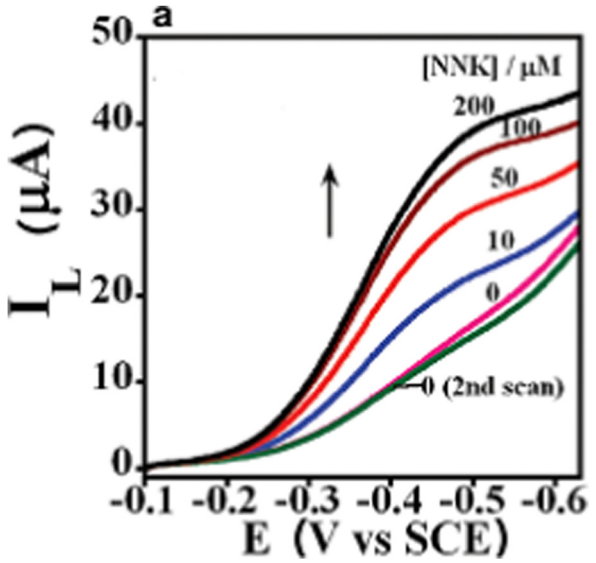

Fig. 3 Rotating disk voltammograms of Cyt P450s/CPR film with increasing the concentration of NNK in pH 7.0 buffer + 0.1 M NaCl at 1000 rpm. Regenerated from *J. Am. Chem. Soc.*, 2011, **133**, 1459–1465 with permission.[131] Copyright, 2011, ACS publications.

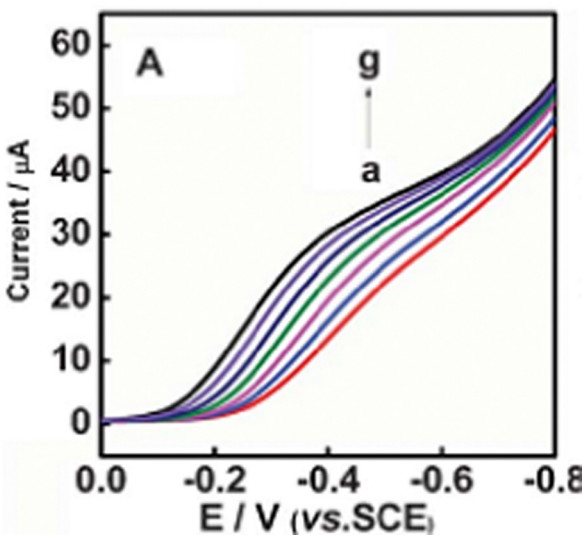

Fig. 4 The RDV (1000 rpm) of CYP3A4/CPR films with increasing the concentration of nifedipine in aerobic 0.1 M phosphate buffer (pH = 7.4) (a) 0, (b) 1.24, (c) 2.48, (d) 3.72, (e) 4.96, (f) 6.2 and (g) 7.44 μM. Regenerated from *RSC Adv.*, 2012, **2**, 12844 with the permission.[127] Copyright, 2012, RSC.

to CPR to CYP3A4 was also observed in this system.[127] The electrochemical catalytic behavior of CYP 3A4/CPR was examined by RDV (1000 rpm) in aerobic pH 7.4 phosphate buffer (0.1 M). The reduction peak current increased with increasing the concentration of nifedipine from 0 to 7.44 μM at −0.5 V (Fig. 4).

As described above, the bioelectrocatalytic pathway in Cyt P450s including CPR on electrode surfaces is the same as the natural human mechanism, featuring the initial electron transfer to microsomal reductase CPR then from CPR to the Cyt P450-heme-iron. We found this to be true as well for both

microsomes and supersomes, already containing CPRs, in LbL films on electrodes.[132,133] While prior work revealed that electrodes can serve as an alternative source of electrons in place of NADPH or NADH for catalysis by Cyt P450s, these systems required peroxide to activate the enzyme for electrocatalytic syntheses oxidation by the H_2O_2 shunt process.[95]

Bioelectrocatalytic activation Cyt P450s supersomes on electrode surfaces in LbL films of DNA has also been developed as a general approach to monitor rates of DNA damage by metabolites.[23–25] The general procedure employs microfluidic arrays featuring individual electrode wells coated with LbL films made with different CYP microsomes, ruthenium polymer $Ru(bpy)_2$-PVP (PVP = polyvinylpyridine) and ds-DNA (ds = double stranded). Reactant flows into the array under an applied oxidation potential that activates the CYP microsomes for oxidation of the reactant to form metabolites that can react with DNA to cause partial ds-DNA unwinding. The relative rates of DNA damage by different Cyt P450s are subsequently detected by electrochemiluminescence (ECL) activated at about +1 V *vs.* SCE and detected with a CDC camera in a dark box.[23–25] Guanines in the partly unraveled DNA act as ECL coreactants that are sensitive to the amount of DNA damage since they are now more accessible to react with the $Ru(bpy)_2$PVP ECL dye. Specific samples of this approach to monitor chemical toxicity are described later in this review.

Additionally, non-natural electrochemical mediators can be used to shuttle electrons to enzymes. For example, Co(II) sepulchrate trichloride can replace NADPH to activate recombinant fusion enzyme rFP450 for the ω-hydroxylation of lauric acid in solution.[134] 1,1′-Dicarboxycobaltocene can replace NADPH to activate $P450_{BM3}$ that catalyzes hydroxylation of lauric acid.[135] Coupling with non-natural electrochemical mediators can extend the practical applicability of electrochemical mediation of electron transfer to P450s as a catalyst for regioselectivity and stereo-selectivity.

3. Challenges in enzyme electrocatalysis and their solutions

Cofactors are nonproteinogenic molecules that are needed for catalytic activity of enzymes which usually bind to enzymes through covalent or electrostatic interactions and are known as prosthetic groups. A broad variety of cofactors are well-known, and may be organic molecules, inorganic ions or metal complexes. In the case of covalent binding, the enzyme is permanently bound to the cofactors. The coenzymes are modified during catalytic reactions by electron transfer or other reactions with the reactant or substrate. Cofactors that are organic molecules are called coenzymes. Regeneration of coenzymes is a key challenge for use in some catalytic reactions.[136] The heme cofactor features a porphyrin ring with a central iron ion. It is found in all known forms of life (bacteria to humans).[137,138] Iron heme is the prosthetic group in hemoproteins such as myoglobin, hemoglobin, peroxidase, cytochromes, catalase, albumin, prion protein, guanylate cyclase and nitric oxide synthase

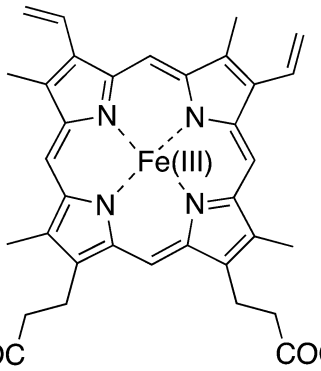

Scheme 3 Iron heme that serves as prosthetic group in Cyt P450s and peroxidases.

(Scheme 3).[139–141] The central iron atom binds the oxygen and transfers it in various forms to small reactant molecules. There are various unbound cofactors used for enzymatic synthesis such as NADH, adenosine triphosphate (ATP), flavin mononucleotide (FMN), and thiamine diphosphate (ThDP).[136] In the Cyt P450 catalytic cycle (Scheme 2), NADH or NADPH transfer electrons in the enzymatic pathways and must be regenerated to continue the catalytic cycle. Regeneration of the co-enzymes can be energetically expensive and may require additional co-substrate or additional enzymes.[142–146] Co-enzymes may also present challenges in terms of availability, and recycling.[147]

Mammalian Cyt P450 enzymes typically accept two electrons originally from reducing agent NADPH that transfers them to flavoprotein NADPH-Cyt P450 oxidoreductase (CPR), the immediate electron donor for Cyt P450s (Scheme 2).[148] However, all reducing agents are not equally effective at donating electrons to Cyt P450s. Hydrogen peroxide or other peroxides may also serve as sources of oxygen for Cyt P450 to catalyze the substrate hydroxylation. CPR can also produce reactive oxygen species (ROS) resulting in NADPH consumption by microsomal P450. These reactive species can cause oxidative damage to enzymes. Thus, it is important to control and minimize generation of reactive oxygen species.[149] This oxidative damage can be controlled by using the more specific electron donor and antioxidants to work alongside Cyt P450 enzymes.[150]

Instability of enzymes can degrade catalytic performance and shorten lifetimes. Numerous factors affect the stability of enzymes, including pH, temperature, and the presence of substrates or inhibitors. Thermostable P450 enzymes can play a significant role in synthesis of the valuable organic compounds. Thermophilic enzymes, such as CYP116B29, CYP116B46, CYP116B64, CYP116B65, CYP119, CYP119A1, CYP119A2, CYP154H1, CYP174A1, CYP175A1, CYP174A1, and CYP231A2 can be used at higher temperature than normal for enzymes.[151–153] The thermal stability of these enzymes makes them attractive for industrial use. For example, a CYP119/sol-gel film remained stable up to 60 °C, but the reduction current decreased to ~45% as compared to that at 30 °C. An enzyme electrode constructed by using LbL films with PDDA and PSS improved thermal stability. CYP119/PDDA/PSS films retained electrochemical activity up to 93% at 80 °C (Fig. 5).[154]

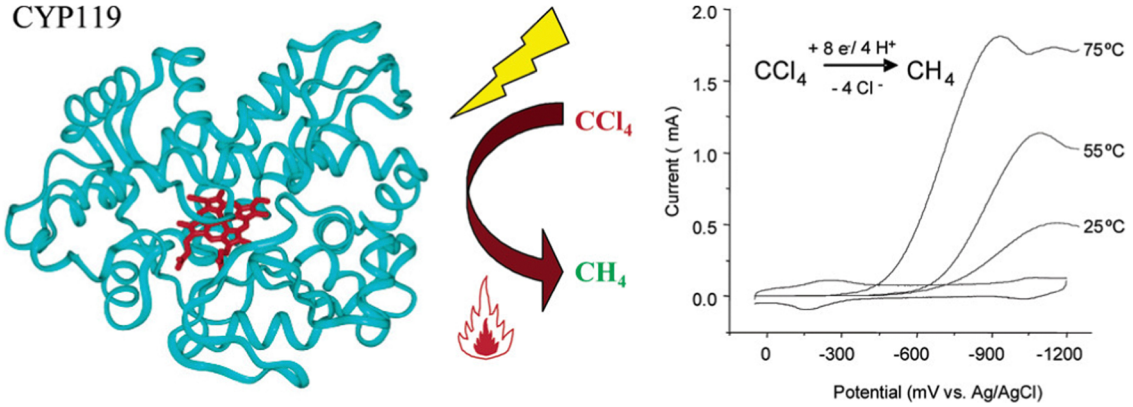

Fig. 5 Catalytic conversion of CCl_4 into CH_4 using CYP119/DDAB/PSS films (left). The effect of temperature on catalytic dehalogenation of CCl_4. Linear sweep voltammograms of CYP119/DDAB/PSS in the presence of CCl_4 at 25 °C, 55 °C, and 75 °C (right). Reproduced from, *J. Am. Chem. Soc.*, 2004, **126**, 8632–8633, with permission.[154] Copyright, 2004, ACS publications.

Higher temperatures can increase the reaction rates significantly, which is of key important for industrial applications. When CYP119 was immobilized in films of dimethyldidodecylammonium bromide and PSS (DDAB/PSS) and used for CCl_4 dehalogenation, the formation rate of methane increased by 35-fold from 25 °C to 55 °C. Other polymers like poly(ethylene oxide) (PEO), when chemically grafted on enzymes, can provide remarkable thermal stability. PEO-modified CYP119A2 was active up to 120 °C in 0.5 M of KCl with a small potential shift of redox potential of ~14 mV between 25 °C and 120 °C.[155] These results show that stability and electrochemical activity of enzymes at temperatures much higher than for the free native enzyme in solution can be improved by making conjugates with suitable polymers as elaborated in more detail below.

3.1 Enzyme film formation and electrode materials

The immobilization of Cyt P450s and peroxidases on electrodes can remarkably improve stability and activity. Immobilization of enzymes can be done by many different methods,[106,112,156–162] *e.g.*, covalently bonding, SAMs, lipid bilayer films, and LbL films. Immobilization often includes the following key steps,

(i) Clean or activate the electrode by mechanical polishing or electrochemical potential cycling. For some films, roughening the electrodes and introducing surface charges chemically can be advantageous for film stability.[163]

(ii) Functionalize electrode surfaces with enzymes *via* drop casting, self-assembled monolayers (SAMs), incorporation into detergent or lipid films, LbL film growth, or chemical attachment.[106,112,164–166]

(iii) Age electrodes at 4 °C in a constant humidity chamber to avoid complete dehydration and remove weakly adsorbed enzymes from the surface by washing.[167–169]

3.1.1 Covalent immobilization of enzymes. Covalent immobilization of enzymes can be used to immobilize the enzyme on the electrode surface. Functionalizations used in attachment of the enzyme include amidization by $-NH_2$ and –COOH coupling catalyzed by *N*-((3-dimethylamino)propyl)-*N*-ethyl carbodiimide hydrochloride (EDC)-*N*-hydroxysulfosuccinimide (NHSS), and thiol–ene click chemistry using cystine (see Table 1). Bioconjugation chemistry using EDC-NHSS cross-linking can immobilize enzymes on electrode surfaces. NHSS is an effective way to stabilize the reaction intermediate and improve coupling reactions with primary amines. NH_2 and COOH groups can be added onto electrodes through surface ligand chemistry (*e.g.*, metal–thiolate coordination on an Au electrode) or physically adsorbed with polyions (*e.g.*, oxidized carbon bound with positively charged polyamines). Surface NH_2 or COOH can now react with enzymes through EDC-NHSS amidization.[170–172] Afterwards, chemically bound enzymes can be partially dried in a constant humidity chamber.[170,173–176] Using human CYPs 3A4, 2D6 and 2C9 in an electrochemical array, Gilardi *et al.* investigated how immobilization would impact the binding affinity (with Michaelis constant K_M as an indicator) of substrates in a high throughput microtiter-based platform.[173] Cyt P450s were immobilized on hydroxyoctanethiol and 10-carboxydecanethiol (1 : 1) self-assembled monolayer (SAM) on a gold (Au) electrode. EDC-NHSS coupled carboxylic groups in the SAM film with amides on Cyt P450s. Michaelis–Menten analysis was done using the current measured at −390 mV with 30 known drugs. K_M values were slightly better or on par with those measured for Cyt P450 microsomes in solution. Also, nanomaterials coupled with enzymes can improve their electrochemical activation. For example, CYP2B6 on a glassy carbon electrode modified with ZrO_2 nanoparticles and platinum-PLL (Pt-PLL) showed reversible electron transfer between heme iron of CYP2B6 and electrode at −0.449 V at pH 7.4 in anaerobic solution.[177] K_M was lowered by two orders of magnitude as compared to CYP3A4 in microsomes.

3.1.2 Incorporation of enzymes through non-covalent interactions. Physisorption has been used frequently to prepare enzyme-coated electrodes due to its simplicity. The enzyme is physically adsorbed on the electrode surface. Adsorption occurs *via* non-covalent forces including electrostatic interaction, van der Waals, hydrophobic interaction, and hydrogen bonding.[178] Although the activity of the enzyme is largely retained as compared to covalently grafted enzymes, the loosely bound enzymes can desorb under reaction conditions, and must be avoided. A comparison of immobilization methods is summarized in Table 1.

Table 1 Immobilization techniques to prepare enzymatic electrodes

Method	Enzyme	Crosslinker and mixture	Incubation time	Electrode	Enzyme activity	Stability	Enzyme leakage	Ref.
Covalent binding	Formate dehydrogenase	EDC and NHS	30 min for enzymes, and 90 min for EDC/NHS	(i) 4-ATP SAMs; (ii) 4-nitrophenyl electrochemically grafted on Au electrode	Low	High	No	188
	P450 BM3	Dendritic mesoporous silica with –OH and $–NH_2$	12 h	CS/GCE				189
	CYP101	*N*-(4-Caboxyphenyl) maleimide and SWCNT	30 min at 4 °C	GCE				190
	P450 BM3	(i) Cystamine-*N*-succinimidyl 3-maleimidopropionate; (ii) dithio-bismaleimidoethane	1 h at 4 °C	Au(111) surfaces				191
	CYP 2B4	EDC/NHS	90 min at R.T.	Carbon and Au SPE				170
	P450 2E1, cysteine mutant MUT261 or MUT268	Dithio-bismaleimidoethane (DTME)	2 h for DTME	Au				124
Physical adsorption	P450 BM3	—	30 min, at 4 °C	ITO	Moderate	Low	Yes	192
	P450 3A4	—	12 h, at 4 °C	DDAB/SPE or MWCNT/SPE				193
	P450 3A4, 2B4, 1A2, 11A1 (P450scc), and 51b1	—	12 h, at 4 °C, Humid chamber	Au nanoparticles-DDAB/PG				157
	CYP2B6	Au-chitosan mixed with CYP2B6	12 h at 4 °C	GCE				158
	CYP2C9	ITO and CS mixed with enzyme	—	GCE				194
	Mb, HRP or hemin	Mb, HRP or hemin mixed with DDAB	Covered with vial and dry overnight (~12 h)	PG				181
LbL films	CYP1A2	PLL or poly-L-ornithine	15 min for polyelectrolyte, 30 min for CYP1A2	Quartz crystal	Moderate	High	No	184
	CYP1A2	PDDA/PSS	—	PG				131
	P4502E1, P450cam, P450 1A2, catalase and Mb	PEI/PSS	—	PG				130
	Mb and P450cam	PEI, PDDA and PSS	15 min for polyions	Au				187
	NADPH-cytochrome P450reductase	PDDA and PSS	20 min for polyions and 1 h for enzymes	PG				195
	CYP3A4	PDDA		GCE				125

Films of insoluble surfactants can accommodate a wide variety of enzymes and heme proteins and have enabled reversible electrochemical reduction of Fe^{III}heme cofactors. These detergent-protein films are made by mixing dispersions of water, insoluble surfactant, and protein, drop casting them on the electrode, and drying before use. They feature multiple layers of bilayers formed with insoluble double chain surfactants such as didodecyldimethylammonium bromide (DDAB) and phospholipids, with the proteins residing between the detergent bilayers. These interlayer regions also contain considerable amounts of water that is available to hydrate the enzymes.[179–181] Direct immobilization of Cyt P450s has been achieved in electrode-supported lipid bilayer membranes, similar to those developed for hydrophobic membrane enzymes.[182,183] For example, CYP2C9, and its polymorphic modification CYP2C9*2 and CYP2C9*3 could be immobilized on DDAB modified screen printed electrodes (SPE).[156] Well-defined reduction and oxidation peaks of the Fe^{III}heme were obtained in CVs. The midpoint potential (E_{mid}) for CYP2C9, CYP2C9*2 and CYP2C9*3 were observed −0.318, −0.324 and −0.318 V *vs.* Ag/AgCl, respectively. In aerobic conditions, the reduction potential of CYP2C9*2 and CYP2C9*3 shifted towards the positive potential in comparison to CYP2C9 with ~50 mV *vs.* Ag/AgCl. The shift in the potential demonstrated easier electron transfer to the heme iron in CYP2C9*2 and CYP2C9*3. Immobilized CYP2C9, CYP2C9*2 and CYP2C9*3 were all active for bioelectrocatalytic 4-hydroxylation of diclofenac in the presence of antioxidants mexidol or taurine at −0.55 V. In comparison with the microsomal systems, the Michaelis constants (K_M) of those three forms of CYP2C9 increased by 10–20 times, suggesting that best structural conformation of CYP2C9 may vary to slightly limit the substrate binding on the electrode.

LbL films first developed by Lvov and Decher have been used to grow stable enzyme films on electrode surfaces.[131,184–186] In this method, also mentioned previously, multiple layers of polyions or nanoparticles are assembled by adsorbing one layer at a time with alternate layers of oppositely charged enzymes, microsomes or supersomes (Scheme 4). These thin films are

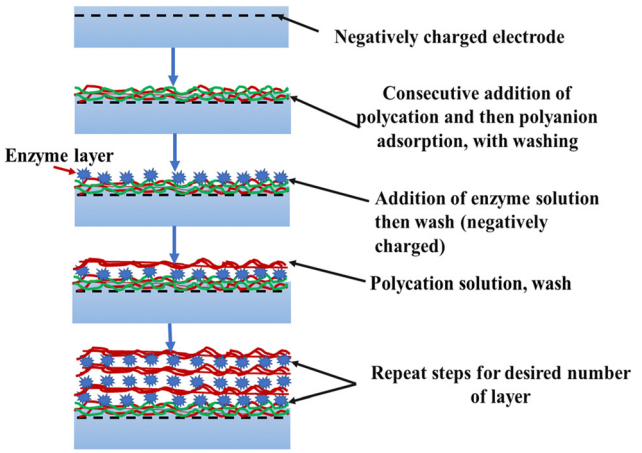

Scheme 4 Illustration of layer-by-layer (LbL) film formation of enzymes and polyions.

strongly absorbed onto the electrode surface, usually by placing single drops of each adsorbate solution on the electrode for 15–20 min. Weakly adsorbed species are washed off the electrode after each adsorption–equilibration step and dried in a stream of nitrogen before application of the next layer.

LbL methods provide high stability to the enzyme film without desorption. Forces between layers are primarily electrostatic in nature, but may include hydrophobic interactions, coordination, hydrogen bonding, or even covalent bonding.[165,185,186] The enzyme attached to the electrode surface through the consecutive addition of negatively or positively charged polyions or layer of the enzymes for example, polyions of PDDA, PSS, PEI, *etc.* (see Table 1), all of which provide multiple electrostatic attraction sites of bound enzymes to strongly hold them on electrodes. Lvov working in our group reported the first LbL film direct voltammetry of enzymes and redox proteins.[187] Myoglobin (Mb) and bacterial Cyt P450cam were used in LbL films with DNA and polyions on an Au electrode coated with chemisorbed mecaptopropanesulfonic acid to provide stable, electroactive multi-layered films. Mb films were made by successive adsorption of PSS, DNA or PDDA. The Cyt P450cam film was grown with layers of PSS or PDDA. LbL films of Cyt P450s using microsomes or supersomes can be assembled on electrodes similarly, as discussed above (see Table 1.)[131]

3.2 Cells and electrode materials

Electrochemical cells and electrodes sizes used in synthesis need to be significantly different from those used for techniques such as voltammetry. In voltammetry, working electrodes are typically disks of 10 μm to several mm in diameter, and counter electrodes are typically a Pt wire. However, in constant potential electrolysis, the goal is to make a measurable amount of product, and

$$\text{The rate of electrolysis} = (\text{const}) \times e^{-k_{elect}t} \quad (7)$$

where k_{elect} is the synthetic rate constant and t is the reaction time. The reaction rate decreases exponentially with t as the decrease of the reactant concentration. The synthetic rate constant $k_{elect} = m_0\frac{A}{V}$, where m_0 is mass transfer coefficient, A is the electrode area, and V is the solution volume, respectively.[196]

The mass transfer coefficient m_0 is calculated as $\frac{D_0}{\delta_0}$, where δ_0 is the Nernst diffusion layer thickness and D_0 is the diffusion coefficient. More efficient stirring gives a smaller δ_0, leading to faster mass transfer and synthetic rate. The concentration of the reactant at any given reaction time is $C(t)$,

$$C(t) = C_O e^{-m_0\frac{A}{V}t}; \quad (8)$$

where C_O is the initial reactant concentration, and the current I_t at an any given reaction time is given by

$$I_t = I_O e^{-m_0\frac{A}{V}t} \quad (9)$$

Thus, to obtain good synthetic yields in a high kinetics, the synthetic rate constant should be maximized by using a large electrode area to solution volume ratio (A/V), and ensuring efficient mass transport. If a large working electrode is used, a similar sized counter electrode should be used to keep current density on both electrodes similar. Symmetric placement of working and counter electrodes with the reference electrode tip close to the working electrode also helps to keep the potential constant across the entire working electrode.

The current I of the bioelectrocatalytic reaction can be measured during synthetic reaction to obtain current efficiency, which is the fraction of charge Q being used to produce the desired product. where

$$Q_t = \int_0^t I\,dt \quad (10)$$

Current efficiency = Q_r/Q_t. Here, Q_r is the charge needed to produce the amount of product formed obtained from Faraday's law.[196]

Binding of the enzymes on the working electrode depends to a certain extent on the electrode material and surface pretreatments. Several electrode materials including glassy carbon (GC), PG, graphitic carbon, carbon felt, carbon cloth, indium tin oxide (ITO), platinum, gold, reticulated carbon, and screen-printed carbon (SPE) have been used to immobilize enzymes.[123,157,159,170,197–201] Au is often used for immobilization in smaller scale projects because it can covalently bind with sulfide groups (*e.g.*, thiol, disulfides, thiolate, and thioesters), with the resulting Au–S–R leading to versatility in the structure of R. For example, R could be a charged group to electrostatically bind to an oppositely charged enzyme, or a reactive group that can be chemically coupled to an enzyme. However, Au and Pt are probably too expensive for industrial scale electrosynthesis. Among the many types of carbons, rough PG is particularly useful for film formation since it is high energy surface capable of adsorbing many different types of polyions. Polished glassy carbon has low surface energy and is not particularly good for film formation. High surface area materials such as carbon felt, carbon cloth and reticulated carbon are also advantageous due to the requirement for high A/V ratios (eqn (8)).

The biocatalytic activity of the electrode can sometimes be improved by using nanomaterials such as metal nanoparticles, conducting polymers, carbon nanomaterials, and thiolate compounds for protein-electrode attachment. When oxidized, these materials can provide functional groups to effectively interact with enzymes and shuttle electrons. The efficiency of the electrochemical synthesis can be improved by using nanostructured surface modifiers on the electrode.[157,159,198–201] For example, multi-walled carbon nanotubes (MWCNTs) and DDAB on screen printed carbon electrodes (SPE) were compared for electrocatalysis with CYP3A4.[193] For catalytic oxygen reduction, the cathodic current increased up to 3-times with CYP3A4/SWCNT/SPE in comparison to CYP3A4/DDAB/SPE. Additionally, CYP3A4 and gold nanoparticles (AuNPs) stabilized by DDAB films on SPE were used to investigate the effect of the B Vitamins (B1, B2, and B6) on the hydroxylation of diclofenac.[202] Similarly, Cyt P450/carbon nanofiber (CNF) films were used on electrodes without a mediator layer and direct electron transfer between CNF and CYP3A4 was observed at −0.30 V *vs.* Ag/AgCl.[199] High catalytic activity for oxygen reduction was found at CYP3A4/CNF compared to other carbon electrode nanomaterials like carbon black. Thus, catalytic activity of the enzyme electrode can often be improved by using optimal nanomaterials.

3.3 Activation of Cyt P450s

The heme reactive center of Cyt P450s is activated for biocatalytic reactions through the electron transfer in the presence of oxygen (see Scheme 2). In electrochemical reactions, electrons are transferred from electrodes instead of the natural electron donors NADPH or NADP.[203] Direct electron transfer from electrode to the heme iron was reported for electrocatalysis using Cyt P450 as discussed previously.[204] The reversible CV peaks for $Fe^{III/II}$ should be examined prior to any electrochemical catalysis. For example, CYP2C18 immobilized in an insoluble DDAB surfactant film on edge plane pyrolytic graphite (EPG) gave reversible CV peaks for $Fe^{III/II}$. Fig. 6 demonstrates the reversible

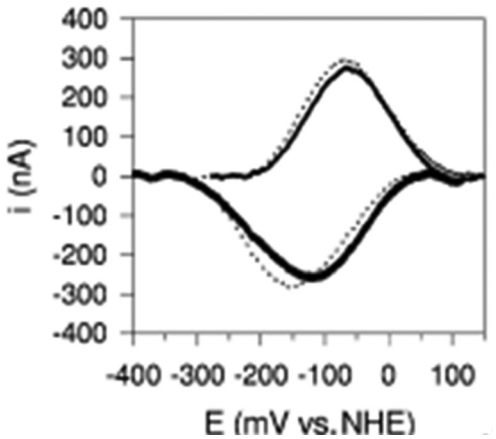

Fig. 6 Background subtracted CVs of CYP2C18 in presence (solid curve) and absence (broken curve) of 150 mM phenytoin at 100 mV s^{-1} scan rate (pH 8.0) showing reduction in upward direction. Reproduced from *Electrochem. Commun.*, 2005, **7**, 437–442 with permission.[205] Copyright, 2005, Elsevier.

Fe(III) → Fe(II) redox couple (anodic peak current (i_{pa})/cathodic peak current (i_{pc}) ~ 1) of CYP2C18. In the presence of trace amounts of dioxygen, well-defined cathodic peaks with a slightly positive shift could be seen and were assigned to catalytic reduction to yield ferrous P450.[205]

Electrocatalysis using Cyt P450s can be assessed using oxygen reduction. CYP27B1 immobilized on an EPG electrode in a DDAB film gave a significant increase in the cathodic current in the presence of oxygen due to electrocatalytic reduction of dioxygen to peroxide.[206] The catalytic oxygen reduction current showed a significant increase along with the positive shift of potential when CYP101 was embedded in DDAB films, as compared to pure DDAB films. As mentioned in Section 3, LBL films of microsomes[207] or supersomes can be electrochemically activated as the natural catalytic cycle involving electron donation first from electrode to CPR, then from CPR to Cyt P450s. Bioelectrochemical oxidation with heme enzymes features specificity and regioselectivity, but, electrochemical oxidation, in the absence of enzymes does not provide this advantage. Direct comparisons of electrochemical and bioelectrochemical reactions are summarized in Table 2. For example, electrochemical oxidation of diclofenac catalyzed by CNT and/or metal nanoparticles (Pt and Ru) shows more than one product (Table 2), while bioelectrocatalysis with CYP3A4 and CYP2C9 is highly regioselective and gives 4-hydroxydiclofenac as the only product. Likewise, the enzymatic electrooxidation of styrene, benzo[*o*]pyrene, and tramadol shows similar trends. With enzymes, the regioselective product is obtained; while, in the absence of enzymes, often more than one product are generated in electrooxidation. Therefore, bioelectrocatalysis provides high selectivity, reduces the electrolysis time, lowers electric energy input, and often produces targeted molecules with no isolation from side-products (see Table 2).

Orientation of enzymes on the electrode surface may play a significant role in maintaining its activity. Enzymes covalently immobilized on electrodes in a single layer may be limited in terms of mobility and configurational dynamics by their orientation. The electron transfer efficiency between electroactive site and the electrode is controlled by the distance between the electrode and enzyme electroactive site. However, it is important to realize that orientation issues will be important mainly in cases where the enzyme has little or no mobility after immobilization, such as in covalent attachment to a solid electrode. In some films, enzymes retain significant mobility to make orientation a non-issue, such as in liquid crystal surfactant films, LbL polyion films, and hydrogel polymer films. In all of these films, enzymes are present in more than a monolayer and electrons transfer occurs predominantly by an electron hopping mechanism involving a reduced enzyme-oxidized enzyme reaction progressing through the film.[208]

Although mediated electron transfer using a molecular redox mediator is possible, direct electron transfer at the enzyme-electrode interface is more efficient with fewer steps and more efficient enzymatic activation process. Therefore, the configuration of heme enzymes in a monolayer, for example, needs to be orientated to minimize the distance between the heme center and electrode (within 14 Å) as a so-called "electroactive"

Table 2 Electrochemical and bioelectrochemical reaction comparison

Electrochemical method						Bioelectrochemical method					
Electrode	Potential, electrolysis time	Substrate	Product (s)	Product identification methods	Ref.	Electrode	Electrolysis time	Substrate	Product (s)	Product identification methods	Ref.
CNT, Pt/CNT and Ru/CNT	1.5 V *vs.* SCE, 8 h	Diclofenac	Formic acid, acetic acid, oxalic acid, oxamic acid, maleic acid, malonic acid, piruvic acid, glioxilic acid, fumaric acid, glicolic acid, succinic acid, butiric acid, tartronic acid	HPLC-MS, ESI-MS, ESI-MS/MS	223	CYP 3A4 + CPR, CYP 2C9 + CPR	−0.6 V *vs.* Ag/AgCl, 45 min	Diclofenac	4-Hydroxydiclofenac	HPLC, MS	224
GF-CoS_2/CoS	4.6–5.1 V, 4 h	Styrene	Benzaldehyde, styrene oxide, dibromide, β-bromostyrene,	GC-MS, ^{1}H-NMR	225	PSS-(CYP1A2-PSS)$_2$	−0.6 V *vs.* SCE, 1 h	Styrene	Styrene epoxide, benzaldehyde	GC	226
Pt electrode, 0.1 M tetra-ethylammonium perchlorate	+1.3 V	Benzo[*a*]-pyrene	6-Acetoxybenzo[*a*]pyrene, and mixture of benzo[*a*]pyrene-quinones	Fluorescence, and absorption spectroscopy	227	CYP1A1/PBA-NGO/GCE	−0.48 V *vs.* SCE, 5 h	Benzo-[*a*]pyrene	Benzo[*a*]pyrene-7,8-diol	HPLC, GC-MS	228
Boron-doped diamond and Pt	10–30 mA, *vs.* Ag/AgCl, 1 h	Tramadol	*N*-Desmethyl- and *O*-desmethyltramadol as well as tramadol-*N*-oxide	LC-MS, NMR	229	CYP2D6/PEI-RGO/GC	−0.52 V *vs.* SCE, 2 h	Tramadol	*O*-Dimethyl-tramadol	HPLC-MS, MS	230

configuration.[209–211] HRP, for example, has a molecular radius of 30 Å[212] that would block the direct electron transfer, since the heme sites buried in the protein frameworks may be too far away from the electrode. Previous literature suggested that the selectivity and stability of enzymes can also be controlled by varying the orientation of enzymes on the electrode surface.[213] Although the orientation of enzymes can be significantly impacted by film formation condition, *e.g.*, pH and ionic strength, there are several methods to control the orientation of enzymes on electrodes, including anchor chain molecular system,[214–216] site-specific attachment,[217] and antibody-based immobilization.[218–222]

Covalent attachment onto a specific site of enzymes may provide some degrees of control over the orientation of enzymes on the surface of electrode.[213,231] The common strategy is to use the cysteine-based selective surface attachment, including cysteine-electrode binding[232] (or metal–thiolate coordination) and thiol–ene click reaction.[124,233] For example, CYP2E1 wild-type and cysteine mutants (MUT261 and MUT268) can be covalently immobilized on an Au electrode using the cross-linking chemistry of dithiobismaleimidoethane (DTME).[124] DTME is a maleimide crosslinker for cysteines. This covalent linkage enables the binding of MUT261 and MUT268 in a way that orientation of the proximal electron transfer side of the heme is close to the electrode; while, the distal substrate-binding side is oriented towards the bulk solution for easy access of the substrate. Efficient electron transfer between heme and electrode can be achieved where MUT261 and MUT268 produced ~2.5 and 2.0 times more products compared to that of wild-type CYP2E1. The site-specific attachment at residues 261 and 268 on proximal side of cysteine mutants are more efficient for electrocatalysis.

Site-specific modification on enzymes that can provide the oriented enzyme-electrode interaction is of increasing interest. Adding a short electrode-binding peptide at a specific terminal of enzymes can guide the binding direction of enzymes to the electrode and avoid the non-specifical orientation of enzymes.[209] This method can provide the oriented immobilization of Cyt P450s.[234] P450 BM3 C-terminally high specific peptide (HSP), as an example can be immobilized on an ITO electrode binding peptide (HSP) made of sequence $(RTRHK)_4$. HSP has a profound effect on the protein orientation thus the electron transfer rate. P450 BM3 without HSP were highly active for de-ethylation of 7-ethoxycoumarin (7-EC) in solution (Fig. 7). When immobilized on the ITO, the orientation of enzymes induced by HSP improved the activity of P450 BM3 in either NADPH-mediated or direct electron transfer pathways. In case of direct electron transfer, P450 BM3 with HSP on ITO under a fixed orientation enhanced the activity of the enzymes up to 10-fold in comparison to that without no HSP (Fig. 7b–d), because random orientation of enzymes limited active center available for electron transfer.

With polyelectrolytes, LbL films can provide a partitioned microenvironment that is hydrated and conductive to allow fast diffusion of ions and substrates as discussed in Section 3.1. LbL films of bacteriorhodopsin with polycations had a high degree of orientation.[235] Bacteriorhodopsin could be oriented by electrostatically adsorption from solution onto an electrode. The nonlinear optical coefficient from the second harmonic generation

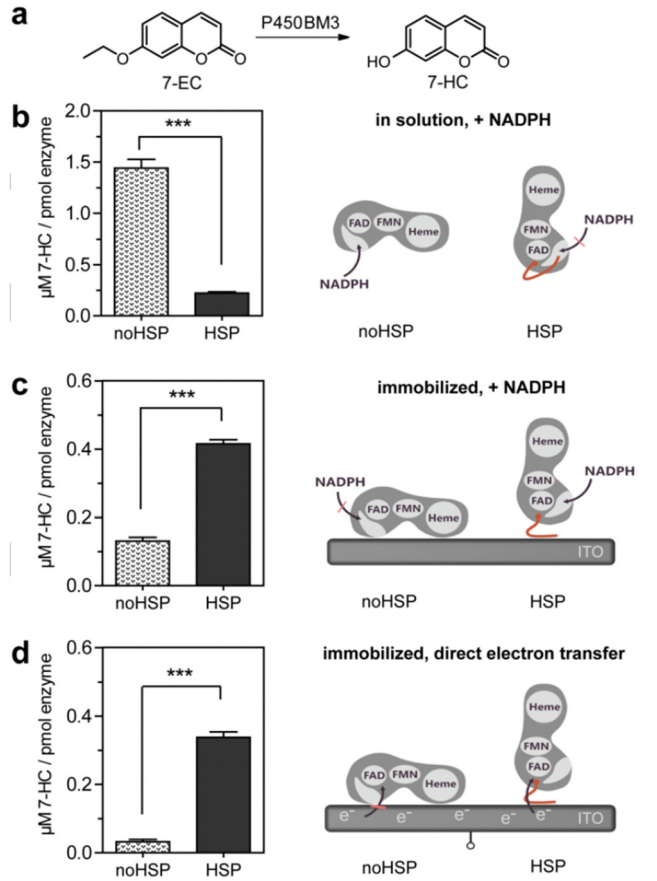

Fig. 7 7-Ethoxycoumarin (7-EC) activity assay on P450 BM3 specifically (HSP) and P450 BM3 unspecific (noHSP) immobilization, (a) dealkylation of 7- EC to 7-hydroxycoumarin (7-HC) by P450 BM3 mutant (A74G, F87V, L188Q). (b–d): Activity assay of noHSP and HSP on the production of 7-HC/pmol enzyme. (b) Set-up I: in solution, NADPH added. (c) Set-up II: immobilized P450 BM3 variants on ITO, NADPH added. (d) Set-up III: immobilized P450 BM3 variants on ITO, electric potential of −0.6 V applied. Reproduced from, *ChemCatChem*, **2018**, 10, 525–530, with permission.[234] Copyrights, 2018, Wiley.

suggested that the second-order susceptibility of the LbL film was greater than that of an electric-field-oriented film. However, this is a special case, and enzymes in LbL films must rely on electron hopping mechanisms involving enzyme throughout the film as described above for thicker films but starting with electron transfer between electrode and the nearest enzyme to the electrode layer. All enzymes in the film may not be accessible for these reactions; in some cases, they may be too far away or improperly oriented from their neighbors. For example, in the LbL films of anionic glucose oxidase with anionic poly(allylamine) modified by ferrocene (PAA-Fc) on an Au electrode, a good fraction of glucose oxidase (~40%) was inactive.[236] To resolve this issue in LbL films, biocatalytic activity has been improved by the use of conductive nanomaterials, as discussed in Section 3.2. The formation of electrically conductive nanomaterial networks and the use of conductive polymers in LBL films[237] can "wire" the electron transfer throughout the film. For example, 4 nm underlayers of conductive sulfonated polyaniline (SPAN) on rough PG were coated with LBL films of polyions and proteins HRP or Mb. With a SPAN underlayer present, >90% of protein electron transfer was coupled to the electrode, but only 40% of enzymatic electroactivity was found without SPAN.[237] This allows utilization of nearly all the enzymes in the LbL film. In this way, the heterogeneous electron transfer rate constant (k_s as discussed in Section 2.1) and the catalytic efficiency of enzymes (k_{cat}, see Table 3) in these films can reach much higher values. However, these more complex approaches are not always necessary, since 40–50% of enzymes as active in LBL films are often sufficient for good catalytic performance in synthetic applications.

4. Reaction conditions: solvent and beyond

Water is needed to hydrate enzymes and it is a major component in bioelectrocatalytic systems. Other components in the fluid may significantly influence the stability of the intermediates, reaction selectivity and yields of products.[162] Supporting electrolyte in the solvents provides conductivity; however, it does much more than that. In general, any salts that dissociate to their ionic forms can work as a supporting electrolyte. The more frequently used supporting electrolytes contain cations including's K^+, Na^+, Li^+, or H^+ and anions ClO_4^-, Cl^-, NO_3^-, HPO_4^{2-} or SO_4^{2-}. The concentration of electrolytes is usually in the range of 0.1 to 1 M and they should be electrochemically inactive.[133] Tuning the supporting electrolyte is important for maximizing the performance of biocatalysts. Specific ion effects are ions interacting specifically with enzymes, and should be avoided.[133] While a higher concentration of electrolyte provides better conductivity, it may enhance background signals.

The use of organic solvents is sometimes needed because the solubility of substrates is limited in aqueous solution. However, enzyme stability issues typically rule out more than 10–20% of organic solvent in water; and at even these levels, organic solvents can denature enzymes by disrupting their internal hydrophobic interactions. Thus, organic solvents can be detrimental to the activity of enzymes. Easterbrook *et al.* demonstrated the influence of dimethyl sulfoxide (DMSO), acetonitrile and methanol (MeOH) in human hepatocytes on activities of Cyt P450s where organic solvents were present in water at of 0.1, 1 and 2% (v/v).[238] DMSO showed the highest enzyme inhibitory effects for several Cyt P450s and activity retentions were approximately 40% (CYP2C9), 23% (CYP2C19), and 11% (CYP2E1) compared to those observed for 0.1% acetonitrile. MeOH showed a solvent-dependent drop of activity of CYP2E1 and CYP2C9, but it had less impact on other Cyt P450s, while acetonitrile in the range of 0.1–2 vol% had no observable effect on Cyt P450 activities.

Electron paramagnetic resonance (EPR) spectroscopy and Soret band optical absorbance suggested that the exposure of the organic solvents decreased the local polarity in enzyme active sites and shifted the Soret absorption band of the Fe^{III}heme center.[239,240] The Soret band of horseradish peroxidase (HRP) in pH 7 buffer is 403 nm, but different microenvironments show a shift in the Soret absorption and intensity.[241]

Table 3 Electrochemical transformations catalyzed by CYPs

Electrode	Substrate	Product	Product identification methods	K_M	k_{cat}	Ref.
CYP1A1/PBA-NGO/GCE	Benzo[*a*]pyrene	Benzo[*a*]pyrene-7,8-diol	HPLC, GC/MS	26 μM	1.9 s^{-1}	228
CYP2C9, CYP2C9*1, CYP2C9*2/4-aminothiophenol/Au electrode	Tolbutamide	4-Hydroxytolbutamide	HPLC	275 μM, 245 μM, and 722 μM	4.5 min^{-1}, 2.3 min^{-1}, and 1.9 min^{-1}	274
CYP101/pyrene maleimide/GCE	Camphor	5-*exo*-Hydroxycamphor	Electrospray ionization mass spectrometry (ESI-MS)	—	—	275
CYP101/N-(4-carboxyphenyl) maleimide(p-CPMI) SWCNT/CGE	Camphor	5-*exo*-Hydroxycamphor	ESI-MS	—	—	190
CYP2C9/ITO/CS/GCE	Tolbutamide	4-Hydroxytolbutamide	HPLC, MS	203 μM	—	194
CYP2C9/AuNPs/TiO_2 NTA	Tolbutamide	4-Hydroxytolbutamide	HPLC, MS	4.8 μM	9.89 s^{-1}	176
CYP1A2 and CYP3A4/AuNP/CS/RGO	Clopidogrel	2-oxo-clopidogrel by CYP1A2, and clopidogrel carboxylic acid by CYP3A4	LC-MS/MS	10.82 μM	2.42 s^{-1}	122
CYP2C19/CS-ceria-graphene	Omeprazole	5-Hydroxyomeprazole	LC-MS, ESI-MS	8.22 μM	5.72 s^{-1}	276
CYP2C9/DDAB/GCE	S-warfarin	7-Hydroxywarfarin	HPLC	—	4.28 min^{-1}	277
Cyt P450 Vdh	Vitamin D3	25-Hydroxyvitamin D_3	HPLC	—	—	278
HLMs/PDA/Au@RGO	Testosterone	6β-OH-testosterone	HPLC-MS	175 μM	8.9 s^{-1}	279
CYP2D6-CPR-PEI-RGO/GCE	Tramadol	*O*-Dimethyl-tramadol	HPLC-MS	23.9 μM	0.47 s^{-1}	230
CYP2D6/AuNPs-CS-RGO and CYP1A1/PAA-AuNPs-CS-RGO	Tramadol	*O*-Dimethyl tramadol	LC-MS, GC-MS	—	—	280
PSS-$(CYP1A2\text{-}PSS)_2$	Styrene	Styrene oxide	GC	—	—	226
PGE/MWCNT/HLM and PGE/MWCNT	Testosterone	6β-OH-testosterone	HPLC	290 ± 33 μM for PGE/MWCNT/HLM and 480 ± 51 μM PGE/HLM	—	281

The dissociation of Fe^{III}heme from enzymes leads to a blue shift to 398 nm. With organic solvents, the Soret band can increase in the intensity without shifting λ_{max}.[239] For example, in H_2O/dioxane and H_2O/methanol mixtures, an enhanced Soret absorbance at 403 nm was seen without a shift of λ_{max}.[239] However, in H_2O/acetonitrile, a peak broadening was found in the range 370–425 nm. The native g values of EPR spectra of HRP in aqueous buffer (pH 7), are observed near $g = 6$ and $g = 2$ because of high spin ferric heme iron, with a rhombic splitting near $g = 6$.[242] There was no change observed in the spectrum in 80% v/v dioxane, while with further increasing dioxane, the EPR spectrum broadened, suggesting the reduced spin-label flexibility. Note that extremely high amounts of organic solvents (*e.g.*, 90% v/v acetonitrile, 95% v/v dioxane and 2% ethyl acetate and 1% v/v aqueous buffer) will directly change the enzyme structure and activity.

Hammett analysis was applied to examine the influence of solvent on the transition-state structure of HRP-catalyzed phenol oxidation.[239] In this analysis, Hammett coefficients (ρ values) showed charge distribution in the reaction transition state, which is highly sensitive to both microenvironment of the transition state and the reaction mechanism. Therefore, variations in ρ value for HRP catalysis in organic solvents may suggest solvent penetration into the enzyme's active site.[239] A deviation in Hammett ρ values reflect changes in the transition state. The catalytic activity of the enzymes decreased as much as 4 orders of magnitude in a mixed solvent containing organic solvents like dimethyl sulfoxide, dioxan, dimethylformamide, tetrahydrofuran and acetonitrile. The catalytic activity of HRP decreased by 30% with only 30 vol% organic solvents other than DMSO.[243] In the case of DMSO, the activity of free enzyme and immobilized enzyme decreased with respect to concentration of DMSO. The stability of the enzyme can be improved by covalent immobilization on silica nanoparticles (NPs), where half-life in buffer at 50 °C was improved from 2 h to 52 h. These covalently immobilized enzymes demonstrated high catalytic activity and stability in comparison to free enzyme.[243] The optimum activity of rice peroxidase on silica NPs was found at 30 °C at pH 7–8 and was stable up to 68 °C. Shelf-life of rice peroxidase was 60 h in 1,4-dioxane (20%) and 12 h in ethanol. The activity of the rice peroxidase was improved up to 12 h (shelf-life) with 0–40% ethanol or 0–30% 1,4-dioxane.[244]

Cyt 450 BM3 can catalyze a broad range of industrially significant compounds in water, but was rapidly inactivated in organic solvents.[245] The impact of acetonitrile, ethanol, acetone, methanol and DMSO on the activity of Cyt P450s in rainbow trout hepatic microsomes was investigated.[246] Acetonitrile, acetone, methanol, ethanol and DMSO below 0.5% did not affect the Cyt P450s BM3 activities. Methanol could be used up to 1% for CYP1A and CYP3A, and up to 2% acetone could be used with CYP2E1.

Cyt 450 BM3 can catalyze a broad range of industrially significant compounds in water, but was rapidly inactivated in organic solvents.[245] The impact of acetonitrile, ethanol, acetone, methanol and DMSO on the activity of Cyt P450s in rainbow trout hepatic microsomes was investigated.[246] Acetonitrile, acetone, methanol, ethanol and DMSO below 0.5% did not affect the Cyt P450s BM3 activities. Methanol could be used up to 1%

for CYP1A and CYP3A,;and up to 2% acetone could be used with CYP2E1.

The pH of the reaction mixture is critical for maximizing activity and electrochemical behavior of the enzyme. Enzymes have a narrow pH range of activity, often near physiological pH and they can denature at temperatures above 40 °C. There are 7 isoenzymes of HRP and in solution they exhibit the maximum catalytic activity at pH 6.0–6.5.[247] Enzymes in thin films may have slightly altered pH-activity profiles and redox potentials than in solution. Electrochemistry of bacterial Cyt $P450_{cin}$ (CYP176A), which hydroxylates cineol in DDAB films gave a significant pH dependence consistent with coupled electron/proton transfer at pH 6 to 10.[248] FAD-reductase and $P450_{BM3}$ immobilized in DDAB film electrodes had mid-point potential of −0.402 V and −0.244 V *vs.* SCE, respectively. A negative shift in the mid-point potential was found in 2 linear relations, one between pH 3 to 8 and another between 8 to 10 pH.[249] In another study, CYP2C9 was immobilized in DDAB films on pyrolytic graphite electrodes. Ionic strength and pH affected the electrochemical behavior of the CYP2C9.[250] The changes in pH led to a shift in midpoint potential of about −55 mV per pH unit, close to the theoretical value −59 mV per pH unit consistent with a single electron, single proton transfer process. In 0.1 M buffer, the change in pH led to a shift in midpoint potential of about −52.4 mV per pH unit (Fig. 8) between pH 5.8 and 8.0 in the absence and presence of substrate. Changes in ionic strength from 0.1 to 1 M showed slightly anodic shifted midpoint potentials, at pH 5.8, ∼22 mV and at pH 8.0, ∼9 mV. The electron transfer rate constant increased slightly with pH, 139 s^{-1} at pH 6.0, 150 s^{-1} at pH 7.4 and 165 s^{-1} at pH 8.5.

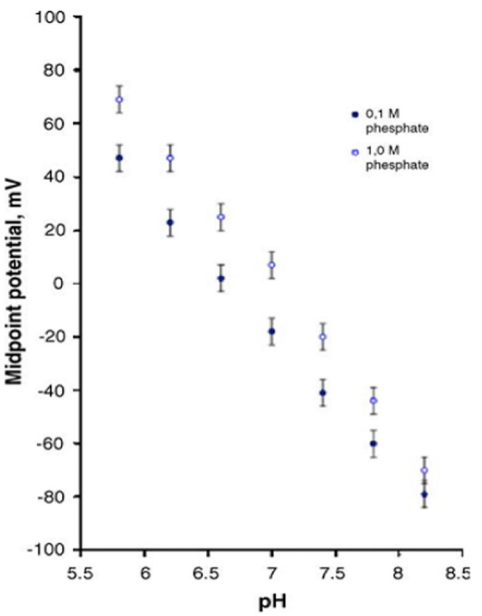

Fig. 8 The effect of ionic strength and pH on the midpoint potential of purified CYP2C9 on DDAB modified PGE. The slope of each plot is 57.5 mV pH^{-1} for 1.0 M (open circles) and 52.4 mV pH^{-1} for 0.1 M (filled circles). Reproduced from *Biochem. Pharmacol.*, 2005, **69**, 1533–1541 with permission.[250] Copyright, 2005, Elsevier.

To this end, microemulsions provide another possible solvent for bioelectrocatalysis, especially valuable for water-insoluble reactants. Microemulsions are clear, stable fluids made of oil, water, surfactant, cosurfactant and electrolyte featuring separate oil and water microphases.[251,252] They can be water-rich, typically 30–80%, which provides hydration of enzymes, and an organic fluid to dissolve non-polar reactants. These fluids have the capability to solubilize polar, nonpolar, and ionic reactants. Cosurfactant is generally required to lower the interfacial tension essential for their formation. Water as the continuous phase contains salt or buffers that are required to enable conductivity necessary for electrochemical synthetic reactors and maintain high activity of enzymes. Structures feature oil droplets in water known as oil-in-water microemulsions or bicontinuous structures of tortuously intertwined mixtures of water and oil, which is often just a common organic solvent. Surfactants reside at oil–water interfaces and decrease interfacial free energy to near zero to stabilize the microemulsions, and additionally provide ionic conductivity for electrolyte. Controlling the compositions of these fluids can provide unique control over some reaction pathways in electrochemical synthesis.[253–258] They are easily prepared from published phase diagrams by mixing components in the correct proportions.[259,260]

Our group pioneered heme enzyme bioelectrocatalysis in microemulsions.[261] Microemulsions are stable mixtures of surfactant, co-surfactant, organic solvent, and water. Oil-in-water and bicontinuous microemulsions look like homogeneous solvents, but have internal microstructures or nanostructures of oil and water phases stabilized by surfactant layers at their interfaces. They are excellent solvents for nonpolar organic molecules, and provide water to hydrate enzymes in films. The use of microemulsions can increase enzyme reactivity, *e.g.*, a 50-fold increase in the yield of styrene oxide from styrene epoxidation catalyzed by and enzyme-like reaction of Fe^{III}heme protein myoglobin (Mb) in CTAB/water/1-pentanol/tetradecane (17.5/35/35/12.5, wt%) microemulsions compared to the reaction in pH 7.4 buffer.[261] The electrochemical reduction of trichloroacetic acid and 1,2-dibromocyclohexane catalyzed by Mb was also demonstrated in microemulsions.[262] The binding and catalytic rates of Mb were more effective for reduction of 1,2-dibromocyclohexane in microemulsion (2000-fold) than in the buffer. For trichloroacetic acid, the faster rate was found in buffer solution (100-fold) because of its hydrophilicity and strong hydration in aqueous phase. The hydrophobic nature of 1,2-dibromocyclohexane provided better access to hydrated Mb in the surfactant film on the electrode and gave a faster reaction rate, while the hydrophilic trichloroacetic acid almost exclusively in the water phase had the poor access to catalyst Mb in the film. Cross-linked films of enzyme-polylysine (PLL) on electrode surfaces improved the thermal, and biocatalytic activity up to 90 °C.[263] The cross-linked Mb/PLL film was stable in microemulsions, which improved the turnover rates for styrene epoxidation compared to loosely cross-linked or non-crosslinked Mb/PLL films.[255] UV circular dichroism supported the stability and the stable conformation of the protein in the film at moderate to high temperatures. UV circular dichroism

(CD) spectra of enzyme-PLL films (HRP/PLL, Mb/PLL, soybean peroxidase (SBP)/PLL) provided evidence of native protein secondary structure in the films.[264] Circular dichroism spectral characteristics for the enzyme-PLL films appear at 193 nm maxima, and 210 and 222 nm minima, when in contact with microemulsion and buffer. All spectra suggested proteins retained native conformations in films (HRP/PLL, Mb/PLL, SBP/PLL) up to 90 °C in SDS microemulsion, and buffer. However, a small change in ratio of 210/222 nm minima was found with CTAB microemulsion in the HRP/PLL films (Fig. 9).

We used *tert*-butylhydroperoxide (*t*-BuOOH) to examine the catalytically active ferryloxy Mb radical formation.[265] Mb/PLL films on a PG electrode were reacted with *t*-BuOOH to generate ferryloxy Mb, and the reaction followed Michaelis–Menten enzyme kinetics. Heterolytic peroxide cleavage then formed *tert*-butyl alcohol and Mb ferryloxy radical, while homolytic cleavage led to formation of the alkoxy radical and nonradical MbFe(IV)=O. The homolytic/heterolytic product ratio was ~0.50, and ~67% products were produced by the heterolytic pathway. Catalytic current from RDV supported the generation of ferryloxy radical, and peroxide-initiated styrene epoxidation in the presence of the *t*-BuOOH by the Mb/PLL films. RDV studies were used to measure catalytic rates of Mb catalyst in CTAB and SDS microemulsions and buffers. Acidic buffer and acidity of the SDS microemulsions had an effect on the reaction kinetics. The values of k_{cat} and K_M were larger in neutral water phases. Values of k_{cat} were close to each other for fluids with pH 2 and 12 water phases. Buffer at pH 6.5, neutral water SDS microemulsion (W/O), and neutral water CTAB micelles, had the largest k_{cat} values.

5. Reactions catalyzed by Cyt P450s

Organic molecules that are commonly unreactive with most chemical oxidants can be activated by Cyt P450s (Scheme 2).[266,267] High-valent iron-oxo species in these enzymes are strong oxidizing agents capable of oxidizing inert C–H bonds through hydrogen atom abstraction, *e.g.*, transforming poorly reactive linear or cyclic alkanes to alcohols and alkenes to epoxides.[267–273] Fig. 10 summarizes bioelectrochemical transformations catalyzed by Cyt P450s, including heteroatom oxygenation, C-hydroxylation, S-oxidation, N-hydroxylation, epoxide formation and heteroatom dealkylation. Additionally, Cyt P450s have also been used in biosensors to produce drug metabolites and inhibitors and some of those representative compounds are also reviewed in this section. The successful reactions catalyzed by Cyt P450s on electrode surfaces are listed in Table 3. The Cyt P450 electrodes used for biocatalytic reactions with K_M, k_{cat}, substrate and respective products are also summarized in Table 3.

5.1 Activation of C–H bonds

Cyt P450s metabolize drugs and xenobiotics (Scheme 1) in mammals through C–H bond activation.[282–286] Hydroxylation of C–H on organic reactants is one of the most common reactions catalyzed by Cyt P450s with addition of an OH group

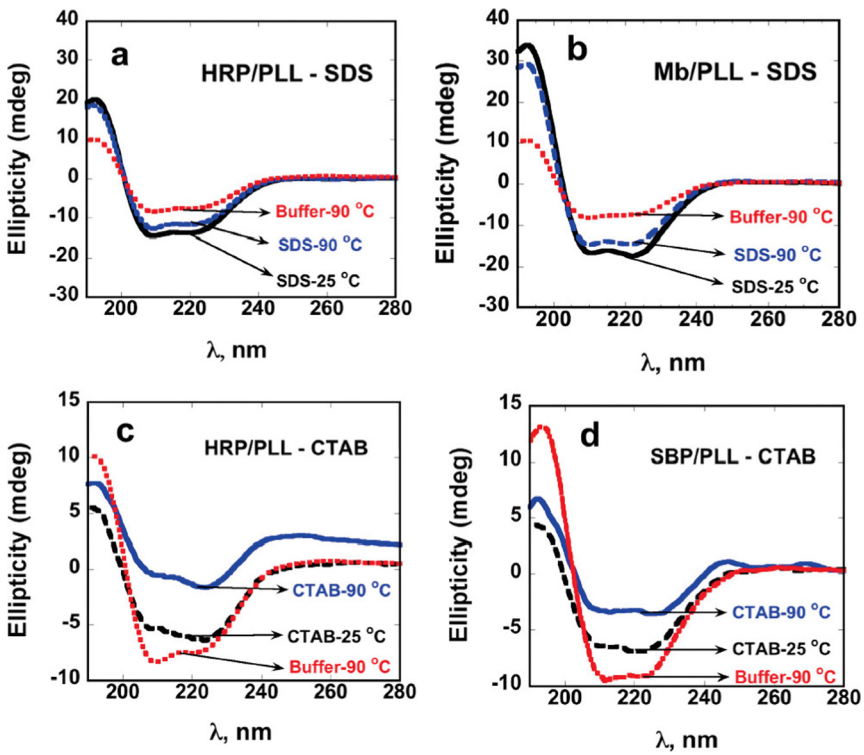

Fig. 9 UV CD spectra of enzyme-PLL films on fused silica slides: (a) HRP/PLL, and (b) Mb/PLL films in SDS, and (c) HRP/PLL, and (d) SBP/PLL films in CTAB microemulsions at 25 and 90 °C. UV CD spectra recorded with pH 5.5 buffer + 0.1 M NaCl at 90 °C were added for comparison. Reproduced from, *Langmuir*, 2008, **24**, 10365–10370, with permission.[264] Copyrights, 2008, ACS Publications.

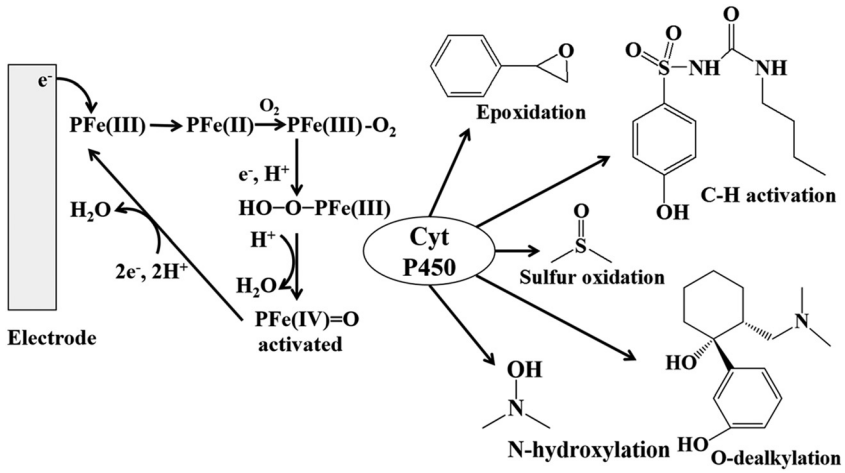

Fig. 10 Schematic representation of products of bioelectrocatalytic reactions catalyzed by Cyt P450s. The down arrow near the electrode with H_2O_2 on it represents the H_2O_2 shunt. With Cyt P450s in microsomes or supersomes, electron transfer proceeds first to CRP, and CPR donates electrons to the Cyt P450 iron heme as shown in Scheme 2 and discussed previously. The same products can form by either pathway.

that can be regio- and stereo-selective. The stereoselectivity of enzymatic catalysis usually arises from specific binding affinities of substrates with different chirality. In the case of most natural Cyt P450s, the heme center is more selective for binding *S**-isomers than *R*-isomers, and/or to produce predominantly an *S**-isomer product from an achiral reactant, although this might vary for different species of Cyt P450s. CYP2C9, as an example, can catalyze the hydroxylation of 5,5-diphenylhydantoin (PPT) to produce the 5-(4′-hydroxyphenyl)-5-phenylhydantoin (*p*-HPPH) through an arene-oxide insertion. CYP2C9 is ~40 times more stereoselective towards *S*-*p*-HPPH,[287] but the *S*/*R* isomer ratio is dependent on the genetic polymorphism of CYP2C9. In case of oxidation of nicotine by CYP2A6, computational simulation suggests hydrogen transfer from either the *trans*-5′- or *cis*-5′-position of (*S*)-(−)-nicotine.[288] The hydroxylation process involves two reactions, starting with the hydrogen transfer from the 5′-position of (*S*)-(−)-nicotine to the oxygen of compound **I** (known as the H-transfer step), followed by recombination of the (*S*)-(−)-nicotine moiety with an iron-bound hydroxyl group, resulting in the formation of the 5′-hydroxynicotine product (known as the O-rebound step). During the 5′-hydroxylation process, there is a preferential loss of the *trans*-5′-hydrogen in a stereoselective manner, because the *trans*-5′-hydrogen is spatially closer to the oxygen of Cpd **I**, as compared to the *cis*-5′-hydrogen. The calculated product stereoselectivity of *S*/*R* isomers for the overall process is 97%, closely matching with the experimentally observed stereoselectivity of 89–94%.

Biologically relevant molecules, *e.g.*, drugs, usually go through metabolic reactions catalyzed by Cyt P450 to form non-toxic or toxic metabolites. This process can play a significant role in development of safe and high-value drugs.[289,290] CYP2C9, as an example, can catalyze the metabolic oxidation of tolbutamide.[274] CYP2C9 was assembled on a *p*-aminothiophenol-modified Au electrode. Thiol derivatives like 4-aminothiophenol, thiophenol, 4-hydroxythiophenol and 4-carboxythiophenol were attached by Au-thiolate bonds overnight in 0.1 mM solutions in ethanol. CYP2C9 microsomes were drop-cast onto those thiol-modified Au electrodes and incubated for 10–30 min at 25 °C. Well-defined redox responses were only found on electrodes modified by thiophenol or 4-aminothiophenol and then coated with CYP2C9 at pH 7.3. The peak potential and the charge transfer rate constant (k_s) were −0.399 V *vs.* Ag/AgCl and 300 s^{-1} for CYP2C9/4-aminothiophenol/Au electrode; and −0.330 V *vs.* Ag/AgCl and 200 s^{-1}, at CYP2C9/thiophenol/Au electrode, respectively. The oxidation of tolbutamide was done at −0.45 V *vs.* Ag/AgCl for 2 h with CYP2C9 with 500 μM tolbutamide in pH 7.3 buffer containing 0.5 vol% of ethanol to give product 4-hydroxytolbutamide. The k_{cat} and K_M for CYP2C9 were 4.5 min^{-1} and 275 μM for CYP2C9*1; 2.3 min^{-1} and 245 μM for CYP2C9*2; and 1.9 min^{-1} and 722 μM for CYP2C9*3, respectively. Similarly, CYP2C9 with CRP coated on ITO with chitosan (CS)/GCE was used to oxidize tolbutamide to 4-hydroxytolbutamide (Fig. 11).[194] The oxidation was studied by titration of tolbutamide at −0.48 V in the buffer solution. There was a clear increase of the cathodic current that reached a stable value within less than 5 s (Fig. 11A). The current increase was due to the catalytic conversion of tolbutamide. The current *vs.* concentration curve was fitted with the Michaelis–Menten model to obtain a Michaelis constant (K_M, characteristics to analyze the binding of substrates to enzymes) of 203 μM (Fig. 11B), close to the K_M of CYP2C9 (60 to 400 μM) in human liver microsomes. The electrolysis was done at −0.48 V *vs.* SCE with 600 μM tolbutamide to give 4-hydroxytolbutamide.

Other approaches have been developed using enzymes with nanomaterials on surfaces of electrodes to improve turnover numbers, and selectivity. When enzymes are immobilized on electrodes, their electrochemical activity depends upon various factors discussed in Section 3. The electrodes with different nanomaterials, nanostructured materials, or ionic surfactants including carbons, conductive polymers, polyions, DDAB, *etc.*, generally improved the activity of Cyt P450s as discussed in Section 3.[226,228,291] The crystallinity of electrode materials varies the activity as well, *e.g.*, a higher electroactivity of CYP3A4

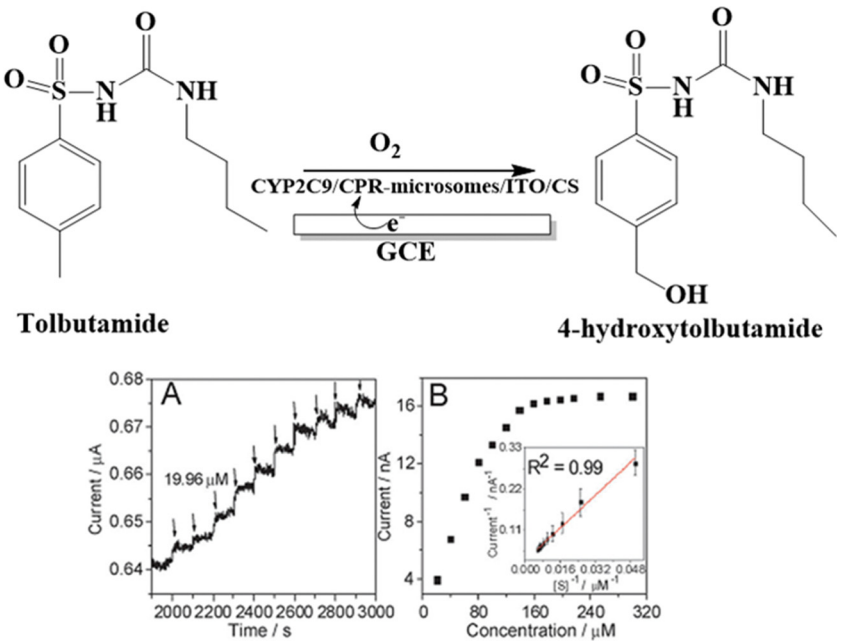

Fig. 11 Bioelectrocatalysis of tolbutamide oxidation: (A) Current *vs.* time plot of consecutive addition of tolbutamide in 0.1 M PBS (pH 7.4) with saturated O_2. (B) Calibration plots demonstrating current *vs.* concentration of tolbutamide. Reprinted from *Chem. Commun.*, 2012, **48** (63), 7802 with permission.[194] Copyright, 2012, Royal Society of Chemistry.

was fund on polycrystalline indium tin oxide (ITO) as compared to that supported on amorphous ITO.[221] CYP3A4 immobilized on polycrystalline ITO enhanced the rate of oxygen reduction and specific coupled with oxidation of drugs (quinidine and testosterone) by oxidation. Similarly, CYP3A4 immobilized with DDAB on a graphite screen-printed electrode (SPE) was highly active for hydroxylation of diclofenac.[292] CYP1A1 on the pyrenebutyric acid modified nitrogen-doped graphene composite (PB-NGO) electrodes can catalyze the oxidation of benzo[*a*]pyrene (B[*a*]P) to benzo[*a*]pyrene-7,8-diol.[228] The redox peak was seen for CYP1A1/PB-NGO/GC electrode at a potential of −0.48 V, while the peak to peak separation was 56 mV at a scan rate of 100 mV s^{-1} in 0.1 M phosphate buffer (pH 7.4) under nitrogen to confirm a one-electron transfer. The Michaelis constant (K_M) was 26 μM and the catalytic rate constant (k_{cat}) was 1.9 s^{-1}. In addition, the linkage of enzymes to electrode can also change the enzymatic activity. For example, bacterial Cyt P450 (CYP101) immobilized on GC through pyrene maleimide enhanced the activity for hydroxylation of camphor.[275] The rate constant of electron transfer (k_s) was ∼2.5 times higher, in comparison to non-specifically bound enzymes.

Nanostructured materials can usually provide a large surface area to improve the activity of Cyt P450s, *e.g.*, on the surface of nanostructured Au and reduced graphene oxide. CYP2C9 when immobilized on AuNPs supported on TiO_2 nanotube arrays (NTAs) was highly active for metabolic reactions of tolbutamide (Fig. 12).[176] NTAs were synthesize by anodization where hollow TiO_2 nanotubes with diameters of 50–100 nm and length up to a few micrometers could be prepared on a Ti foil. Afterwards, the electrochemical deposition of AuNPs (∼5.5 nm) on TNAs was performed by cyclic voltammetry. CYP2C9 was immobilized on AuNPs/TNAs/Ti foil by dip coating in the solution of 1.0 μM CYP2C9 in phosphate buffer 7.4 at 4 °C for 24 h. The electron transfer rate constant (k_s) of CYP2C9 was calculated to be 7.8 s^{-1} at a scan rate of 0.1 V s^{-1}, about 1.3 times greater than CYP2C9 coated on an Au electrode directly. The Michaelis constant (K_M) increased with the tube aspect ratio where the binding of substrates become more difficult in NTAs with a larger diameter. As compared to CYP2C9 directly immobilized on the surface of Ti foil by electrostatic interaction, the K_M decreased by 10-folds from 145.6 μM to approximately 10 μM, indicating that the high surface area favors the binding of substrates. The k_{cat} could reach 9.9 s^{-1} at an optimized tube aspect ratio to produce 4-hydroxytolbutamide. Other conductive nanomaterials *e.g.*, reduced graphene oxide can be used to improve the activity of enzymes as well. CYP2C19 can be immobilized on reduced graphene oxide and CeO_2 nanocomposites for metabolic oxidation of omeprazole into 5-hydroxyomeprazole.[276] The electron transfer rate constant (k_s) of CYP2C19 was 1.77 s^{-1} at the scan rate of 0.1 V s^{-1}. For the Michaelis–Menten fitting of catalytic current and reactant concentration, the Michaelis constant (K_M) of omeprazole to CYP2C19 was calculated to be 8.22 μM and the catalytic rate constant k_{cat} was 5.72 s^{-1}, indicating the faster turnover of substrates. The yield of 5-hydroxyomeprazole was 17% after 4 h electrolysis at −0.520 V *vs.* SCE.

Cyt P450s are active for oxidation of natural drugs as well. Vitamin D3 (VD3) is essential for calcium metabolism in the human body. It is not active in its native form and the activation through 25-hydroxylation catalyzed by Cyt P450s is needed for its biological activity. Human CYP3A4, CYP3A5 and CYP3A7 as examples are active to convert VD3 to 25-dihydroxyvitamin D3 (or denoted as 25(OH) D_3).[96] The bioelectrocatalysis method was

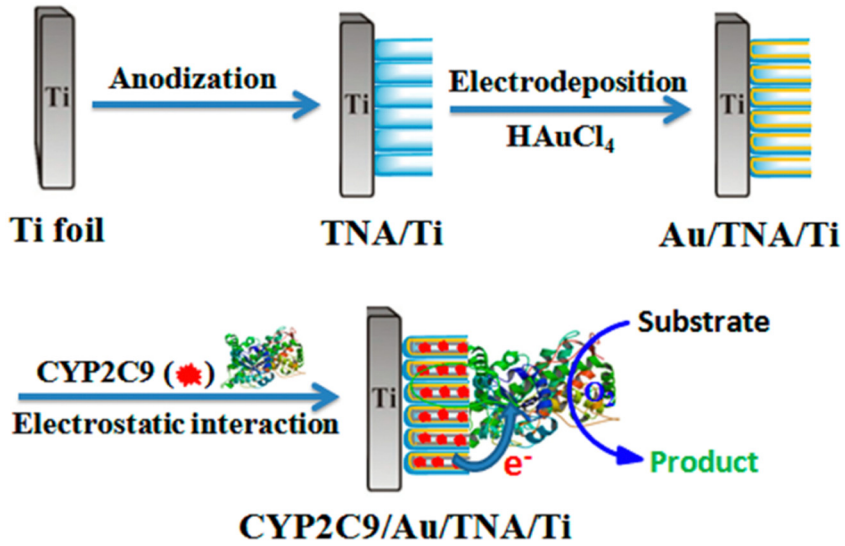

Fig. 12 Synthesis of TiO_2 nanotube arrays system for investigation metabolite of tolbutamide into 4-hydroxytolbutamide. Regenerated from *Anal. Chem.*, 2014, **86**(15), 8003–8009 with permission.[176] Copyright, 2014, ACS Publications.

used for this hydroxylation of VD3 into 25(OH) D_3 by using ferredoxin and other molecules as mediators with Cyt P450 vitamin D_3 hydroxylase (Cyt P450 Vdh) (Fig. 13).[278] In solution, Cyt P450 VdH with NADPH produced 2.3 nmol of 25(OH) D_3 after 30 min using NADH as an electron source. However, Cyt P450 VdH produced 4.8 nM of 25(OH) D_3 at a 0.9 cm^2 electrode by electrolysis at −0.5 V *vs.* SHE for 30 min. The yield of 25(OH) D_3 was nearly doubled in later case without the use of NADPH.

Cyt P450s in human liver microsomes (HLMs) can catalyze the conversion of testosterone into 6β-OH-testosterone on a polydopamine decorated Au-graphene (PDA/Au@RGO) nanocomposite electrode.[279] Fig. 14A shows electrochemical behavior of the HLMs on PDA/Au@RGO. The electrode showed the well-defined redox peak with an anodic peak at −0.37 V and a cathodic peak at −0.45 V *vs.* SCE, under anaerobic conditions, while no peak was observed without microsomes. Fig. 14B shows that the enzymatic electrocatalytic oxygen reduction current and binding of oxygen to reduced iron heme was observed at −0.5 V under aerobic conditions (curve b). However, the oxygen reduction currents on PDA/Au@RGO-CS surface with

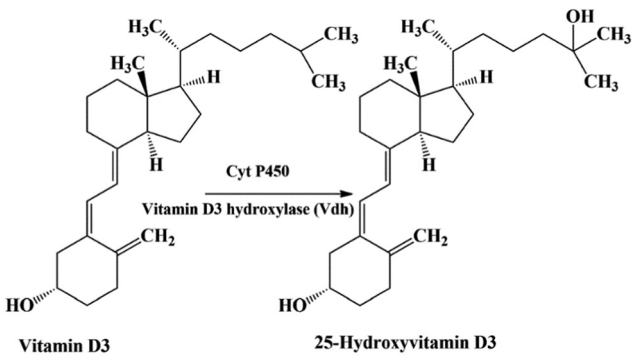

Fig. 13 Conversion of vitamin D3 to 25-dihydroxyvitamin D3 by Cyt P450 vitamin D3 hydroxylase.

microsomes were very low. Thus, microsomal heme proteins catalyzed the oxygen reduction through electron transfer from electrode to reduce CPR then to the heme. In curve c (Fig. 14B), the cathodic current increased on addition of testosterone into the electrolyte, known as a catalytic process. In control study, the testosterone did not make any significant changes in the current (curve c in the insert of Fig. 14B). Electrolysis at −0.5 V in oxygen saturated phosphate buffer was done for testosterone (250 mM) in water/methanol (0.5%) for 2 h. The rate constant and K_M were 8.9 s^{-1} and 175 μM, respectively. The product was confirmed by HPLC-MS (Fig. 14C) and MS (Fig. 14D) where 305.4 (*m*/*z*) and 343.0 (*m*/*z*) were assigned to $[M + H]^+$ and $[M + K]^+$ of 6β-OH-testosterone, respectively.

As mentioned previously, our group used LbL films of DNA, an ECL-generating polymer $[Ru(bpy)_2(PVP)_{10}]^{2+}$ {(PVP = poly(4-vinylpyridine)} (Ru-PVP) and many different human CYPs in supersomes contain CPR on multi-well microfluidic arrays built on top or PG electrodes to make metabolites that damage DNA. Test compounds flow into the array, and the bioelectrocatalytic enzyme film under potential control produces the metabolites close to the DNA layers. If the metabolite is reactive, DNA is damaged and detected by a subsequent electrochemiluminescence measurement in the same array as described earlier.[23–25] Multiple wells in the array can accommodate many different types of Cyt P450s in a single experiment (Fig. 15).[293] Here we provide a few examples of this approach. A microfluidic 64-nanowell chip array was used to evaluate genotoxicity of metabolites formed by liver, lung, kidney and intestinal Cyt P450 enzymes. LbL films contained DNA, RuBPY and the metabolic enzymes. Multiple enzyme reactions for a reactant are run *via* bioelectrocatalysis, then ECL measuring the DNA damage is recorded with a sensitive camera in a dark box. LC-MS studies of the same reactions are used for confirmation of array results, and to detect specific products. Results reveal rates and nucleobase adducts from DNA damage, enzymes responsible from

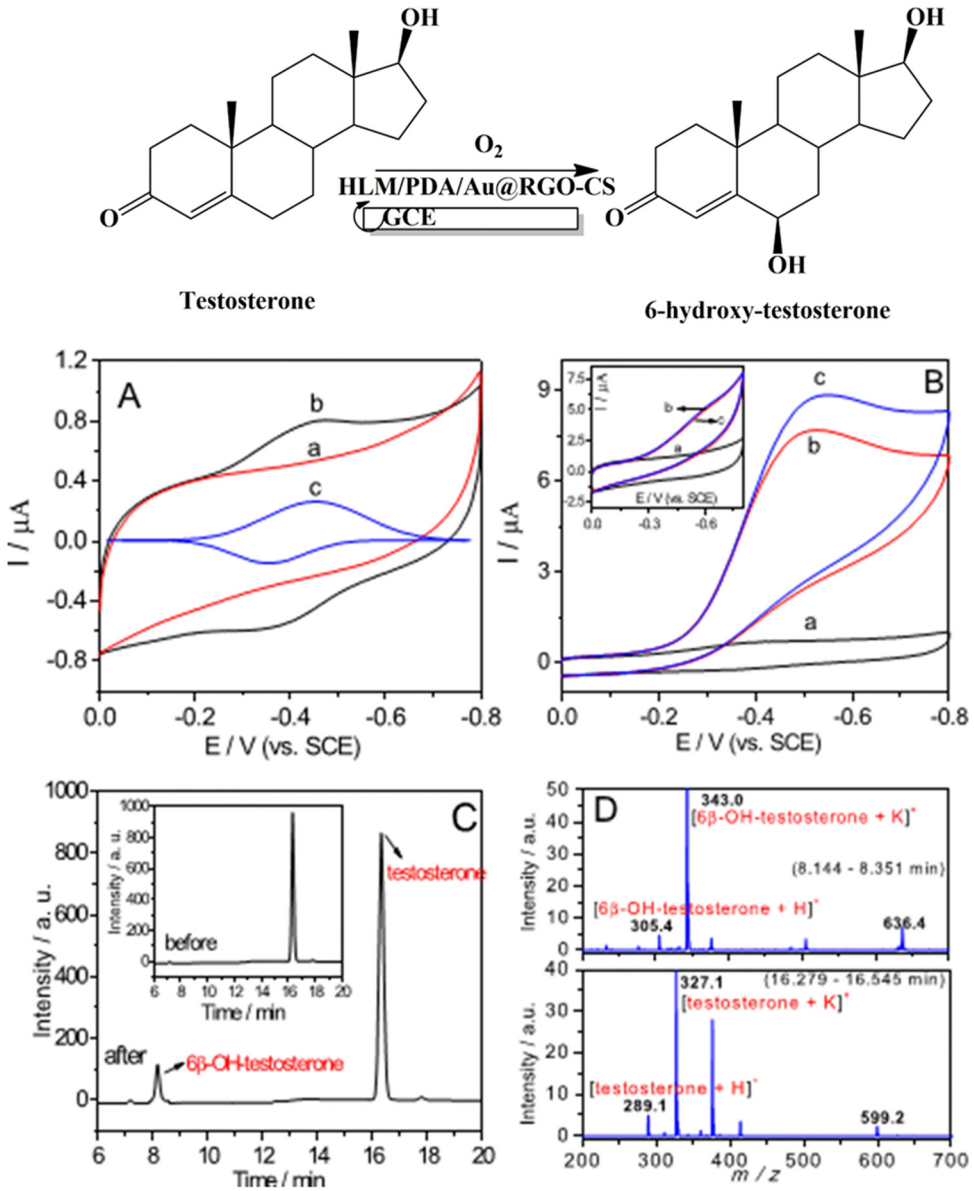

Fig. 14 (A) CVs on (a) without microsomal PDA/Au@RGO-CS/GCE, (b) with microsomal PDA/Au@RGO-CS/GCE and (c) background subtracted response of curve b in anaerobic 0.1 M PBS (pH 7.4). (B) Cyclic voltammograms on microsomal PDA/Au@RGO-CS/GCE, (a) anaerobic, (b) aerobic PBS and (c) with testosterone (200 mM) Insert: curves on without microsomal PDA/Au@RGO-CS/GCE in (a) anaerobic, (b) aerobic PBS and (c) with testosterone (200 mM). (C) HPLC of the electrolysis at −0.5 V for 2 h and (D) the mass spectra of the product observed after the reaction. Regenerated from *Electrochimica Acta*, 2017, **258**, 1365–1374 with the permission.[279] Copyright, 2017, Elsevier.

different organs, and pathways of genotoxic chemistry.[293] DNA damage rates were found using the cell-free array and correlated with organ-specific cell-based DNA damage. In DNA, deoxyguanosine is the oxidized into 8-oxo-7,8-dihydroxy-2-deoxyguanosine (8-oxodG) by reactive oxygen species, which is an important oxidative DNA damage product in humans.[294,295]

We developed similar arrays to measure DNA oxidation facilitated by redox-active metabolites formed by the Cyt P450s. The metabolites of nitrosamines from cigarette smoke can lead to DNA oxidation and genotoxicity.[296] Metabolites of nitrosamines 4-(methylnitrosamino)-1-(3-pyridyl)-1-butanone (NNK) and *N*-nitrosonornicotine (NNN) were formed by bioelectrocatalysis in a 3d-printed microfluidic array loaded with thin films of DNA, CYPs and other enzymes that make metabolites in presence of Cu^{2+} and NADPH to obtain relative rates of DNA oxidation. Here, electrochemiluminescence (ECL) measurements employing a soluble ECL dye, $[Os(tpy\text{-}benz\text{-}COOH)_2]^{2+}$ were carried out to detect the primary DNA oxidation product 8-oxo-7,8-dihydro-2-deoxyguanosine (8-oxodG, Fig. 15). Results showed that metabolites of NNK and NNN + Cu^{2+} + NADPH generated high rates of DNA oxidation by forming reactive oxygen species (ROS) in a complex pathway as the ultimate oxidants.[296]

In biological catalysis, multiple enzymes can mediate multistep conversions. Clopidogrel as a thienopyridine antiplatelet

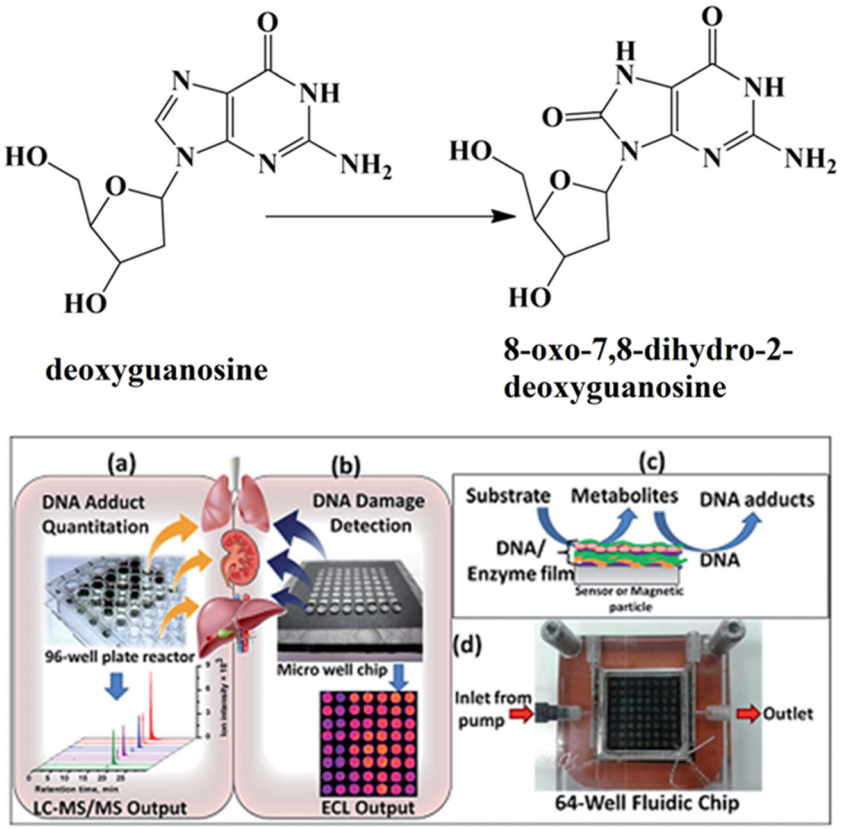

Fig. 15 Conceptual representation of (a) microfluidic bioelectrocatalytic arrays to determine DNA damage by ECL, combined with (b) biocatalytic reactive metabolite-DNA adduct formation and measurements by LC-MS/MS; (c) representation of reactive metabolite-DNA adducts formation; (d) ECL chip contains a flow cell, and 64-well PG electrode with each well containing LbL films of different CYPs, DNA, and Ru-PVP. Reproduced from *Chem. Sci.*, 2015, **6**, 2457–2468 with permission.[293] Copyright, 2015, RSC.

agent is used for treatment of cardiovascular diseases. The activation of clopidogrel is a two-step reaction both catalyzed by Cyt P450s.[297] The first oxidation is clopidogrel to 2-oxo-clopidogrel as a sp^2 C–H activation and the second step is the ring opening of 2-oxo-clopidogrel into a thiol-containing active form (Fig. 16). Metabolic reaction of clopidogrel was done using a bi-enzymatic system on the surface of a AuNP/chitosan/reduced graphene oxide (RGO) nanocomposite (Fig. 16).[122] Two enzymes, namely CYP1A2 and CYP3A4, were co-immobilized on an electrode to catalyze the two cascade reactions. CYP1A2 was covalently attached to primary amine sites of chitosan with glutaraldehyde and CYP3A4 by hydroxyl sites of chitosan *via* amide bonds using carbonyldiimidazole. Enzymes were immobilized on the surface to provide consecutive oxidation of clopidogrel into 2-oxo-clopidogrel catalyzed by CYP1A2 and 2-oxo-clopidogrel converted into clopidogrel carboxylic acid catalyzed by CYP3A4. The co-loading of the two enzymes provides good electron communication to the two heme centers with a fast heterogeneous electron transfer rate constant (k_s) 13.09 s^{-1}. The Michaelis constant (K_M) of clopidogrel metabolism by the two enzymes was calculated to be 19.6 μM and the catalytic rate constant k_{cat} was 1.33 s^{-1}, suggesting the two enzymes working cooperatively. The conversion of clopidogrel to clopidogrel carboxylic acid was up to 7.2% in 1 h electrolysis at −0.53 V (*vs.* SCE).

In native Cyt P450s, high-valent iron-oxo species oxidize C–H bonds by oxygen transfer as discussed previously (Scheme 2). Conversion of C–H into C–OH bonds was been reported even for non-biologically relevant substrates, *e.g.*, 4-cyclohexylbenzoic acid hydroxylation by CYP199A4,[298] butane and propane hydroxylation by CYP450cam,[299] methane oxidation by CYP153A6,[300] ethane and octane hydroxylation by P450 BM3,[301,302] cyclohexane hydroxylation by Cyt P450 from *Acidovorax* sp. CHX100 in recombinant *P. taiwanensis* VLB120,[303] and *Synechocystis* sp. PCC 6803,[304] and toluene oxidation by P450 2A13.[305] These non-biologically relevant substrates may have weak binding to Cyt P450s as not being their biologically relevant function. Therefore, the yield is low in solution or in electrosynthesis.[298,301] Similarly, the amination of C–H bonds by Cyt P450s is difficult with low selectivity.[306] To increase the reactivity of enzymes, protein engineering on either heme or the secondary coordination sphere of heme has been used. Engineered enzymes can provide customized binding pockets for non-biologically relevant substrates. For example, replacing the heme cofactor of CYP119 by an iridium porphyrin (Ir(Me)-PIX), Ir(Me)-CYP119 can provide catalytic insertion of nitrenes into C–H bonds in sulfonyl azide derivatives with an enantiomeric excess of 95 : 5, er.[307] Similarly, the modification of the secondary coordination sphere close to the Fe-heme center can enhance the demethylation activity of CYP2D6.10.

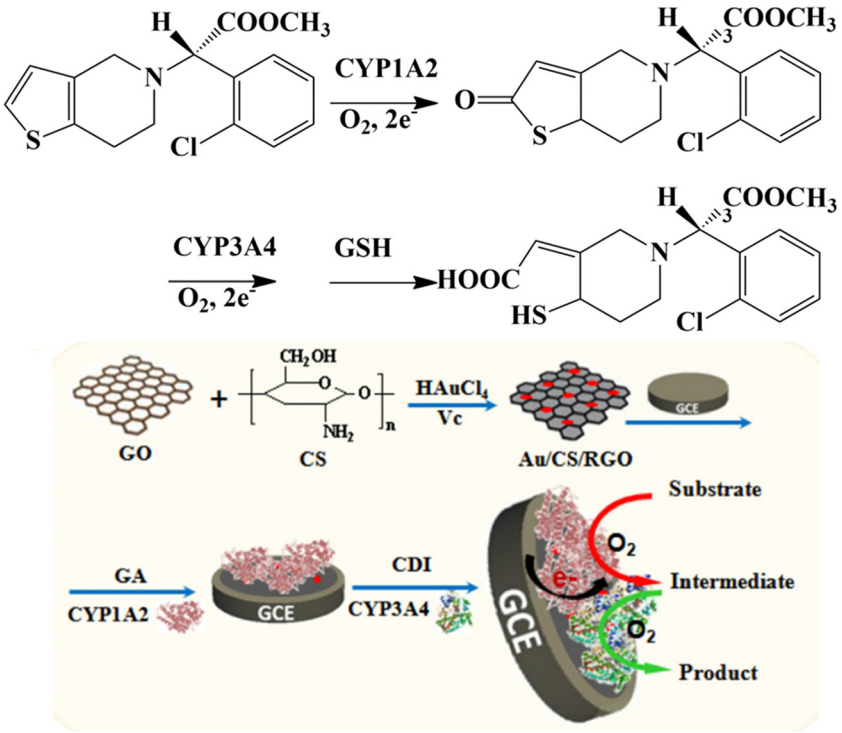

Fig. 16 Electrochemical investigation of metabolites of clopidogrel by using 2 Cyt P450 enzymes at AuNPs/chitosan/rGO/GCE. Reproduced from *Electrochimica Acta*, 2015, **165**, 36–44 with permission.[122] Copyright, 2015, Elsevier.

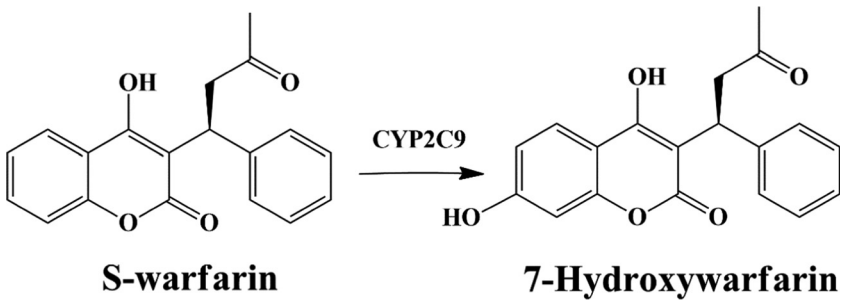

Fig. 17 Electroenzymatic conversion of S-warfarin into 7-hydroxywarfarin at DDAB/GCE.

CYP2D6-C, with valine (V) at position 122 instead of alanine (A) present in CYP2D6.10 was twice as active in converting codeine into morphine with a yield of >70%.[308] CYP2C9 and its polymorphic variants CYP2C9-FLD prepared through CYP2C9 gene fusion at a genetic level with D. vulgaris flavodoxin (FLD) redox module showed altered catalytic activity to oxidize S-warfarin into S-7-hydroxywarfarin (Fig. 17).[277] CYP2C9-FLD immobilized in DDAB films on a GC electrode (DDAB/GCE) was 4 times more active for this hydroxylation reaction, as compared to CYP2C9 under the same conditions.

5.2 Epoxidation

Epoxides are useful synthetic precursors to produce chiral molecules *via* ring-opening. Chiral epoxides are used widely in the pharma industry for synthesis of drugs.[309,310] Manganese (Mn) chiral salen complexes are useful for enantioselective epoxidations.[311] Epoxidation is considered to proceed through multiple mechanisms and different reactive intermediates.[311,312] The enzyme can catalyze the oxygenation of alkenes (non-chiral substrates) to produce chiral epoxides.[40,313–315] Predicting epoxide formation in drugs usage is difficult but important because the formation of epoxide is often linked with drug toxicity.[316,317] Cyt P450s are capable of converting alkenes into epoxides.[316,318–323] Several chemical reactions based on enzymes Cyt P450 BM3, CYP152A1, CYP199A and CYP199A4 have been reported for epoxidation, *e.g.*, linolenic acid, linear aliphatic alkenes, 4-vinylbenzoic acid and styrene. Cyt P450 BM3 can catalyze stereo- and regioselective epoxidation of linolenic acid to epoxy-linolenic acid.[324] The epoxidation is highly regioselective (100%) where only the C15═C16 vinyl group is converted among the three vinyl groups in linolenic acid. The configuration of epoxy-linolenic acid is identified to be 15(*R*),16(*S*)-epoxyoctadeca-9,12-dienoic acid with

an enantiomeric ratio excess of 60%. Epoxidation of 4-vinylbenzoic acid was reported using bacterial CYP199A4 as a biocatalyst with a high stereoselectivity and activity to produce (*S*)-epoxide with an enantioselectivity of 99%.[318] In another approach, H_2O_2 also drives the epoxidation of styrene to styrene epoxide catalyzed by Cyt P450s, although selectivity is much lower.[325] However, most alkenes are very hydrophobic with a limited solubility in aqueous reaction media. At a low concentration of substrates, Cyt P450s also reduce oxygen through two-electron pathways to produce H_2O_2 that can oxidize alkenes directly or activate the Cyt P450 *via* the peroxide shunt (Scheme 2) to epoxide or aldehyde as a mixture.[309,325,326]

In our group, the LBL films of pure CYP1A2, and bacterial Cyt P450cam with conductive polymer PSS on a carbon cloth electrode were used for electrochemical oxidation of styrene to styrene oxide.[226] The epoxidation was facilitated at −0.6 V *vs.* SCE by initial biocatalytic reduction of molecular oxygen to H_2O_2 which activates iron heme enzymes to PFe^{IV}=O by a complex mechanism (Fig. 10) for catalytic oxidation of styrene. Here, iron porphyrin (PFe^{III}) reacts with bioelectrocatalytically-formed hydrogen peroxide to form high valent PFe^{IV}=O oxidant, which oxidizes styrene to styrene oxide. The turnover rate was 39 h^{-1} to produced styrene oxide at PSS-$(CYP1A2\text{-}PSS)_2$ by electrolysis at −0.6 V *vs.* SCE for 1 h. The yield of styrene oxide and benzaldehyde were found to be 8.8 and 22 nmol, respectively.

5.3 Oxidative *N*-, and *O*-dealkylation

Products formed through *O*-dealkylation and *N*-dealkylation follow similar reaction mechanisms to remove alkyl groups to yield alcohols, carbonyls, or amines. Oxidative *N*-dealkylation is commonly catalyzed by Cyt P450s in secondary and tertiary amines, and related *N*-alkylated amines.[327] In the first step, hydroxylation takes place at an α-carbon atom or carbon-adjacent heteroatom, leading to the formation of carbinol species which further undergo chemical rearrangement followed by dealkylation on the heteroatom. The dealkylation can be initiated either by single electron transfer or hydrogen atom transfer.[328–335] For oxidative *N*-dealkylation,[336–339] two elementary steps are involved, *i.e.*, hydrogen atom transfer and single electron transfer. *N*-Oxidation proceeds through charge transfer to the oxo-ferryl group, followed by the formation of radical cation and homolysis of the iron–oxygen bond to generate the new N–O bond. For example, *O*-dealkylation of tramadol was done using CYP2D6 and CPR in a PEI film on graphene-modified GCE (Fig. 18).[230] The electron transfer rate constant and Michaelis constant (K_M) were 0.47 s^{-1} and 23.9 μM, respectively. Electrolysis was done at −0.52 V *vs.* SCE for 2 h at CYP2D6/PEI-RGO/GC electrode (RGO = reduced graphene oxide) with 300 μM tramadol. The conversion of tramadol into *O*-desmethyl tramadol was confirmed by MS with a *m*/*z* of 250.18 and the yield was ∼15% after electrolysis for 2 h.

Bioelectrochemical conversion of tramadol to *O*-desmethyl tramadol was done by using CYP2D6 and CYP1A1 immobilized on AuNPs-chitosan (CS), RGO, and polyacrylic acid on GCE (Fig. 19).[280] The modification of AuNPs-CS-RGO/GCE with PAA gave the net negative charge on the electrode that further immobilized CYP2D6 and CYP1A1 through electrostatic interaction. PAA, while increasing the size of the gold nanoparticles from ∼15 to ∼25 nm, led to the potential shift from −492 to −513 mV for CYP2D6 and −504 mV to −509 mV for CYP1A1, respectively. The presence of PAA resulted in the decrease of the electron transfer rate constant (k_s) from 5.19 s^{-1} to 4.10 s^{-1} for CYP2D6 and 3.24 s^{-1} to 2.78 s^{-1} for CYP1A1, respectively. The electrolysis converted tramadol to *O*-desmethyl tramadol at −0.530 V for 1 h, as confirmed by HPLC, GC-MS and LC-MS. The conversion per unit time was 2.3 h^{-1} for CYP2D6/PAA-AuNPs-CS-RGO and 3.2 h^{-1} for CYP2D6/AuNPs-CS-RGO.

6. Reactions catalyzed by peroxidases

As mentioned earlier, peroxidases are universal oxidoreductases that use hydrogen peroxide or organic hydroperoxides to

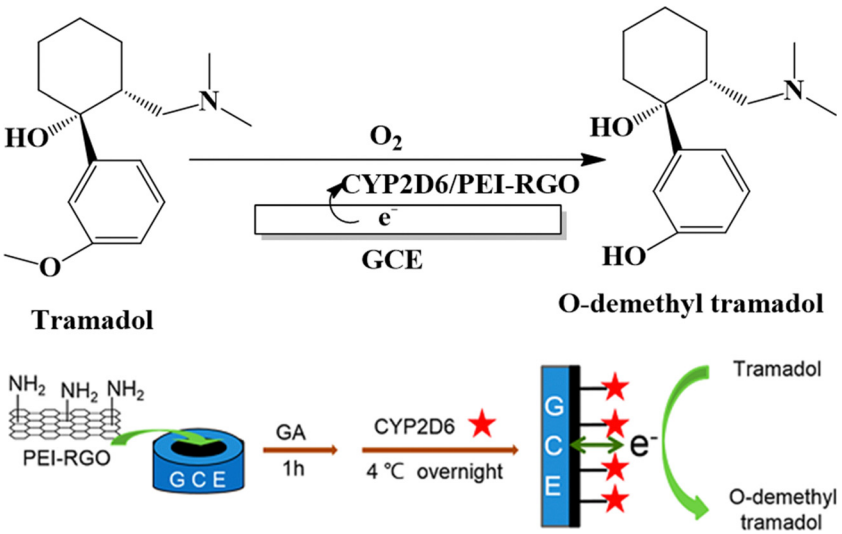

Fig. 18 Scheme of bioelectrocatalytic oxidation of tramadol. Reproduced from *Langmuir*, 2014, **30**, 11833–11840, with permission.[230] Copyright, 2014, ACS Publications.

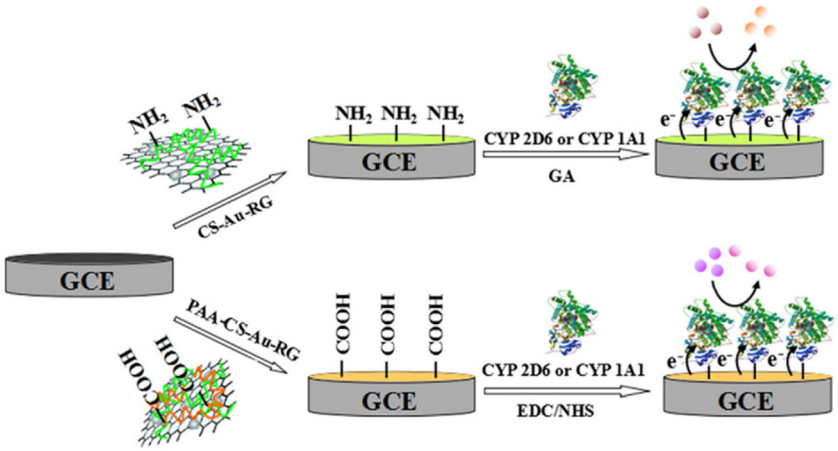

Fig. 19 Immobilization of enzymes on nanocomposite modified electrode and electrochemical system for metabolism of tramadol. Reproduced from *J. Electroanal. Chem.*, 2016, **772**, 46–51 with permission.[280] Copyright, 2016, Elsevier.

oxidize prosthetic group metal atoms to higher valent oxidants. These enzymes catalyze reactions *via* free radicals where reactants get oxidized or in some cases polymerized (Fig. 20). Peroxidases are synthesized by bacteria, fungi, and plants. The reactive centers can be heme, selenium, cysteine thiols, manganese, and other chemical moieties.[340] Several types of peroxidases have been used frequently for catalyzing organic and inorganic reactions such as Fe heme-containing (*e.g.*, HRP, soybean peroxidase (SBP), chloroperoxidase (CPO)) and non-heme containing (*e.g.*, manganese peroxidase, lignin peroxidase). Heme-containing peroxidases predominantly oxidize Fe(III) into highly reactive Fe(IV)=O species by reducing hydrogen peroxide or other peroxides and catalyzing the reactions as discussed in Section 1 (see eqn (1)–(3)). However, the activation of peroxidases requires the use of H_2O_2 to produce the oxidative compound I form. In bioelectrochemistry, *in situ* H_2O_2 production through electrochemical oxygen reduction can also be used to activate the heme center for catalytic conversions. There is a fundamental need for direct electrochemical activation of peroxidases on an electrode for catalytic oxidation of organic compounds.[341]

HRP is obtained from the roots of the horseradish plant,[342] and has been widely used in biocatalytic oxidations of many organic and inorganic substrates.[57] SBPs obtained from soybean plants carry out reactions similar to HRP.[343] Chloroperoxidases are heme-containing enzymes found in fungi and catalyze chlorinations.[344] In the same fashion, non-heme containing peroxidases, not our focus in the current review, also generate highly reactive species by reaction with peroxides. Manganese peroxidase as an example is a lignin-modified peroxidase found from wood-colonizing basidiomycetous fungi.[345] This non-heme peroxidase is oxidized from Mn(II) to highly reactive Mn(III) by peroxides. It is stabilized by chelation with dicarboxylic acid and catalyzes the oxidation of phenolic lignin.

While pure peroxidases are less expensive compared to Cyt P450s, they are unstable under a higher temperature (*e.g.*, >40 °C) or in the presence of excess peroxide.[346,347] In our group, Guto demonstrated that chemical cross-linking in an LbL film can stabilize peroxidases, like HRP, Mb and SBP, for biocatalytic applications up to 90 °C.[263] In the thin crosslinked LbL films with

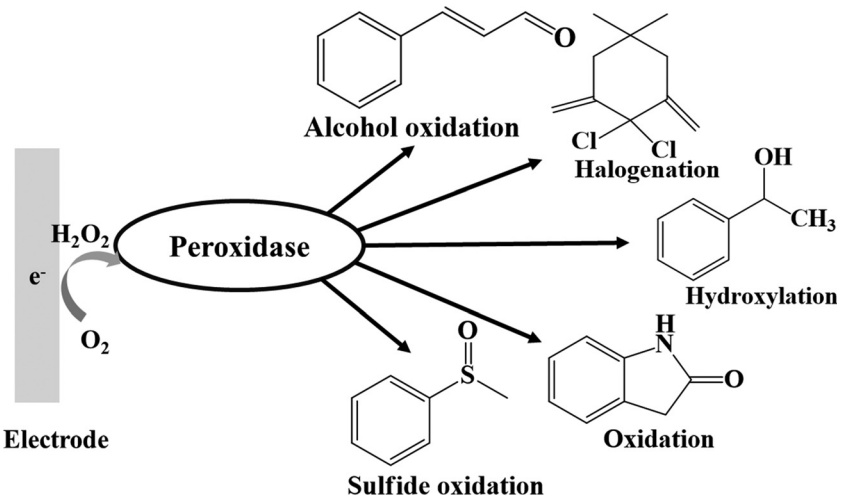

Fig. 20 Bioelectrocatalytic reactions catalyzed by peroxidases.

PLL on PG electrodes, HRP, SBP and Mb were catalytically stable for about 9 h at 90 °C; but were denatured completely in 20–30 min at 90 °C in solution. The HRP-PLL film was 3-fold more active than the SBP-PLL film at 25 °C; whereas, at 90 °C, SBP gave 8-fold better catalytic activity compared to HRP-PL. This is related to the inherent temperature stability of SBP as well as stabilization by the film where the unfolding of enzymes is limited by chemical cross-linking. The oxidation of *o*-methoxyphenol to 3,3′-dimethoxy-4,4′-biphenoquinone by crosslinked peroxidase-PLL films also showed better yields at 90 °C than 25 °C. Results demonstrated that peroxidase catalytic activity can be enhanced at elevated temperatures. Microemulsions of oil, water, and surfactant were used as supporting electrolytes for biocatalysis and bioelectrocatalysis at low and high temperature by using PLL-HRP, PLL-SBP and PLL-Mb activated by *t*-BuOOH.[264] The enzyme-PLL films were stable at 90 °C for >12 h in microemulsions. Oxidation of *o*-methoxyphenol into 3,3′-dimethoxy-4,4′-biphenoquinone gave 3–5 times better yield in microemulsion at 90 °C than at 25 °C. Product yields increased 5-fold with increasing the temperature from 25 to 90 °C for both HRP and SBP in CTAB microemulsions and ~3 fold in SDS microemulsions.

As mentioned, peroxides may be unstable and potentially inactivate by peroxidases at a higher concentration, although these enzymes are stable at mM peroxide concentrations. Continuous electrocatalytic synthesis of hydrogen peroxide by reduction of oxygen is a strategy to activate peroxidases while avoiding high levels of peroxide. Using dissolved oxygen in water, *in situ* reduction can generate hydrogen peroxide by, (i) a two-electron process at the electrode surface as a cathode, or (ii) enzymatic reduction of oxygen by glucose oxidase.[348–354] *In situ* generation of hydrogen peroxide was effective for activation of peroxidase enzymes. For example, *in situ* generated hydrogen peroxide was achieved at pH 3.0 at applied potentials +0.2 to −0.4 V *vs.* Ag/AgCl by oxygen reduction by using Pt-coated titanium and vitreous carbon.[355] The generation of hydrogen peroxide increased at the more negative potential, but a higher concentration of hydrogen peroxide decreased the activity of catalyst lignin peroxidase. The optimal potential was +0.1 V *vs.* Ag/AgCl for generation of hydrogen peroxide and bioelectrocatalytic degradation of 2,4,6-trinitrotoluene by lignin peroxidase into 4-diamino-6-dinitrotoluene. The peroxidase-driven bioelectrocatalytic reactions are summarized in Table 4.

6.1 Oxidation of alcohols, aldehydes, and related compounds

HRP can catalyze oxidation of organic compounds like phenols, alcohols, aldehydes, and chlorinated organics.[60,365–372] HRP can be covalently immobilized on beads. The covalently bound HRP can be activated by H_2O_2 produced electrochemically to catalyze the oxidation of organic compounds. For example, HRP immobilized on beads *via* aminopropylation with 3-aminopropyltriethoxysilane and glutaraldehyde can oxidize phenol derivatives in an electrochemical reactor.[348] *In situ* electro-generation of H_2O_2 by reduction of dissolved oxygen was carried out using Pt coated on a Ti plate as the anode and stainless steel as the cathode. To generate the hydrogen peroxide, initially protons were generated by anodic oxidation of water ($2H_2O \rightarrow O_2 + 4H^+ + 4e^-$) and combined with dissolved oxygen to produce hydrogen peroxide at the cathode (O_2 + 2H+ + $2e^- \rightarrow H_2O_2$). The aqueous phase of phenol was converted to *p*-benzoquinone, other organic acids, and carbon dioxide. The removal efficiency of the phenol reaction was 93%.

Combining peroxidases with electrochemistry can be applied to remove environmental hazards in biochemical processes. For example, bisphenol-A has biological toxicity to aquatic organisms and humans. HRP has high activity for oxidizing bisphenol-A in the presence of H_2O_2. Bioelectrocatalytic oxidation of bisphenol-A by HRP was done in a membraneless electrochemical reactor.[373] Silk fibroin (a natural fibrous protein), Fe_3O_4 nanoparticles and poly(amido amine) were dispersed in a phosphate buffer (pH = 7.4, 50 mM) for 8 h to assemble into magnetic composite nanoparticles (~50 nm). Those magnetic nanoparticles were filtered and transferred to phosphate buffer containing HRP and 25% glutaraldehyde. After incubation at 4 °C for 8 h, the resulting magnetic particles decorated with HRP were isolated magnetically. In 0.1 M PBS buffer, H_2O_2 was produced by oxygen reduction on a carbon fiber cathode. The removal efficiency of bisphenol-A was 80% with an applied potential of 1.6 V, pH 5.0, and 25 mL min^{-1} oxygen flow rate at 25 °C.

Chloroperoxidase (CPO) is a fungal heme-thiolate enzyme that also has peroxidase activity. CPO is negatively charged, and it can assemble with polycations. For example, CPO and PDDA could assemble on a 3-mercaptopropanesulfonic acid-coated Au electrode. These PDDA-CPO-PDDA films were stable and retained 97% activity after storage for 48 h in pH 5 buffer.[374] CPO films can electrochemically oxidize cinnamyl alcohol.[356] CPO could be assembled on a DDAB/Nafion film on a GC electrode for bioelectrocatalytic oxidation of cinnamyl alcohol into cinnamyl aldehyde (Fig. 21A). GC modified with a Nafion film could hold a DDAB-CPO film after coating with chitosan. A well-defined, quasi-reversible redox pair for CPO at −0.2 V *vs.* SCE (phosphate buffer, pH 4.5) was obtained (Fig. 21B, curve a) with an electron transfer rate constant (k_s) of 2.3 s^{-1}. CPO reduced oxygen electrochemically to H_2O_2. Under saturated oxygen, a catalytic reduction peak was assigned to the production of H_2O_2 by CPO in the film as shown in Fig. 21B (curve b). H_2O_2 generated *in situ* by electrochemical reduction further drives the catalytic oxidation of cinnamyl alcohol, also catalyzed by CPO in the composite films. Cinnamyl aldehyde was formed at a yield of 52% after electrolysis for 2 h at −0.6 V *vs.* SCE. The product formation was confirmed by GC-MS.

Lignin peroxidase (LPO) activated by H_2O_2 can catalyze oxidative degradation of organic biopolymers, nonphenolic veratryl-type compounds, and a wide range of organic pollutants, such as phenol and non-phenolic compounds.[47,375–380] Lee and Moon reported the oxidation of veratryl alcohol into veratraldehyde catalyzed in by LPO in solution with H_2O_2 generated by electrochemical reduction of oxygen.[357] H_2O_2 was produced on a reticulated vitreous carbon cathode. The formation rate of veratraldehyde was 30 μM min^{-1} at −0.4 V *vs.* Ag/AgCl in a broad pH range of 2.5–5.5. The concentration of the veratraldehyde produced during the reaction was measured by UV-vis.

Table 4 Electrochemical transformations catalyzed by peroxidase

Electrode	Substrate	Product	Product identification methods	Yield	Ref.
CS-DDAB-CPO-Nafion/GCE	Cinnamyl alcohol	Cinnamyl aldehyde	GC-MS	52%	356
LPO	Veratryl alcohol	Veratraldehyde	UV-vis	30 μM min^{-1}	357
CPO	Thioanisole	(*R*)-Methylphenylsulfoxide	GC, NMR	30 g L^{-1} d^{-1}	341
CPO	Thioanisole	(*R*)-Methylphenylsulfoxide	HPLC	104 g L^{-1} d^{-1}	358
CPO	Methyl *p*-tolyl sulfide	(*R*)-Methyl *p*-tolyl sulfoxide	GC, NMR	76% (ee 93%)	359
	N-MOC-L-methionine methyl ester	(*R*)-N-MOC-L-methionine methyl ester sulfoxide		60% (dr 81 : 19)	
	1-methoxy-4-(methylthio)benzene	(*R*)-Methoxyphenylmethylsulfoxide		83% (ee 99%)	
CPO	Thioanisole	Methyl phenyl sulfoxide	GC-MS	23 g L^{-1} d^{-1}	360
	Monochlorodimedone	Dichlorodimedone		9.5 g L^{-1} d^{-1}	
	Indole	Oxindole		8.3 g L^{-1} d^{-1}	
CPO-Au@HMS	Ethylbenzene	*R*-1-phenylethanol	GC	~1.6 mM in 12 h	361
AaeUPO	Ethylbenzene	1-Phenethyl alcohol, acetophenone	GC	~1 g L^{-1} h^{-1}	362
Vanadium chloroperoxidase	4-Pentenoic acid	Bromolactone	GC	1.4 g (~80% yield) in 24 h	363
CPO-ILEMB/rGO/PEI/carbon cloth	Phenol	*o*-Chlorophenol and *p*-chlorophenol	HPLC	—	364

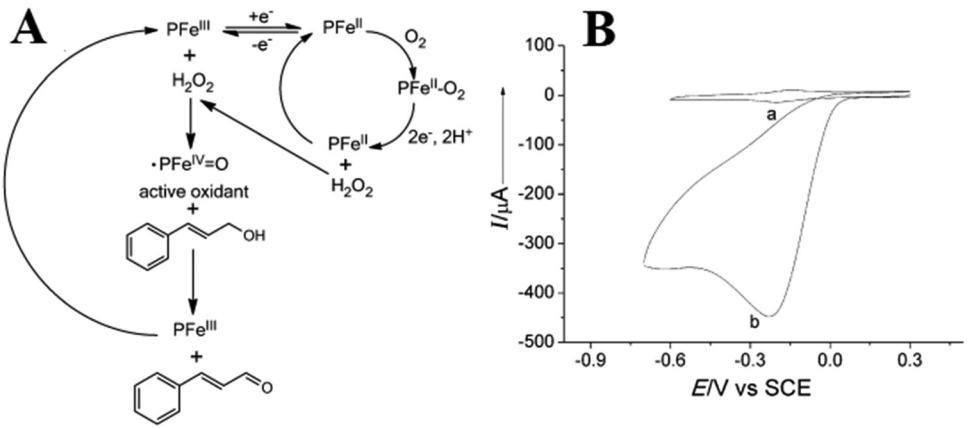

Fig. 21 (A) Oxidation of cinnamyl alcohol. (B) CVs of the CS-DDAB-CPO-Nafion/GCE (a) in nitrogen-saturated and (b) in oxygen-saturated phosphate buffer solution (50 mM, pH 4.5) at 100 mV s^{-1} scan rate. Reproduced from *ChemCatChem*, 2012, **4**, 1850–1855 with permission.[356] Copyright, 2012, John Wiley & Son.

6.2 Oxidation of sulfur-containing compounds

Peroxidases can oxidize organo-sulfur compounds like thiols, sulfides and disulfides.[381–384] The oxidation of aromatic sulfides has been reported by using LPO, SBP and CPO. The yield of sulfoxide decreased with electron donating power of substituents.[385] Manganese peroxidase was reported to cleave the sulfide bond in di(2-methylpent-2-enyl) sulfide.[386] The oxidation of omeprazole sulfide to (*S*)-omeprazole was catalyzed by SBP in CTAB/isooctane/*n*-butyl alcohol/water water-in-oil microemulsions.[387] A bioelectrocatalytic system was developed with CPO for oxidation of thioanisole to (*R*)-methylphenylsulfoxide (Fig. 22).[341] H_2O_2 generated by electroreduction of dissolved oxygen at the cathode could activate CPO to oxidize thioanisole. The enantioselectivity was >98% for *R*-methylphenylsulfoxide. The yield was 30 g L^{-1} d^{-1} at −0.5 V *vs.* Ag/AgCl in 300 mL sodium citrate buffer containing 30 vol% of *t*-butanol at pH 5. Similarly, the conversion of thioanisole into (*R*)-methylphenylsulfoxide was performed by using CPO.[358] The electrolysis at a constant current produced H_2O_2 (eqn (11) and (12)). The product was (*R*)-methylphenylsulfoxide at formation rate 104 g L^{-1} d^{-1} as confirmed by HPLC and the product up to 1.2 g (enantiomeric excess >98.5%, purity >98%) was obtained.

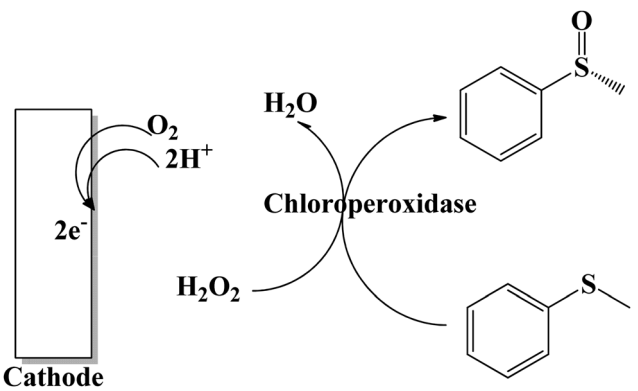

Fig. 22 A schematic representation of electroenzymatic sulfoxidation with chloroperoxidase.

The oxidation of methyl *p*-tolyl sulfide, N-MOC-L-methionine methyl ester and 1-methoxy-4-(methylthio)benzene into methyl *p*-tolyl sulfoxide, N-MOC-L-methionine methyl ester sulfoxide and methoxyphenylmethylsulfoxide was catalyzed by CPOs.[359] Using a similar approach, H_2O_2 was generated electrochemically by reduction of oxygen at −0.5 V *vs.* Ag/AgCl. Under saturated oxygen, an irreversible reduction peak was found for reduction of oxygen to hydrogen peroxide between −0.5 V to −1.0 V *vs.* Ag/AgCl. The product conversion was 60% for N-MOC-L-methionine methyl ester, 76% for methyl *p*-tolyl sulfide, and 83% for 1-methoxy-4-(methylthio)benzene. The products of the reaction were identified by GC and NMR.

Cathode reaction:

$$O_2 + 2H^+ + 2e^- \rightarrow H_2O_2 \quad (11)$$

Anode reaction:

$$H_2O \rightarrow 2e^- + 1/2O_2 + 2H^+ \quad (12)$$

Gas-diffusion electrodes have also been used for the peroxidase-catalyzed reactions. Gas-diffusion electrodes provide high concentrations of H_2O_2 in the vicinity of the enzyme.[388] These gas-diffusion electrodes consisted of solid, liquid and gaseous interfaces and catalyst (*e.g.*, carbon materials or carbon particles) for electrochemical reaction between liquid and gaseous phase, polytetrafluoroethylene (PTFE) and additives. PTFE provided a hydrophobic matrix to bind the catalyst and liquid attracting materials. Hydrogen peroxide produced at gas–liquid–solid interface diffuses into the liquid phase to the enzyme. For example, the gas-diffusion electrode was applied for enzymatic sulfoxidation, chlorination and oxidation by using CPO.[360] The turnover numbers of enzymatic conversions of thioanisole to methyl phenyl sulfoxide, monochlorodimedone to dichlorodimedone, and indole to oxindole could reach 3120, 203 100 and 39 000, respectively. The reaction products were identified by GC-MS. The space time yields (STYs) for each reaction were observed 23, 9.5 and 8.3 g L^{-1} d^{-1}, respectively (Fig. 23).

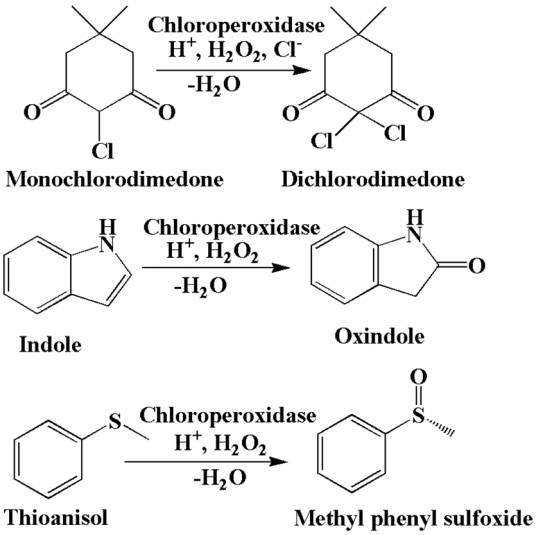

Fig. 23 Biocatalytic reactions catalyzed by chloroperoxidase.

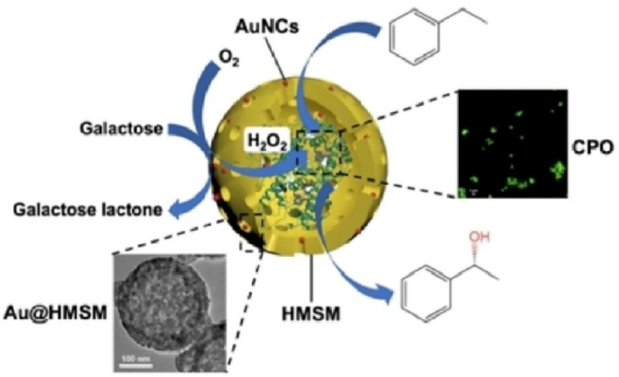

Fig. 24 Hydroxylation of C–H bond using chloroperoxidase to convert ethyl benzene into 1-phenethyl alcohol. Reproduced from *ChemCatChem*, 2022, **14**(4), e202101732 with permission.[361] Copyright, 2022, John Wiley & Son.

6.3 Hydroxylation

Selective hydroxylation of C–H bonds is typically slow with peroxidases.[389] CPO was used for selective bromo-hydroxylation of alkenes,[390] halo-hydroxylation of monoterpenes,[391] and hydroxylation of C–H bonds in ethylbenzene (Fig. 24).[361] Asymmetric hydroxylation of ethylbenzene to *R*-1-phenylethanol was carried out in the presence of *in situ* H_2O_2 generation by oxidation of monosaccharides catalyzed by gold nanoclusters (AuNCs). AuNCs were incorporated into mesoporous silica with hydroxyl groups (HMS-OH), denoted Au@HMS. CPO was loaded on the surface of Au@HMS (CPO-Au@HMS) and placed into the reaction solution with acetate buffer (pH 5.5), ethylbenzene and galactose for 12 h at 30 °C. The oxidation of galactose by AuNCs produced a high concentration of H_2O_2 (1.2 mM) that further activates CPO. The yield of *R*-1-phenylethanol was ~1.6 mM in 12 h when 120 mM of galactose was used in this consecutive reaction.

In recent years, unspecific peroxygenases (UPOs) containing heme-thiolate have attracted much attention to catalyze monooxygenation of various organic compounds with H_2O_2. UPOs can be isolated from the natural fungus, *e.g.*, the edible mushroom *Agrocybe aegerita*.[392,393] Similar to other peroxidases, UPOs do not catalyze the reductive activation of oxygen, but it directly uses H_2O_2 to generate the catalytic active oxyferryl.[392] An excess of H_2O_2, however, can decrease peroxygenase activity; and in some cases, it can drive over oxidation which leads to low turnover and byproduct formation. Electroenzymatic hydroxylation of ethylbenzene to 1-phenethyl alcohol with UPOs produced by fungus *Agrocybe aegerita* (AaeUPO) has been demonstrated by Horst *et al.*[362] Oxygen was used from ambient air and protons from the buffer for electrochemical *in situ* generation of H_2O_2 on a carbon black gas diffusion electrode. The current efficiency was 65–78% in 30 mL of reaction mixtures containing AaeUPO (50 nM) with phosphate buffer (100 mM, pH, 7.0) containing 3 vol% of acetone and 500 μL of ethylbenzene. The product was quantified on a GC. The highest turnover number was 400 000 at −10 mA cm^{-2} after 4 h electrolysis and the space-time-yield was up to ~1 g L^{-1} h^{-1}. However, the AaeUPO was non-specific to produce 1-phenethyl

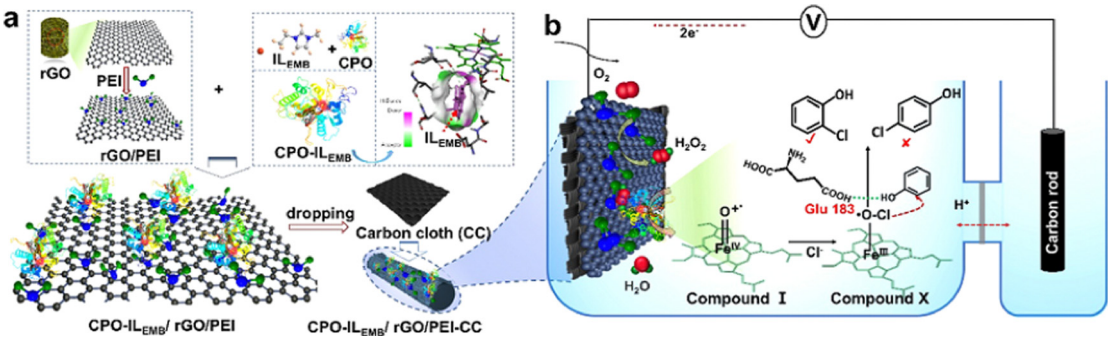

Fig. 25 (a) Scheme for fabrication of CPO-ILEMB/rGO/PEI/carbon cloth electrode and (b) electroenzymatic protocol on carbon cloth to synthesis of *ortho*-chlorophenol. Reproduced from *ACS Sustainable Chem. Eng.*, **10**, 12497–12503 with permission.[364] Copyright, 2022, ACS Publications.

alcohol and 10–20% of acetophenone as an overoxidized byproduct was seen under constant-current electrolysis.

6.4 Halogenation

CPO and vanadium peroxidase are active for enzymatic halogenation.[360,363,394] CPO can catalyze the halogenation by using free halide ions and H_2O_2. Bioelectrochemical synthesis of chlorinated barbituric acid was studied by using CPO.[395] H_2O_2 was produced in an electrolytic cell at −0.5 V *vs.* SCE and activates CPO in a membrane chamber to produce 5-chlorobarbituric acid. The conversion of barbituric acid into 5-chlorobarbituric acid was >96% after 24 h. The enzymatic conversion of 4-pentenoic acid to bromolactone was catalyzed by vanadium chloroperoxidase with *in situ* generation of H_2O_2.[363] An oxidized carbon nanotube (o-CNT) gas-diffusion electrode was used as a cathode where H_2O_2 was produced from oxygen reduction. Vanadium chloroperoxidase was used in solution for conversion of 4-pentenoic acid to bromolactone product identified by GC. The isolated yield of bromolactone was 1.4 g (~80% yield) in 24 h. Chlorination of phenol was demonstrated with ionic liquid modified CPO (CPO-IL$_{EMB}$) assembled on a reduced graphene oxide electrode (rGO)/PEI (rGO/PEI).[364] The enzymatic reaction was performed in the range −0.3 V to −0.7 V *vs.* SCE with chloride ions (Cl^-) as the source for chlorination. The composite of rGO/PEI and CPO-IL$_{EMB}$ catalyzed *ortho*-selective phenol chlorination (Fig. 25). At −0.3 V to −0.7 V, the yield of *ortho*-chlorophenol increased with potential. Two products, *o*-chlorophenol and *p*-chlorophenol, were found only at −0.6 V *vs.* SCE. The protocol was selective at −0.3 V and −0.4 V for synthesis of *o*-chlorophenol. Catalytic efficiency was improved 5.5-fold as compared to manually added H_2O_2 and 2.3-fold compared to the use of free CPO. The products were confirmed by HPLC.

7. Conclusions and prospective

Selective oxidations are of critical importance in organic and pharmaceutical syntheses. Effective bioelectrocatalytic approaches using heme-containing enzymes, especially Cyt P450s and peroxidases, have been demonstrated to serve this purpose as described above, and have attracted tremendous interest. While bioelectrocatalytic reactions are important as a synthetic tool, a major goal is to refine the methodologies to generate products with high yields and high selectivity. The practical utility of bioelectrocatalysis is heavily impacted by the stability of enzymes, and selected immobilization methods can achieve high stability and large turnover numbers. For example, crosslinking enzymes into thin polyion films enables high enzyme stability and reaction chemistry at temperatures well above the solution decomposition temperature of the enzyme and provide much higher reaction rates at much higher temperatures than those where unmodified enzymes are stable in solution.

Key challenges with enzymes include thermodynamics, kinetics, and non-aqueous solvent stability (*e.g.*, in organic solvents). The first two aspects have been addressed well by crosslinking and other film strategies, while non-aqueous solvents can be used in microemulsions that do not denature enzymes in films. In addition, genetic molecular engineering by site-directed mutagenesis of enzymes offers a pathway to high thermodynamic and kinetic stability as well as improved reactivity of enzymes, some resistance to organic solvents, accessibility to new or improved reactions, and alternative product selectivity.[396,397] These genetically engineered enzymes can play a significant role for highly specific and selective organic synthesis. For example, Arnold *et al.* reported a number of engineered heme-containing enzymes, *e.g.*, P450$_{BM3}$ as high efficient and specific for C–H activation.[398] In a recent study, engineered P450 nitrene transferase was demonstrated for conversion of aliphatic C–H bonds to chiral amines and cyclohexane C–H bonds to acetamide.[399] These engineered enzymes have not been used much in bioelectrocatalysis, but could offer effective pathways to improve the specificity and access to organic molecules that natural enzymes do not catalyze. However, the cost of genetically engineered enzyme production is an important issue compared to natural enzymes that are often easily obtained from natural sources.

As mentioned above, immobilizing enzymes in stable films, *e.g.*, crosslinked LbL films using polyions with amine groups, offers excellent promise for high stability and retention of activity under synthetic conditions at relatively high temperatures. This has been demonstrated for peroxidases up to 90 °C in aqueous buffer and in microemulsions. More attention

should be paid to electrocatalysis in microemulsions, which provides solvation of water-insoluble hydrophobic reactants, as well as the sufficient water to hydrate enzymes in films and allow them to function in a close-to-natural environment at a relatively low cost.

As discussed, for Cyt P450s in microsomes or supersomes, electron transfer proceeds from electrodes to Cyt P450 reductase (CPR), then to the Cyt P450 Fe^{III}heme, and subsequently formed species utilize molecular oxygen directly as in the natural pathway (Scheme 2). For peroxidases, however, an external source of peroxide is required to activate the enzyme. *In situ*, on-demand, controlled generation of H_2O_2 is attractive for this purpose to enhance atom economy, yields, and enzyme stability. Thus, more feasible and effective total systems are required to provide hydrogen peroxide using electrochemical or alternative approaches. For example, complete flow reactor systems that catalytically produce and biocatalyze synthetic reactions have so far seen little attention. Photocatalytic production of H_2O_2 from O_2 is also a viable option and could be combined with an electrochemical cell to activate enzymes. In our opinion, Fe^{III}heme enzymes are the most stable, versatile, and best utilized for biosynthetic applications in thin films on an electrode or on nanoparticles with electrochemical generation of activators such as H_2O_2. In view of scaleup, new designs of effective reaction cells and protocols which can produce product at larger scale or in a high-throughput fashion are very important future goals.

Finally, bioelectrocatalytic synthesis is limited somewhat by the numbers and types of enzymes available. Biological reactions are often catalyzed by a group of enzymes in sequence, and this approach may also have a role in chemical syntheses. A good example of such chemoenzymatic pathways was reported by Cai *et al.*[400] who demonstrated the enzymatic conversion of CO_2 into starch using 11 sequential reactions. The surface of electrodes in bioelectrochemical synthesis indeed can support the formation of multienzyme complexes with spatial proximity to catalyze cascade reactions, but there are few reports of bioelectrocatalytic syntheses involving consecutive reactions. Alternatively, using synthetic catalysts to replace some recalcitrant enzyme steps in multienzyme syntheses could also be a viable alternative for scaleup. In a recent study, an electrobiosystem was reported using nanostructured copper to convert CO_2 to acetate and genetically engineered *Saccharomyces cerevisiae* to then produce glucose from the acetate.[401] Integrating synthetic catalysts with multienzyme syntheses may be able to improve overall reaction efficiency and could broaden synthetic capacity and the applications of bioelectrocatalytic synthesis.

Conflicts of interest

The authors declare no conflict of interest.

Acknowledgements

The authors are grateful for financial support from a National Science Foundation grant (CBET-2035669) and partial support from the University of Connecticut Research Excellence Program.

References

1 J. J. Sangster, J. R. Marshall, N. J. Turner and J. Mangas-Sanchez, *ChemBioChem*, 2022, **23**, e202100464.
2 R. Siedentop, C. Claaßen, D. Rother, S. Lütz and K. Rosenthal, *Catalysts*, 2021, **11**, 1183.
3 M. Ghaffari-Moghaddam, H. Eslahi, Y. A. Aydin and D. Saloglu, *J. Biol. Methods*, 2015, **2**, e25.
4 E. L. Bell, W. Finnigan, S. P. France, A. P. Green, M. A. Hayes, L. J. Hepworth, S. L. Lovelock, H. Niikura, S. Osuna, E. Romero, K. S. Ryan, N. J. Turner and S. L. Flitsch, *Nat. Rev. Methods Primer*, 2021, **1**, 46.
5 K. M. Koeller and C.-H. Wong, *Nature*, 2001, **409**, 232–240.
6 R. P. Sheridan, K. R. Korzekwa, R. A. Torres and M. J. Walker, *J. Med. Chem.*, 2007, **50**, 3173–3184.
7 M. Zhao, J. Ma, M. Li, Y. Zhang, B. Jiang, X. Zhao, C. Huai, L. Shen, N. Zhang, L. He and S. Qin, *Int. J. Mol. Sci.*, 2021, **22**, 12808.
8 F. P. Guengerich, *Chem. Res. Toxicol.*, 2001, **14**, 611–650.
9 S. M. Mousavi, S. A. Hashemi, S. M. Iman Moezzi, N. Ravan, A. Gholami, C. W. Lai, W.-H. Chiang, N. Omidifar, K. Yousefi and G. Behbudi, *Biochem. Res. Int.*, 2021, **2021**, 1–12.
10 S. Rathore, A. Varshney, S. Mohan and P. Dahiya, *Biotechnol. Genet. Eng. Rev.*, 2022, **38**, 1–32.
11 J. Gan, M. Bilal, X. Li, S. Z. Hussain Shah, B. A. Mohamed, T. Hadibarata and H. Cheng, *Chemosphere*, 2022, **307**, 136035.
12 *Cytochrome P450: Structure, Mechanism, and Biochemistry*, ed. P. R. O. de Montellano, Springer US, Boston, MA, 1995.
13 *Cytochrome P450*, ed. P. R. Ortiz de Montellano, Springer US, Boston, MA, 2005.
14 P. Anzenbacher and E. Anzenbacherová, *Cell. Mol. Life Sci.*, 2001, **58**, 737–747.
15 L. L. von Moltke, D. J. Greenblatt, J. Schmider, J. S. Harmatz and R. I. Shader, *Clin. Pharmacokinet.*, 1995, **29**, 33–44.
16 A. M. McDonnell and C. H. Dang, *J. Adv. Pract. Oncol.*, 2013, **4**, 263–268.
17 T. Lynch and A. Price, *Cytochrome P*, 2007, **76**, 6.
18 S. Uehara, Y. Uno and H. Yamazaki, *Biochem. Pharmacol.*, 2020, **171**, 113721.
19 U. M. Zanger and M. Schwab, *Pharmacol. Ther.*, 2013, **138**, 103–141.
20 S. Li, L. Du and R. Bernhardt, *Trends Microbiol.*, 2020, **28**, 445–454.
21 M. J. Cryle, J. E. Stok and J. J. De Voss, *Aust. J. Chem.*, 2003, **56**, 749.
22 S. Cholerton, A. K. Daly and J. R. Idle, *Trends Pharmacol. Sci.*, 1992, **13**, 434–439.
23 M. Spatzenegger and W. Jaeger, *Drug Metab. Rev.*, 1995, **27**, 397–417.
24 E. Morgan, *Clin. Pharmacol. Ther.*, 2009, **85**, 434–438.
25 E. G. Hvastkovs, J. B. Schenkman and J. F. Rusling, *Annu. Rev. Anal. Chem.*, 2012, **5**, 79–105.
26 E. G. Hvastkovs and J. F. Rusling, *Anal. Chem.*, 2016, **88**, 4584–4599.

27 J. F. Rusling and E. G. Hvastkovs, *Drug Metabolism Handbook*, Wiley, 2022, vol. 2.
28 S. B. Lamb, D. C. Lamb, S. L. Kelly and D. C. Stuckey, *FEBS Lett.*, 1998, **431**, 343–346.
29 T. Sakaki, K. Yamamoto and S. Ikushiro, *Biotechnol. Appl. Biochem.*, 2013, **60**, 65–70.
30 J. B. Y. H. Behrendorff, *Front. Microbiol.*, 2021, **12**, 649273.
31 M. A. Alonso-Lomillo, J. Gonzalo-Ruiz, O. Domínguez-Renedo, F. J. Muñoz and M. J. Arcos-Martínez, *Biosens. Bioelectron.*, 2008, **23**, 1733–1737.
32 L. Asturias-Arribas, M. A. Alonso-Lomillo, O. Domínguez-Renedo and M. J. Arcos-Martínez, *Anal. Chim. Acta*, 2011, **685**, 15–20.
33 P. Sun and Y. Wu, *Sens. Actuators B Chem.*, 2013, **178**, 113–118.
34 J. Ducharme and K. Auclair, *Biochim. Biophys. Acta, Proteins Proteomics*, 2018, **1866**, 32–51.
35 R. W. Estabrook, K. M. Faulkner, M. S. Shet and C. W. Fisher, *Methods in Enzymology*, Elsevier, 1996, vol. 272, pp. 44–51.
36 L. Zhang, Z. Xie, Z. Liu, S. Zhou, L. Ma, W. Liu, J.-W. Huang, T.-P. Ko, X. Li, Y. Hu, J. Min, X. Yu, R.-T. Guo and C.-C. Chen, *Nat. Commun.*, 2020, **11**, 2676.
37 K. J. McLean, D. Luciakova, J. Belcher, K. L. Tee and A. W. Munro, in *Monooxygenase, Peroxidase and Peroxygenase Properties and Mechanisms of Cytochrome P450*, ed. E. G. Hrycay and S. M. Bandiera, Springer International Publishing, Cham, 2015, vol. 851, pp. 299–317.
38 B. Meunier, S. P. de Visser and S. Shaik, *Chem. Rev.*, 2004, **104**, 3947–3980.
39 J. T. Groves, *J. Inorg. Biochem.*, 2006, **100**, 434–447.
40 F. P. Guengerich, *ACS Catal.*, 2018, **8**, 10964–10976.
41 J. F. Rusling, E. G. Hvastkovs, D. O. Hull and J. B. Schenkman, *Chem. Commun.*, 2008, 141–154.
42 A. Claesson and O. Spjuth, *Mini-Rev. Med. Chem.*, 2013, **13**, 720–729.
43 T. L. de Albuquerque, J. S. Silva, A. C. de Macedo, L. R. B. Gonçalves and M. V. P. Rocha, *Reference Module in Chemistry, Molecular Sciences and Chemical Engineering*, Elsevier, 2019.
44 S. Colonna, N. Gaggero, C. Richelmi and P. Pasta, *Trends Biotechnol.*, 1999, **17**, 163–168.
45 K. N. Ingenbosch, S. Quint, M. Dyllick-Brenzinger, D. S. Wunschik, J. Kiebist, P. Süss, U. Liebelt, R. Zuhse, U. Menyes, K. Scheibner, C. Mayer, K. Opwis, J. S. Gutmann and K. Hoffmann-Jacobsen, *ChemBioChem*, 2021, **22**, 398–407.
46 S. Chen and P. Schopfer, *Eur. J. Biochem.*, 1999, **260**, 726–735.
47 A. O. Falade, U. U. Nwodo, B. C. Iweriebor, E. Green, L. V. Mabinya and A. I. Okoh, *MicrobiologyOpen*, 2017, **6**, e00394.
48 M. Tien and D. Ma, *J. Biol. Chem.*, 1997, **272**, 8912–8917.
49 M. Tanaka, K. Matsuura, S. Yoshioka, S. Takahashi, K. Ishimori, H. Hori and I. Morishima, *Biophys. J.*, 2003, **84**, 1998–2004.
50 E. G. Hrycay and S. M. Bandiera, in *Monooxygenase, Peroxidase and Peroxygenase Properties and Mechanisms of Cytochrome P450*, ed. E. G. Hrycay and S. M. Bandiera, Springer International Publishing, Cham, 2015, vol. 851, pp. 1–61.
51 D. C. Goodwin, S. D. Aust and T. A. Grover, *Biochemistry*, 1995, **34**, 5060–5065.
52 V. Christian, R. Shrivastava, D. Shukla, H. Modi and B. R. M. Vyas, *Enzyme Microb. Technol.*, 2005, **36**, 327–332.
53 R. S. Koduri and M. Tien, *J. Biol. Chem.*, 1995, **270**, 22254–22258.
54 E. Vignali, F. Tonin, L. Pollegioni and E. Rosini, *Appl. Microbiol. Biotechnol.*, 2018, **102**, 10579–10588.
55 N. Khatoon, A. Jamal and M. I. Ali, *Environ. Technol.*, 2019, **40**, 1366–1375.
56 J. Guo, X. Liu, X. Zhang, J. Wu, C. Chai, D. Ma, Q. Chen, D. Xiang and W. Ge, *Int. J. Biol. Macromol.*, 2019, **138**, 433–440.
57 N. C. Veitch, *Phytochemistry*, 2004, **65**, 249–259.
58 M. Aldhahri, Y. Q. Almulaiky, R. M. El-Shishtawy, W. M. Al-Shawafi, N. Salah, A. Alshahrie and H. A. H. Alzahrani, *Catal. Lett.*, 2021, **151**, 232–246.
59 J. P. McEldoon and J. S. Dordick, *J. Biol. Chem.*, 1991, **266**, 14288–14293.
60 M. Jonović, B. Jugović, M. Žuža, V. Đorđević, N. Milašinović, B. Bugarski and Z. Knežević-Jugović, *Polymers*, 2022, **14**, 2614.
61 M. Pešić, C. López, G. Álvaro and J. López-Santín, *J. Mol. Catal. B: Enzym.*, 2012, **84**, 144–151.
62 A. But, A. van Noord, F. Poletto, J. P. M. Sanders, M. C. R. Franssen and E. L. Scott, *Mol. Catal.*, 2017, **443**, 92–100.
63 E. Kiljunen and L. T. Kanerva, *J. Mol. Catal. B: Enzym.*, 2000, **9**, 163–172.
64 G. Masdeu, M. Pérez-Trujillo, J. López-Santín and G. Álvaro, *Process Biochem.*, 2016, **51**, 1204–1211.
65 A. D'Annibale, C. Crestini, E. D. Mattia and G. G. Sermanni, *J. Biotechnol.*, 1996, **48**, 231–239.
66 P. Chowdhary, G. Shukla, G. Raj, L. F. R. Ferreira and R. N. Bharagava, *SN Appl. Sci.*, 2019, **1**, 45.
67 J. M. Naapuri, P. K. Wagner, F. Hollmann and J. Deska, *ChemistryOpen*, 2022, **11**, e2021002.
68 Md Belal, S. Sarkar, R. Subramanian and A. T. Khan, *Org. Biomol. Chem.*, 2022, **20**, 2562–2579.
69 Q. Luo, J. Li, W. Wang, Y. Li, Y. Li, X. Huo, J. Li and N. Wang, *ACS Appl. Mater. Interfaces*, 2022, **14**, 14218–14225.
70 P. Dhankhar, V. Dalal, V. Singh, A. K. Sharma and P. Kumar, *Int. J. Biol. Macromol.*, 2021, **193**, 601–608.
71 J. He, Y. Zhang, Q. Yuan and H. Liang, *Ind. Eng. Chem. Res.*, 2019, **58**, 3555–3560.
72 F. Gao, L. Wang, Y. Liu, S. Wang, Y. Jiang, M. Hu, S. Li and Q. Zhai, *Biochem. Eng. J.*, 2015, **93**, 243–249.
73 B. Valderrama, M. Ayala and R. Vazquez-Duhalt, *Chem. Biol.*, 2002, **9**, 555–565.
74 H. L. Wapshott-Stehli and A. M. Grunden, *Enzyme Microb. Technol.*, 2021, **145**, 109744.
75 S. Ortega Ugalde, C. P. de Koning, K. Wallraven, B. Bruyneel, N. P. E. Vermeulen, T. N. Grossmann, W. Bitter, J. N. M. Commandeur and J. C. Vos, *Appl. Microbiol. Biotechnol.*, 2018, **102**, 9231–9242.

76 S. B. Mellor, A. Z. Nielsen, M. Burow, M. S. Motawia, D. Jakubauskas, B. L. Møller and P. E. Jensen, *ACS Chem. Biol.*, 2016, **11**, 1862–1869.
77 L. Waskell and J.-J. P. Kim, in *Cytochrome P450*, ed. P. R. Ortiz de Montellano, Springer International Publishing, Cham, 2015, pp. 33–68.
78 M. J. I. Paine, N. S. Scrutton, A. W. Munro, A. Gutierrez, G. C. K. Roberts and C. R. Wolf, in *Cytochrome P450*, ed. P. R. Ortiz de Montellano, Springer US, Boston, MA, 2005, pp. 115–148.
79 Z. E. Chiliza, J. Martínez-Oyanedel and K. Syed, *Biophys. Rev.*, 2020, **12**, 1217–1222.
80 S. A. Child, J. M. Bradley, T. L. Pukala, D. A. Svistunenko, N. E. Le Brun and S. G. Bell, *Chem. Sci.*, 2018, **9**, 7948–7957.
81 M. Sasaki, A. Akahira, K. Oshiman, T. Tsuchido and Y. Matsumura, *Appl. Environ. Microbiol.*, 2005, **71**, 8024–8030.
82 D. C. Lamb, Y. Kim, L. V. Yermalitskaya, V. N. Yermalitsky, G. I. Lepesheva, S. L. Kelly, M. R. Waterman and L. M. Podust, *Structure*, 2006, **14**, 51–61.
83 A. W. Munro, H. M. Girvan and K. J. McLean, *Biochim. Biophys. Acta, Gen. Subj.*, 2007, **1770**, 345–359.
84 S. Bellosta, R. Paoletti and A. Corsini, *Circulation*, 2004, **109**, III-50–III-57.
85 O. V. Maksymchuk and V. I. Kashuba, *Pharmacol. Rep.*, 2020, **72**, 1161–1172.
86 H. Hashimoto, K. Toide, R. Kitamura, M. Fujita, S. Tagawa, S. Itoh and T. Kamataki, *Eur. J. Biochem.*, 1993, **218**, 585–595.
87 F. P. Guengerich, in *Cytochrome P450*, ed. P. R. Ortiz de Montellano, Springer International Publishing, Cham, 2015, pp. 523–785.
88 F. P. Guengerich, in *Cytochrome P450*, ed. P. R. Ortiz de Montellano, Springer US, Boston, MA, 2005, pp. 377–530.
89 M. R. McGill and H. Jaeschke, *Pharm. Res.*, 2013, **30**, 2174–2187.
90 H.-J. Xie, Ü. Yasar, S. Lundgren, L. Griskevicius, Y. Terelius, M. Hassan and A. Rane, *Pharmacogenomics J.*, 2003, **3**, 53–61.
91 P. Roy, L. J. Yu, C. L. Crespi and D. J. Waxman, *Drug Metab. Dispos.*, 1999, **27**, 655–666.
92 D. D. Bikle, *Chem. Biol.*, 2014, **21**, 319–329.
93 G. Jones, D. E. Prosser and M. Kaufmann, *J. Lipid Res.*, 2014, **55**, 13–31.
94 I. Aiba, T. Yamasaki, T. Shinki, S. Izumi, K. Yamamoto, S. Yamada, H. Terato, H. Ide and Y. Ohyama, *Steroids*, 2006, **71**, 849–856.
95 O. Pelkonen, M. Turpeinen, J. Hakkola, P. Honkakoski, J. Hukkanen and H. Raunio, *Arch. Toxicol.*, 2008, **82**, 667–715.
96 X. Qin and X. Wang, *Acta Pharm. Sin. B*, 2019, **9**, 1087–1098.
97 S. Hiraga, K. Sasaki, H. Ito, Y. Ohashi and H. Matsui, *Plant Cell Physiol.*, 2001, **42**, 462–468.
98 K. G. Welinder, *Curr. Opin. Struct. Biol.*, 1992, **2**, 388–393.
99 V. S. Ferreira-Leitão, J. G. da Silva and E. P. S. Bon, *Appl. Catal.*, 2003, **42**, 213–221.
100 M. Zámocký, P. G. Furtmüller and C. Obinger, *Arch. Biochem. Biophys.*, 2010, **500**, 45–57.
101 F. Passardi, G. Theiler, M. Zamocky, C. Cosio, N. Rouhier, F. Teixera, M. Margis-Pinheiro, V. Ioannidis, C. Penel, L. Falquet and C. Dunand, *Phytochemistry*, 2007, **68**, 1605–1611.
102 N. Bistolas, U. Wollenberger, C. Jung and F. W. Scheller, *Biosens. Bioelectron.*, 2005, **20**, 2408–2423.
103 A. Yarman, U. Wollenberger and F. W. Scheller, *Electrochim. Acta*, 2013, **110**, 63–72.
104 V. A. Dixit, L. A. Lal and S. R. Agrawal, *WIREs Comput. Mol. Sci.*, 2017, **7**, e1323.
105 O. A. Fatunde and S.-A. Brown, *Int. J. Mol. Sci.*, 2020, **21**, 604.
106 D. Valikhani, J. M. Bolivar and J. N. Pelletier, *ACS Catal.*, 2021, **11**, 9418–9434.
107 J. B. Y. H. Behrendorff and E. M. J. Gillam, *Chem. Res. Toxicol.*, 2017, **30**, 453–468.
108 V. V. Shumyantseva, A. V. Kuzikov, R. A. Masamrekh, T. V. Bulko and A. I. Archakov, *Biosens. Bioelectron.*, 2018, **121**, 192–204.
109 B. D. Fleming, D. L. Johnson, A. M. Bond and L. L. Martin, *Expert Opin. Drug Metab. Toxicol.*, 2006, **2**, 581–589.
110 L. Asturias-Arribas, M. A. Alonso-Lomillo, O. Domínguez-Renedo and M. J. Arcos-Martínez, *Talanta*, 2013, **105**, 131–134.
111 S. Kumar, *Expert Opin. Drug Metab. Toxicol.*, 2010, **6**, 115–131.
112 E. Schneider and D. S. Clark, *Biosens. Bioelectron.*, 2013, **39**, 1–13.
113 J. Genovino, D. Sames, L. G. Hamann and B. B. Touré, *Angew. Chem. Int. Ed.*, 2016, **55**, 14218–14238.
114 V. B. Urlacher and M. Girhard, *Trends Biotechnol.*, 2019, **37**, 882–897.
115 P. R. Ortiz de Montellano, in *Cytochrome P450*, ed. P. R. Ortiz de Montellano, Springer International Publishing, Cham, 2015, pp. 111–176.
116 S. Krishnan, J. B. Schenkman and J. F. Rusling, *J. Phys. Chem. B*, 2011, **115**, 8371–8380.
117 G.-D. Roiban and M. T. Reetz, *Chem. Commun.*, 2015, **51**, 2208–2224.
118 J. F. Rusling and Z. Zhang, *Handbook of Surfaces and Interfaces of Materials*, Elsevier, 2001, pp. 33–71.
119 U. Bussy, R. Boisseau, C. Thobie-Gautier and M. Boujtita, *TrAC, Trends Anal. Chem.*, 2015, **70**, 67–73.
120 U. Bussy, Y.-W. Chung-Davidson, K. Li and W. Li, *Environ. Sci. Technol.*, 2015, **49**, 4450–4457.
121 L. Portychová and K. A. Schug, *Anal. Chim. Acta*, 2017, **993**, 1–21.
122 J. Lu, D. Cui, H. Li, Y. Zhang and S. Liu, *Electrochim. Acta*, 2015, **165**, 36–44.
123 F. W. Scheller, U. Wollenberger, C. Lei, W. Jin, B. Ge, C. Lehmann, F. Lisdat and V. Fridman, *Rev. Mol. Biotechnol.*, 2002, **82**, 411–424.
124 L. H. Mak, S. J. Sadeghi, A. Fantuzzi and G. Gilardi, *Anal. Chem.*, 2010, **82**, 5357–5362.
125 S. J. Sadeghi, S. Ferrero, G. Di Nardo and G. Gilardi, *Bioelectrochemistry*, 2012, **86**, 87–91.
126 V. V. Shumyantseva, A. A. Makhova, E. V. Shikh, T. V. Bulko, A. V. Kuzikov, R. A. Masamrekh, T. Shkel, S. Usanov, A. Gilep and A. I. Archakov, *Bionanoscience*, 2019, **9**, 79–86.

127 M. Huang, X. Xu, H. Yang and S. Liu, *RSC Adv.*, 2012, **2**, 12844.
128 S. J. Sadeghi, A. Fantuzzi and G. Gilardi, *Biochim. Biophys. Acta, Proteins Proteomics*, 2011, **1814**, 237–248.
129 V. V. Shumyantseva, Y. D. Ivanov, N. Bistolas, F. W. Scheller, A. I. Archakov and U. Wollenberger, *Anal. Chem.*, 2004, **76**, 6046–6052.
130 S. Krishnan, A. Abeykoon, J. B. Schenkman and J. F. Rusling, *J. Am. Chem. Soc.*, 2009, **131**, 16215–16224.
131 S. Krishnan, D. Wasalathanthri, L. Zhao, J. B. Schenkman and J. F. Rusling, *J. Am. Chem. Soc.*, 2011, **133**, 1459–1465.
132 R. Nerimetla, G. Premaratne, H. Liu and S. Krishnan, *Electrochim. Acta*, 2018, **280**, 101–107.
133 C. Carucci, A. Salis and E. Magner, *Curr. Opin. Electrochem.*, 2017, **5**, 158–164.
134 K. M. Faulkner, M. S. Shet, C. W. Fisher and R. W. Estabrook, *Proc. Natl. Acad. Sci. U. S. A.*, 1995, **92**, 7705–7709.
135 A. K. Udit, F. H. Arnold and H. B. Gray, *J. Inorg. Biochem.*, 2004, **98**, 1547–1550.
136 K. Drauz, H. Gröger and O. May, *Enzyme Catalysis in Organic Synthesis*, John Wiley & Sons, 2012, vol. 1.
137 S. M. Mense and L. Zhang, *Cell Res.*, 2006, **16**, 681–692.
138 F. Scott Mathews, *Prog. Biophys. Mol. Biol.*, 1985, **45**, 1–56.
139 P. Ponka, *Am. J. Med. Sci.*, 1999, **318**, 241–256.
140 J. D. Dimitrov and T. L. Vassilev, *Nat. Biotechnol.*, 2009, **27**, 892.
141 Y. Xing, S. Gao, X. Zhang and J. Zang, *Foods*, 2022, **11**, 3594.
142 W. Hummel and H. Gröger, *J. Biotechnol.*, 2014, **191**, 22–31.
143 M.-R. Kula and C. Wandrey, *Methods in Enzymology*, Elsevier, 1987, vol. 136, pp. 9–21.
144 Y. Wu, H. Li, X.-M. Zhang, J.-S. Gong, H. Li, Z.-M. Rao, J.-S. Shi and Z.-H. Xu, *Steroids*, 2015, **101**, 15–20.
145 F. Hollmann and A. Schmid, *Biocatal. Biotransform.*, 2004, **22**, 63–88.
146 D. Valikhani, J. M. Bolivar, A. Dennig and B. Nidetzky, *Biotechnol. Bioeng.*, 2018, **115**, 2416–2425.
147 A. M. Chánique and L. P. Parra, *Front. Microbiol.*, 2018, **9**, 194.
148 J. P. Gray, V. Mishin, D. E. Heck, D. L. Laskin and J. D. Laskin, *Toxicol. Appl. Pharmacol.*, 2010, **247**, 76–82.
149 R. Zangar, *Toxicol. Appl. Pharmacol.*, 2004, **199**, 316–331.
150 I. Hanukoglu, *Drug Metab. Rev.*, 2006, **38**, 171–196.
151 S.-Y. Park, K. Yamane, S. Adachi, Y. Shiro, K. E. Weiss, S. A. Maves and S. G. Sligar, *J. Inorg. Biochem.*, 2002, **91**, 491–501.
152 K. Nguyen, N. Nguyen, M. Milhim, V. Nguyen, T. Lai, H. Nguyen, T. Le, T. Phan and R. Bernhardt, *FEBS Open Bio*, 2021, **11**, 124–132.
153 H. Matsumura, S. Wiwatchaiwong, N. Nakamura, M. Yohda and H. Ohno, *Electrochem. Commun.*, 2006, **8**, 1245–1249.
154 E. Blair, J. Greaves and P. J. Farmer, *J. Am. Chem. Soc.*, 2004, **126**, 8632–8633.
155 H. Matsumura, N. Nakamura, M. Yohda and H. Ohno, *Electrochem. Commun.*, 2007, **9**, 361–364.
156 V. V. Shumyantseva, T. V. Bulko, P. I. Koroleva, E. V. Shikh, A. A. Makhova, M. S. Kisel, I. V. Haidukevich and A. A. Gilep, *Processes*, 2022, **10**, 383.
157 V. V. Shumyantseva, T. V. Bulko, G. P. Kuznetsova, N. F. Samenkova and A. I. Archakov, *Biochem. Mosc.*, 2009, **74**, 438–444.
158 S. Liu, L. Peng, X. Yang, Y. Wu and L. He, *Anal. Biochem.*, 2008, **375**, 209–216.
159 A. Fantuzzi, M. Fairhead and G. Gilardi, *J. Am. Chem. Soc.*, 2004, **126**, 5040–5041.
160 C. Garcia-Galan, Á. Berenguer-Murcia, R. Fernandez-Lafuente and R. C. Rodrigues, *Adv. Synth. Catal.*, 2011, **353**, 2885–2904.
161 C. M. Silveira, P. R. Rodrigues, W. Ghach, S. A. Pereira, F. Esteves, M. Kranendonk, M. Etienne and M. G. Almeida, *ChemElectroChem*, 2021, **8**, 500–507.
162 T. Gul, R. Bischoff and H. P. Permentier, *TrAC, Trends Anal. Chem.*, 2015, **70**, 58–66.
163 D. P. Manica, Y. Mitsumori and A. G. Ewing, *Anal. Chem.*, 2003, **75**, 4572–4577.
164 P. J. R. Roche, S.-M. Ng, K. Page, N. Goddard and R. Narayanaswamy, *Sens. Actuators B Chem.*, 2009, **139**, 97–103.
165 Y. Lvov, R. Price, B. Gaber and I. Ichinose, *Colloids Surf., A*, 2002, **198–200**, 375–382.
166 Z. Tang, Y. Wang, P. Podsiadlo and N. A. Kotov, *Adv. Mater.*, 2006, **18**, 3203–3224.
167 G.-X. Wang, W.-J. Bao, J. Wang, Q.-Q. Lu and X.-H. Xia, *Electrochem. Commun.*, 2013, **35**, 146–148.
168 A. K. Yagati, J. Min and S. Cho, *J. Electrochem. Soc.*, 2014, **161**, G133–G140.
169 A. V. Kuzikov, R. A. Masamrekh, T. A. Filippova, Y. I. Haurychenka, A. A. Gilep, T. V. Shkel, N. V. Strushkevich, S. A. Usanov and V. V. Shumyantseva, *Electrochim. Acta*, 2020, **333**, 135539.
170 M. A. Alonso-Lomillo, C. Yardimci, O. Domínguez-Renedo and M. J. Arcos-Martínez, *Anal. Chim. Acta*, 2009, **633**, 51–56.
171 P. M. Gannett, J. Kabulski, F. A. Perez, Z. Liu, D. Lederman, C. W. Locuson, R. R. Ayscue, N. M. Thomsen and T. S. Tracy, *J. Am. Chem. Soc.*, 2006, **128**, 8374–8375.
172 L. A. Wollenberg, J. L. Kabulski, M. J. Powell, J. Chen, D. R. Flora, T. S. Tracy and P. M. Gannett, *Appl. Biochem. Biotechnol.*, 2014, **172**, 1293–1306.
173 A. Fantuzzi, L. H. Mak, E. Capria, V. Dodhia, P. Panicco, S. Collins and G. Gilardi, *Anal. Chem.*, 2011, **83**, 3831–3839.
174 D. Bartczak and A. G. Kanaras, *Langmuir*, 2011, **27**, 10119–10123.
175 S. Keleştemur, M. Altunbek and M. Culha, *Appl. Surf. Sci.*, 2017, **403**, 455–463.
176 J. Lu, H. Li, D. Cui, Y. Zhang and S. Liu, *Anal. Chem.*, 2014, **86**, 8003–8009.
177 L. Peng, X. Yang, Q. Zhang and S. Liu, *Electroanalysis*, 2008, **20**, 803–807.
178 K. R. Jegannathan, S. Abang, D. Poncelet, E. S. Chan and P. Ravindra, *Crit. Rev. Biotechnol.*, 2008, **28**, 253–264.
179 J. F. Rusling and A. E. F. Nassar, *J. Am. Chem. Soc.*, 1993, **115**, 11891–11897.
180 J. F. Rusling, *Acc. Chem. Res.*, 1998, **31**, 363–369.
181 P. M. Guto and J. F. Rusling, *Electrochem. Commun.*, 2006, **8**, 455–459.

182 J. K. Cullison, F. M. Hawkridge, N. Nakashima and S. Yoshikawa, *Langmuir*, 1994, **10**, 877–882.
183 J. D. Burgess, M. C. Rhoten and F. M. Hawkridge, *Langmuir*, 1998, **14**, 2467–2475.
184 P. Quantin, E. Colaço, K. El Kirat, C. Egles, H. Ficheux and J. Landoulsi, *ACS Omega*, 2018, **3**, 12535–12544.
185 F. Hua, T. Cui and Y. M. Lvov, *Nano Lett.*, 2004, **4**, 823–825.
186 Y. M. Lvov, *Handbook of Surfaces and Interfaces of Materials*, Elsevier, 2001, pp. 169–188.
187 Y. M. Lvov, Z. Lu, J. B. Schenkman, X. Zu and J. F. Rusling, *J. Am. Chem. Soc.*, 1998, **120**, 4073–4080.
188 J. Alvarez-Malmagro, A. R. Oliveira, C. Gutiérrez-Sánchez, B. Villajos, I. A. C. Pereira, M. Vélez, M. Pita and A. L. De Lacey, *ACS Appl. Mater. Interfaces*, 2021, **13**, 11891–11900.
189 Q. Dai, L. Yang, Y. Wang, X. Cao, C. Yao and X. Xu, *Anal. Bioanal. Chem.*, 2020, **412**, 4703–4712.
190 M. Ray, S. D. Mhaske, S. K. Haram and S. Mazumdar, *Anal. Biochem.*, 2021, **626**, 114204.
191 V. E. V. Ferrero, L. Andolfi, G. Di Nardo, S. J. Sadeghi, A. Fantuzzi, S. Cannistraro and G. Gilardi, *Anal. Chem.*, 2008, **80**, 8438–8446.
192 R. Frank, C. Prönnecke, R. Azendorf, H.-G. Jahnke, A. G. Beck-Sickinger and A. A. Robitzki, *Lab Chip*, 2020, **20**, 1449–1460.
193 A. V. Kuzikov, T. V. Bulko, P. I. Koroleva, R. A. Masamrekh, S. S. Babkina, A. A. Gilep and V. V. Shumyantseva, *Biochem. Mosc. Suppl. Ser. B Biomed. Chem.*, 2020, **14**, 252–259.
194 X. Xu, W. Wei, M. Huang, L. Yao and S. Liu, *Chem. Commun.*, 2012, **48**, 7802.
195 N. Sultana, J. B. Schenkman and J. F. Rusling, *Electroanalysis*, 2007, **19**, 2499–2506.
196 A. J. Bard and L. R. Faulkner, *Electrochemical methods: fundamentals and applications*, Wiley, New York, 2nd edn, 2001.
197 C. Baj-Rossi, G. D. Micheli and S. Carrara, *Sensors*, 2012, **12**, 6520–6537.
198 T. Yuan, H. Permentier and R. Bischoff, *TrAC, Trends Anal. Chem.*, 2015, **70**, 50–57.
199 Q. Xue, D. Kato, T. Kamata, Q. Guo, T. You and O. Niwa, *The Analyst*, 2013, **138**, 6463.
200 V. V. Shumyantseva, S. Carrara, V. Bavastrello, D. Jason Riley, T. V. Bulko, K. G. Skryabin, A. I. Archakov and C. Nicolini, *Biosens. Bioelectron.*, 2005, **21**, 217–222.
201 H. F. Ozbakir and D. A. Sambade, *J. Biosens. Bioelectron.*, 2015, **7**, 1000193.
202 A. A. Makhova, V. V. Shumyantseva, E. V. Shich, T. V. Bulko, V. G. Kukes, O. S. Sizova, G. V. Ramenskaya, S. A. Usanov and A. I. Archakov, *Bionanoscience*, 2011, **1**, 46–52.
203 Y. Mie, M. Suzuki and Y. Komatsu, *J. Am. Chem. Soc.*, 2009, **131**, 6646–6647.
204 V. V. Shumyantseva, T. V. Bulko, Yu. O. Rudakov, G. P. Kuznetsova, N. F. Samenkova, A. V. Lisitsa, I. I. Karuzina and A. I. Archakov, *J. Inorg. Biochem.*, 2007, **101**, 859–865.
205 A. Shukla, E. M. Gillam, D. J. Mitchell and P. V. Bernhardt, *Electrochem. Commun.*, 2005, **7**, 437–442.
206 S. Y. Rhieu, D. R. Ludwig, V. S. Siu and G. T. R. Palmore, *Electrochem. Commun.*, 2009, **11**, 1857–1860.
207 D. P. Wasalathanthri, S. Malla, R. C. Faria and J. F. Rusling, *Electroanalysis*, 2012, **24**, 2049–2052.
208 D. A. Buttry and F. C. Anson, *J. Electroanal. Chem. Interfacial Electrochem.*, 1981, **130**, 333–338.
209 S. S. Reginald, H. Lee, N. Fazil, B. Sharif, M. Lee, M. J. Kim, H. Beyenal and I. S. Chang, *Commun. Biol.*, 2022, **5**, 390.
210 C. C. Page, C. C. Moser, X. Chen and P. L. Dutton, *Nature*, 1999, **402**, 47–52.
211 N. D. J. Yates, M. A. Fascione and A. Parkin, *Chem. – Eur. J.*, 2018, **24**, 12164–12182.
212 H. G. Rennke and M. A. Venkatachalam, *J. Histochem. Cytochem.*, 1979, **27**, 1352–1353.
213 M. Hoarau, S. Badieyan and E. N. G. Marsh, *Org. Biomol. Chem.*, 2017, **15**, 9539–9551.
214 X. Yan, J. Tang, D. Tanner, J. Ulstrup and X. Xiao, *Catalysts*, 2020, **10**, 1458.
215 K. P. Fears, B. Sivaraman, G. L. Powell, Y. Wu and R. A. Latour, *Langmuir*, 2009, **25**, 9319–9327.
216 Y. Liu, T. L. Ogorzalek, P. Yang, M. M. Schroeder, E. N. G. Marsh and Z. Chen, *J. Am. Chem. Soc.*, 2013, **135**, 12660–12669.
217 N. Lalaoui, P. Rousselot-Pailley, V. Robert, Y. Mekmouche, R. Villalonga, M. Holzinger, S. Cosnier, T. Tron and A. Le Goff, *ACS Catal.*, 2016, **6**, 1894–1900.
218 W.-H. Shao, X.-E. Zhang, H. Liu, Z.-P. Zhang and A. E. G. Cass, *Bioconjug. Chem.*, 2000, **11**, 822–826.
219 A. Ménard, Y. Huang, P. Karam, G. Cosa and K. Auclair, *Bioconjug. Chem.*, 2012, **23**, 826–836.
220 J. Park, S. Lee, Y. Kim and T. H. Yoo, *Bioorg. Med. Chem.*, 2021, **30**, 115946.
221 K. Yoshioka, D. Kato, T. Kamata and O. Niwa, *Anal. Chem.*, 2013, **85**, 9996–9999.
222 D. L. Johnson and L. L. Martin, *J. Am. Chem. Soc.*, 2005, **127**, 2018–2019.
223 M. Ferreira, S. Güney, I. Kuźniarska-Biernacka, O. S. G. P. Soares, J. L. Figueiredo, M. F. R. Pereira, I. C. Neves, A. M. Fonseca and P. Parpot, *New J. Chem.*, 2021, **45**, 12622–12633.
224 R. Nerimetla, C. Walgama, V. Singh, S. D. Hartson and S. Krishnan, *ACS Catal.*, 2017, **7**, 3446–3453.
225 Y. Zhang, A. Iqbal, J. Zai, S.-Y. Zhang, H. Guo, X. Liu, I. Ul Islam, H. Fazal and X. Qian, *Org. Chem. Front.*, 2022, **9**, 436–444.
226 C. Estavillo, Z. Lu, I. Jansson, J. B. Schenkman and J. F. Rusling, *Biophys. Chem.*, 2003, **104**, 291–296.
227 L. Jeftic and R. N. Adams, *J. Am. Chem. Soc.*, 1970, **92**, 1332–1337.
228 L. Mi, F. He, L. Jiang, L. Shangguan, X. Zhang, T. Ding, A. Liu, Y. Zhang and S. Liu, *J. Electroanal. Chem.*, 2017, **804**, 23–28.
229 C. Lütke Eversloh, M. Schulz, M. Wagner and T. A. Ternes, *Water Res.*, 2015, **72**, 293–304.
230 D. Cui, L. Mi, X. Xu, J. Lu, J. Qian and S. Liu, *Langmuir*, 2014, **30**, 11833–11840.
231 K. Elouarzaki, D. Cheng, A. C. Fisher and J.-M. Lee, *Nat. Energy*, 2018, **3**, 574–581.

232 E. A. Della Pia, J. E. Macdonald, M. Elliott and D. D. Jones, *Small*, 2012, **8**, 2341–2344.
233 F. A. Al-Lolage, M. Meneghello, S. Ma, R. Ludwig and P. N. Bartlett, *ChemElectroChem*, 2017, **4**, 1528–1534.
234 S. Zernia, R. Frank, R. H.-J. Weiße, H.-G. Jahnke, K. Bellmann-Sickert, A. Prager, B. Abel, N. Sträter, A. Robitzki and A. G. Beck-Sickinger, *ChemCatChem*, 2018, **10**, 525–530.
235 J.-A. He, L. Samuelson, L. Li, J. Kumar and S. K. Tripathy, *Langmuir*, 1998, **14**, 1674–1679.
236 J. Hodak, R. Etchenique, E. J. Calvo, K. Singhal and P. N. Bartlett, *Langmuir*, 1997, **13**, 2708–2716.
237 X. Yu, G. A. Sotzing, F. Papadimitrakopoulos and J. F. Rusling, *Anal. Chem.*, 2003, **75**, 4565–4571.
238 J. Easterbrook, C. Lu, Y. Sakai and A. P. Li, *Drug Metab. Dispos.*, 2001, **29**, 141–144.
239 K. Ryu and J. S. Dordick, *Biochemistry*, 1992, **31**, 2588–2598.
240 T. T. Herskovits, B. Gadegbeku and H. Jaillet, *J. Biol. Chem.*, 1970, **245**, 2588–2598.
241 Y. Zhang, P. He and N. Hu, *Electrochim. Acta*, 2004, **49**, 1981–1988.
242 W. E. Blumberg, J. Peisach, B. A. Wittenberg and J. B. Wittenberg, *J. Biol. Chem.*, 1968, **243**, 1854–1862.
243 A. M. Azevedo, D. M. F. Prazeres, J. M. S. Cabral and L. P. Fonseca, *J. Mol. Catal. B: Enzym.*, 2001, **15**, 147–153.
244 P. Singh, R. Prakash and K. Shah, *Talanta*, 2012, **97**, 204–210.
245 T. Seng Wong, F. H. Arnold and U. Schwaneberg, *Biotechnol. Bioeng.*, 2004, **85**, 351–358.
246 S. Sakalli, V. Burkina, V. Zlabek and G. Zamaratskaia, *Toxicol. Mech. Methods*, 2015, **25**, 501–506.
247 Horseradish Peroxidase (HRP) Enzymes, **https://www.sigmaaldrich.com/US/en/technical-documents/technical-article/protein-biology/enzyme-activity-assays/peroxidase-enzymes**, (accessed January 3, 2023).
248 K.-F. Aguey-Zinsou, P. V. Bernhardt, J. J. De Voss and K. E. Slessor, *Chem. Commun.*, 2003, 418–419.
249 B. D. Fleming, Y. Tian, S. G. Bell, L.-L. Wong, V. Urlacher and H. A. O. Hill, *Eur. J. Biochem.*, 2003, **270**, 4082–4088.
250 D. L. Johnson, B. C. Lewis, D. J. Elliot, J. O. Miners and L. L. Martin, *Biochem. Pharmacol.*, 2005, **69**, 1533–1541.
251 J. F. Rusling, *Pure Appl. Chem.*, 2001, **73**, 1895–1905.
252 J. F. Rusling and C. J. Campbell, in *Encyclopedia of surface and colloid science*, ed. A. T. Hubbard, Marcel Dekker, New York, 2002, vol. 1, pp. 1754–1770.
253 H. Y. Karasulu, *Expert Opin. Drug Deliv.*, 2008, **5**, 119–135.
254 A. Vaze and J. F. Rusling, *Langmuir*, 2006, **22**, 10788–10795.
255 A. Vaze, M. Parizo and J. F. Rusling, *Langmuir*, 2004, **20**, 10943–10948.
256 V. A. Tamhane, D. G. Dhaware, N. Khandelwal, A. P. Giri and V. Panchagnula, *J. Colloid Interface Sci.*, 2012, **383**, 177–183.
257 S. A. Raya, I. Mohd Saaid, A. Abbas Ahmed and A. Abubakar Umar, *J. Pet. Explor. Prod. Technol.*, 2020, **10**, 1711–1728.
258 N. Kumar and R. N. Goyal, *Electroanalysis*, 2018, **30**, 892–900.
259 J. F. Rusling, in *Encyclopedia of Electrochemistry*, ed. A. J. Bard, Wiley, 1st edn, 2003.
260 J. F. Rusling, *Pure Appl. Chem.*, 2001, **73**, 1895–1905.
261 A. C. Onuoha, X. Zu and J. F. Rusling, *J. Am. Chem. Soc.*, 1997, **119**, 3979–3986.
262 G. N. Kamau, M. P. Guto, B. Munge, V. Panchagnula and J. F. Rusling, *Langmuir*, 2003, **19**, 6976–6981.
263 P. M. Guto, C. V. Kumar and J. F. Rusling, *J. Phys. Chem. B*, 2007, **111**, 9125–9131.
264 P. M. Guto, C. V. Kumar and J. F. Rusling, *Langmuir*, 2008, **24**, 10365–10370.
265 P. M. Guto and J. F. Rusling, *J. Phys. Chem. B*, 2005, **109**, 24457–24464.
266 W. Nam, *Acc. Chem. Res.*, 2007, **40**, 522–531.
267 M. Mukherjee and A. Dey, *ACS Cent. Sci.*, 2019, **5**, 671–682.
268 T. Kamachi, T. Kouno, W. Nam and K. Yoshizawa, *J. Inorg. Biochem.*, 2006, **100**, 751–754.
269 J. C. Price, E. W. Barr, T. E. Glass, C. Krebs and J. M. Bollinger, *J. Am. Chem. Soc.*, 2003, **125**, 13008–13009.
270 P. Hlavica, *Eur. J. Biochem.*, 2004, **271**, 4335–4360.
271 M. N. Podgorski, J. S. Harbort, J. H. Z. Lee, G. T. H. Nguyen, J. B. Bruning, W. A. Donald, P. V. Bernhardt, J. R. Harmer and S. G. Bell, *ACS Catal.*, 2022, **12**, 1614–1625.
272 J. J. D. Sacramento and D. P. Goldberg, *Acc. Chem. Res.*, 2018, **51**, 2641–2652.
273 J. Yang, Y. Qi, J. A. V. Blodgett and T. A. Wencewicz, *J. Nat. Prod.*, 2022, **85**, 47–55.
274 Y. Mie, E. Tateyama and Y. Komatsu, *Electrochim. Acta*, 2014, **115**, 364–369.
275 S. D. Mhaske, M. Ray and S. Mazumdar, *Inorganica Chim. Acta*, 2010, **363**, 2804–2811.
276 J. Tian, J. Wang, Y. Li, M. Huang and J. Lu, *J. Electrochem. Soc.*, 2017, **164**, H470–H476.
277 P. Panicco, S. Castrignanò, S. J. Sadeghi, G. D. Nardo and G. Gilardi, *Bioelectrochemistry*, 2021, **138**, 107729.
278 Y. Mie, Y. Yasutake, H. Takayama and T. Tamura, *J. Catal.*, 2020, **384**, 30–36.
279 X. Xu, G. Bai, L. Song, Q. Zheng, Y. Yao, S. Liu and C. Yao, *Electrochim. Acta*, 2017, **258**, 1365–1374.
280 L. Shangguan, Y. Zhao, L. Mi, L. Jiang and S. Liu, *J. Electroanal. Chem.*, 2016, **772**, 46–51.
281 R. Nerimetla and S. Krishnan, *Chem. Commun.*, 2015, **51**, 11681–11684.
282 J. Rittle and M. T. Green, *Science*, 2010, **330**, 933–937.
283 D. F. Lewis and Y. Ito, *Expert Opin. Drug Metab. Toxicol.*, 2008, **4**, 1181–1186.
284 M. Pickl, S. Kurakin, F. G. Cantú Reinhard, P. Schmid, A. Pöcheim, C. K. Winkler, W. Kroutil, S. P. de Visser and K. Faber, *ACS Catal.*, 2019, **9**, 565–577.
285 H. Park, G. Park, W. Jeon, J.-O. Ahn, Y.-H. Yang and K.-Y. Choi, *Biotechnol. Adv.*, 2020, **40**, 107504.
286 X. Zhang, Y. Hu, W. Peng, C. Gao, Q. Xing, B. Wang and A. Li, *Front. Chem.*, 2021, **9**, 649000.
287 U. A. Argikar, J. C. Cloyd, A. K. Birnbaum, I. E. Leppik, J. Conway, S. Kshirsagar, W. S. Oetting, E. C. Klein and R. P. Remmel, *Epilepsy Res.*, 2006, **71**, 54–63.
288 D. Li, X. Huang, K. Han and C.-G. Zhan, *J. Am. Chem. Soc.*, 2011, **133**, 7416–7427.

289 R.-J. Li, Z. Zhang, C. G. Acevedo-Rocha, J. Zhao and A. Li, *Green Synth. Catal.*, 2020, **1**, 52–59.
290 A. R. Jalalvand, *Microchem. J.*, 2020, **157**, 105104.
291 D. Holtmann, K.-M. Mangold and J. Schrader, *Biotechnol. Lett.*, 2009, **31**, 765–770.
292 V. V. Shumyantseva, T. V. Bulko, A. V. Kuzikov, R. A. Masamrekh, A. Y. Konyakhina, I. Romanenko, J. B. Max, M. Köhler, A. A. Gilep, S. A. Usanov, D. V. Pergushov, F. H. Schacher and L. V. Sigolaeva, *Electrochim. Acta*, 2020, **336**, 135579.
293 D. P. Wasalathanthri, D. Li, D. Song, Z. Zheng, D. Choudhary, I. Jansson, X. Lu, J. B. Schenkman and J. F. Rusling, *Chem. Sci.*, 2015, **6**, 2457–2468.
294 B. Song, S. Pan, C. Tang, D. Li and J. F. Rusling, *Anal. Chem.*, 2013, **85**, 11061–11067.
295 N. Kumar, Rosy and R. N. Goyal, *Talanta*, 2017, **166**, 215–222.
296 R. N. T. Kankanamage, A. B. Ghosh, D. Jiang, K. Gkika, T. Keyes, L. A. Achola, S. Suib and J. F. Rusling, *Chem. Res. Toxicol.*, 2020, **33**, 2072–2086.
297 M. Kazui, Y. Nishiya, T. Ishizuka, K. Hagihara, N. A. Farid, O. Okazaki, T. Ikeda and A. Kurihara, *Drug Metab. Dispos.*, 2010, **38**, 92–99.
298 T. Coleman, A. M. Kirk, J. H. Z. Lee, D. Z. Doherty, J. B. Bruning, E. H. Krenske, J. J. De Voss and S. G. Bell, *ACS Catal.*, 2022, **12**, 1258–1267.
299 S. G. Bell, J.-A. Stevenson, H. D. Boyd, S. Campbell, A. D. Riddle, E. L. Orton and L.-L. Wong, *Chem. Commun.*, 2002, 490–491.
300 M. M. Chen, P. S. Coelho and F. H. Arnold, *Adv. Synth. Catal.*, 2012, **354**, 964–968.
301 P. Meinhold, M. W. Peters, M. M. Y. Chen, K. Takahashi and F. H. Arnold, *ChemBioChem*, 2005, **6**, 1765–1768.
302 E. T. Farinas, U. Schwaneberg, A. Glieder and F. H. Arnold, *Adv. Synth. Catal.*, 2001, **343**, 601–606.
303 R. Karande, L. Debor, D. Salamanca, F. Bogdahn, K.-H. Engesser, K. Buehler and A. Schmid, *Biotechnol. Bioeng.*, 2016, **113**, 52–61.
304 A. Hoschek, J. Toepel, A. Hochkeppel, R. Karande, B. Bühler and A. Schmid, *Biotechnol. J.*, 2019, **14**, 1800724.
305 T. Fukami, M. Katoh, H. Yamazaki, T. Yokoi and M. Nakajima, *Chem. Res. Toxicol.*, 2008, **21**, 720–725.
306 S. C. Dodani, J. K. B. Cahn, T. Heinisch, S. Brinkmann-Chen, J. A. McIntosh and F. H. Arnold, *ChemBioChem*, 2014, **15**, 2259–2267.
307 P. Dydio, H. M. Key, H. Hayashi, D. S. Clark and J. F. Hartwig, *J. Am. Chem. Soc.*, 2017, **139**, 1750–1753.
308 I. S. Williams, L. Gatchie, S. B. Bharate and B. Chaudhuri, *ACS Omega*, 2018, **3**, 8903–8912.
309 M. P. Mayhew, V. Reipa, M. J. Holden and V. L. Vilker, *Biotechnol. Prog.*, 2000, **16**, 610–616.
310 E. N. Jacobsen, W. Zhang and M. L. Guler, *J. Am. Chem. Soc.*, 1991, **113**, 6703–6704.
311 G. Yin, A. M. Danby, D. Kitko, J. D. Carter, W. M. Scheper and D. H. Busch, *Inorg. Chem.*, 2007, **46**, 2173–2180.
312 G. Yin, M. Buchalova, A. M. Danby, C. M. Perkins, D. Kitko, J. D. Carter, W. M. Scheper and D. H. Busch, *Inorg. Chem.*, 2006, **45**, 3467–3474.
313 H. F. Fisher, E. E. Conn, B. Vennesland and F. H. Westheimer, *J. Biol. Chem.*, 1953, **202**, 687–697.
314 J. T. Groves and R. S. Myers, *J. Am. Chem. Soc.*, 1983, **105**, 5791–5796.
315 V. Polic, K. J. Cheong, F. Hammerer and K. Auclair, *Adv. Synth. Catal.*, 2017, **359**, 3983–3989.
316 R. Lonsdale, J. N. Harvey and A. J. Mulholland, *J. Phys. Chem. B*, 2010, **114**, 1156–1162.
317 P. Rydberg, R. Lonsdale, J. N. Harvey, A. J. Mulholland and L. Olsen, *J. Mol. Graph. Model.*, 2014, **52**, 30–35.
318 T. Coleman, A. M. Kirk, R. R. Chao, M. N. Podgorski, J. S. Harbort, L. R. Churchman, J. B. Bruning, P. V. Bernhardt, J. R. Harmer, E. H. Krenske, J. J. De Voss and S. G. Bell, *ACS Catal.*, 2021, **11**, 1995–2010.
319 C.-H. Yun, K.-H. Kim, D.-H. Kim, H.-C. Jung and J.-G. Pan, *Trends Biotechnol.*, 2007, **25**, 289–298.
320 L. Zhang and Q. Wang, *ChemBioChem*, 2022, **23**, e202100439.
321 D. Kumar, S. P. de Visser and S. Shaik, *Chem. – Eur. J.*, 2005, **11**, 2825–2835.
322 S. Jin, T. M. Makris, T. A. Bryson, S. G. Sligar and J. H. Dawson, *J. Am. Chem. Soc.*, 2003, **125**, 3406–3407.
323 R. R. Chao, I. C.-K. Lau, T. Coleman, L. R. Churchman, S. A. Child, J. H. Z. Lee, J. B. Bruning, J. J. De Voss and S. G. Bell, *Chem. – Eur. J.*, 2021, **27**, 14765–14777.
324 A. Çelik, D. Sperandio, R. E. Speight and N. J. Turner, *Org. Biomol. Chem.*, 2005, **3**, 2688.
325 H. Kawana, T. Miwa, Y. Honda and T. Furuya, *ACS Omega*, 2022, **7**, 20259–20266.
326 A. W. Munro, K. J. McLean, J. L. Grant and T. M. Makris, *Biochem. Soc. Trans.*, 2018, **46**, 183–196.
327 J. Zitko, B. Servusová, A. Janoutová, P. Paterová, J. Mandíková, V. Garaj, M. Vejsová, J. Marek and M. Doležal, *Bioorg. Med. Chem.*, 2015, **23**, 174–183.
328 U. Bussy and M. Boujtita, *Chem. Res. Toxicol.*, 2014, **27**, 1652–1668.
329 I. Geronimo, C. A. Denning, D. K. Heidary, E. C. Glazer and C. M. Payne, *Biophys. J.*, 2018, **115**, 1251–1263.
330 S. H. Lee, Y.-C. Kwon, D.-M. Kim and C. B. Park, *Biotechnol. Bioeng.*, 2013, **110**, 383–390.
331 P. Rydberg, U. Ryde and L. Olsen, *J. Chem. Theory Comput.*, 2008, **4**, 1369–1377.
332 L. T. Burka, F. P. Guengerich, R. J. Willard and T. L. Macdonald, *J. Am. Chem. Soc.*, 1985, **107**, 2549–2551.
333 C. Li, W. Wu, K. Cho and S. Shaik, *Chem. – Eur. J.*, 2009, **15**, 8492–8503.
334 F. P. Guengerich, C.-H. Yun and T. L. Macdonald, *J. Biol. Chem.*, 1996, **271**, 27321–27329.
335 T. Johansson, L. Weidolf and U. Jurva, *Rapid Commun. Mass Spectrom.*, 2007, **21**, 2323–2331.
336 E. Nouri-Nigjeh, H. P. Permentier, R. Bischoff and A. P. Bruins, *Anal. Chem.*, 2010, **82**, 7625–7633.
337 A. H. Meyer, A. Dybala-Defratyka, P. J. Alaimo, I. Geronimo, A. D. Sanchez, C. J. Cramer and M. Elsner, *Dalton Trans.*, 2014, **43**, 12175–12186.
338 A. A. Najmi, R. Bischoff and H. P. Permentier, *Molecules*, 2022, **27**, 3293.

339 F. Rao, Z. Chen, D. Zhou, Y. Kang, L. Guo and Y. Xue, *J. Mol. Graph. Model.*, 2018, **84**, 109–117.
340 A. M. Carmona-Ribeiro, T. Prieto and I. L. Nantes, *Front. Mol. Biosci.*, 2015, **2**, 50.
341 S. Lütz, E. Steckhan and A. Liese, *Electrochem. Commun.*, 2004, **6**, 583–587.
342 C. Regalado, J. A. Asenjo and D. L. Pyle, *Enzyme Microb. Technol.*, 1996, **18**, 332–339.
343 A. Henriksen, *Protein Sci.*, 2001, **10**, 108–115.
344 Y. Bhandari, H. Sajwan, P. Pandita and V. Koteswara Rao, *Biocatal. Biotransform.*, 2022, 1–18.
345 M. Hofrichter, *Enzyme Microb. Technol.*, 2002, **30**, 454–466.
346 O. D. V. Biko, M. Viljoen-Bloom and W. H. van Zyl, *Enzyme Microb. Technol.*, 2020, **141**, 109669.
347 W. Zhang, W. Ye, Y. Wang and Y. Yan, *Biotechnol. J.*, 2022, **17**, 2200098.
348 S.-H. Cho, J. Shim, S.-H. Yun and S.-H. Moon, *Appl. Catal. Gen.*, 2008, **337**, 66–72.
349 K. S. Yang, G. Mul and J. A. Moulijn, *Electrochim. Acta*, 2007, **52**, 6304–6309.
350 R. D. C. Soltani, A. Rezaee, A. R. Khataee and H. Godini, *Res. Chem. Intermed.*, 2013, **39**, 4277–4286.
351 V. Viswanathan, H. A. Hansen and J. K. Nørskov, *J. Phys. Chem. Lett.*, 2015, **6**, 4224–4228.
352 W. R. P. Barros, T. Ereno, A. C. Tavares and M. R. V. Lanza, *ChemElectroChem*, 2015, **2**, 714–719.
353 A. Khataee, S. Sajjadi, S. Rahim Pouran and A. Hasanzadeh, *J. Ind. Eng. Chem.*, 2017, **56**, 312–320.
354 Y.-C. Yin, Y. Shi, Y.-B. Sun, D.-R. Yang, Y. Liu and X.-H. Xia, *ACS Appl. Energy Mater.*, 2021, **4**, 10843–10848.
355 K. B. Lee, M. B. Gu and S.-H. Moon, *J. Chem. Technol. Biotechnol.*, 2001, **76**, 811–819.
356 H. Tian, S. Mu, H. Li, X. Wu and Z. Lu, *ChemCatChem*, 2012, **4**, 1850–1855.
357 K. Lee and S.-H. Moon, *J. Biotechnol.*, 2003, **102**, 261–268.
358 S. Lütz, K. Vuorilehto and A. Liese, *Biotechnol. Bioeng.*, 2007, **98**, 525–534.
359 C. Kohlmann and S. Lütz, *Eng. Life Sci.*, 2006, **6**, 170–174.
360 T. Krieg, S. Hüttmann, K.-M. Mangold, J. Schrader and D. Holtmann, *Green Chem.*, 2011, **13**, 2686.
361 M. Xia, Z. Wang, L. Du, Z. Fu, G. Jiang, D. Lu, J. Wu and Z. Liu, *ChemCatChem*, 2022, **14**, e202101732.
362 A. E. W. Horst, S. Bormann, J. Meyer, M. Steinhagen, R. Ludwig, A. Drews, M. Ansorge-Schumacher and D. Holtmann, *J. Mol. Catal. B: Enzym.*, 2016, **133**, S137–S142.
363 S. Bormann, M. M. C. H. Schie, T. P. De Almeida, W. Zhang, M. Stöckl, R. Ulber, F. Hollmann and D. Holtmann, *ChemSusChem*, 2019, **12**, 4759–4763.
364 X. Zhu, Y. Ding, S. Li, Y. Chen, Q. Zhai and Y. Jiang, *ACS Sustainable Chem. Eng.*, 2022, **10**, 12497–12503.
365 N. Ž. Šekuljica, J. R. Jovanović, S. M. Jakovetić Tanasković, N. D. Ognjanović, I. V. Gazikalović, Z. D. Knežević-Jugović and D. Ž. Mijin, *Biotechnol. Prog.*, 2020, **36**, e2991.
366 B. E. Keshta, A. H. Gemeay and A. A. Khamis, *Environ. Sci. Pollut. Res.*, 2022, **29**, 6633–6645.
367 J. Wang, Z. Shu, Z. Chen, J. Su and C. Liu, *J. Clean. Prod.*, 2022, **337**, 130489.
368 D. Tarasek, B. Gąsowska-Bajger, B. Frąckowiak-Wojtasek, C. Kersten, M. Jewgiński, Ł. Kołodziej, R. Latajka and H. Wojtasek, *J. Mol. Struct.*, 2022, **1252**, 132169.
369 G. Zambrano, A. Sekretareva, D. D'Alonzo, L. Leone, V. Pavone, A. Lombardi and F. Nastri, *RSC Adv.*, 2022, **12**, 12947–12956.
370 J. Rocha-Martin, S. Velasco-Lozano, J. M. Guisán and F. López-Gallego, *Green Chem.*, 2014, **16**, 303–311.
371 V. M. Samokyszyn, J. P. Freeman, K. R. Maddipati and R. V. Lloyd, *Chem. Res. Toxicol.*, 1995, **8**, 349–355.
372 H. Nunavath, C. Banoth, V. R. Talluri and B. Bhukya, *Bioinformation*, 2016, **12**, 318–323.
373 J. Xu, T. Tang, K. Zhang, S. Ai and H. Du, *Process Biochem.*, 2011, **46**, 1160–1165.
374 Z. Lu, W. Hou, X. Wu, H. Li and J. Chen, *Chem. Lett.*, 2007, **36**, 564–565.
375 K. Piontek, A. T. Smith and W. Blodig, *Biochem. Soc. Trans.*, 2001, **29**, 111–116.
376 S. Parveen, M. Asgher and M. Bilal, *Environ. Technol. Innov.*, 2021, **21**, 101226.
377 V. D. Giap, D. H. Nghi, L. H. Cuong and D. T. Quynh, *BioResources*, 2022, **17**, 4480–4498.
378 E. E. Ferapontova, J. Castillo and L. Gorton, *Biochim. Biophys. Acta, Gen. Subj.*, 2006, **1760**, 1343–1354.
379 C. Yang, S. Maldonado and C. R. J. Stephenson, *ACS Catal.*, 2021, **11**, 10104–10114.
380 Y. Ding, K. Cui, X. Liu, Q. Xie, Z. Guo and Y. Chen, *J. Hazard. Mater.*, 2022, **431**, 128544.
381 Z. Liu, Y. Lv, A. Zhu and Z. An, *ACS Macro Lett.*, 2018, **7**, 1–6.
382 E. Gantumur, S. Sakai, M. Nakahata and M. Taya, *ACS Macro Lett.*, 2017, **6**, 485–488.
383 A. Bindoli, J. M. Fukuto and H. J. Forman, *Antioxid. Redox Signal.*, 2008, **10**, 1549–1564.
384 V. M. Dembitsky and M. Srebnik, *Eurasian Chem.-Technol. J.*, 2017, **4**, 221.
385 E. Baciocchi, M. F. Gerini, P. J. Harvey, O. Lanzalunga and S. Mancinelli, *Eur. J. Biochem.*, 2000, **267**, 2705–2710.
386 S. Sato, Y. Ohashi, M. Kojima, T. Watanabe, Y. Honda and T. Watanabe, *Chemosphere*, 2009, **77**, 798–804.
387 H. Tang, Y. Zhang, Y. Deng, S. Du, D. Li, Z. Wang, H. Li, X. Gao and F. Wang, *Catal. Lett.*, 2022, **152**, 720–731.
388 H. Rabiee, L. Ge, X. Zhang, S. Hu, M. Li and Z. Yuan, *Energy Environ. Sci.*, 2021, **14**, 1959–2008.
389 J. J. Mieyal and D. W. Starke, *Methods in Enzymology*, Elsevier, 1994, vol. 231, pp. 573–598.
390 S. Aoun and M. Baboulène, *J. Mol. Catal. B: Enzym.*, 1998, **4**, 101–109.
391 B.-A. Kaup, U. Piantini, M. Wüst and J. Schrader, *Appl. Microbiol. Biotechnol.*, 2007, **73**, 1087–1096.
392 M. Hobisch, D. Holtmann, P. Gomez de Santos, M. Alcalde, F. Hollmann and S. Kara, *Biotechnol. Adv.*, 2021, **51**, 107615.
393 M. Hofrichter, H. Kellner, R. Herzog, A. Karich, C. Liers, K. Scheibner, V. W. Kimani and R. Ullrich, in *Grand*

Challenges in Fungal Biotechnology, ed. H. Nevalainen, Springer International Publishing, Cham, 2020, pp. 369–403.
394 D. Holtmann, T. Krieg, L. Getrey and J. Schrader, *Catal. Commun.*, 2014, **51**, 82–85.
395 C. Laane, A. Weyland and M. Franssen, *Enzyme Microb. Technol.*, 1986, **8**, 345–348.
396 F. Arnold, *Trends Biotechnol.*, 1990, **8**, 244–249.
397 A. Shaw, *Curr. Opin. Struct. Biol.*, 1996, **6**, 546–550.
398 P. S. Coelho, E. M. Brustad, A. Kannan and F. H. Arnold, *Science*, 2013, **339**, 307–310.
399 S. V. Athavale, S. Gao, A. Das, S. C. Mallojjala, E. Alfonzo, Y. Long, J. S. Hirschi and F. H. Arnold, *J. Am. Chem. Soc.*, 2022, **144**, 19097–19105.
400 T. Cai, H. Sun, J. Qiao, L. Zhu, F. Zhang, J. Zhang, Z. Tang, X. Wei, J. Yang, Q. Yuan, W. Wang, X. Yang, H. Chu, Q. Wang, C. You, H. Ma, Y. Sun, Y. Li, C. Li, H. Jiang, Q. Wang and Y. Ma, *Science*, 2021, **373**, 1523–1527.
401 T. Zheng, M. Zhang, L. Wu, S. Guo, X. Liu, J. Zhao, W. Xue, J. Li, C. Liu, X. Li, Q. Jiang, J. Bao, J. Zeng, T. Yu and C. Xia, *Nat. Catal.*, 2022, **5**, 388–396.